EXPERIMENTAL INVESTIGATIONS ON PERFORMANCE OF PASSIVE DIRECT METHANOL FUEL CELL WITH DIFFERENT CURRENT COLLECTOR MATERIALS USING TAPERED CYLINDRICAL OPENINGS, EMPLOYING VARIABLE DYNAMIC REGIONS, AND IDENTIFICATION OF SERVICE-ORIENTED DEGRADATION

A Dissertation
Submitted in partial fulfilment of the requirements for
the award of Degree of

DOCTOR OF PHILOSOPHY

in

MECHANICAL ENGINEERING

by

Nelaturi V Raghavaiah
(Roll No.719059)

Supervisor:

Dr. G. Naga Srinivasulu
Professor

DEPARTMENT OF MECHANICAL ENGINEERING
NATIONAL INSTITUTE OF TECHNOLOGY,
WARANGAL (TS), INDIA,
2023

DECLARATION

This is to certify that the work presented in the thesis entitled "**EXPERIMENTAL INVESTIGATIONS ON PERFORMANCE OF PASSIVE DIRECT METHANOL FUEL CELL WITH DIFFERENT CURRENT COLLECTOR MATERIALS USING TAPERED CYLINDRICAL OPENINGS, EMPLOYING VARIABLE DYNAMIC REGIONS, AND IDENTIFICATION OF SERVICE-ORIENTED DEGRADATION**" is a bonafide work done by me under the supervision of Dr. G. Naga Srinivasulu, and was not submitted elsewhere for the award of any degree. I declare that this written submission represents my ideas in my own words and where others' ideas or words have been included, I adequately cited and referenced the original sources. I also declare that I have adhered to all the principles of academic honesty and integrity and have not misrepresented, fabricated, or falsified any idea/data/fact/source in my submission. I understand that any violation of the above will cause disciplinary action by the Institute and can also evoke penal action from the sources that have thus not been properly cited or from whom proper permission has not been taken when needed.

(Nelaturi V Raghavaiah)

(Roll No.719059)

Date:

DEPARTMENT OF MECHANICAL ENGINEERING
NATIONAL INSTITUTE OF TECHNOLOGY,
WARANGAL, TS, INDIA – 506004

CERTIFICATE

This is to certify that the dissertation work entitled — **EXPERIMENTAL INVESTIGATIONS ON PERFORMANCE OF PASSIVE DIRECT METHANOL FUEL CELL WITH DIFFERENT CURRENT COLLECTOR MATERIALS USING TAPERED CYLINDRICAL OPENINGS, EMPLOYING VARIABLE DYNAMIC REGIONS, AND IDENTIFICATION OF SERVICE-ORIENTED DEGRADATION,** which is being submitted by Mr. Nelaturi V Raghavaiah (Roll No.719059), is a bonafide work submitted to the Department of Mechanical Engineering, National Institute of Technology, Warangal in partial fulfilment of the requirement for the award of the degree of Doctor of Philosophy in Mechanical Engineering.

To the best of our knowledge, the work incorporated in this thesis has not been submitted elsewhere for the award of any degree.

Prof. G. Naga Srinivasulu,
Supervisor
Department of Mechanical Engineering
National Institute of Technology
Warangal- 506004

Prof. V. Suresh Babu,
Head
Department of Mechanical Engineering
National Institute of Technology
Warangal- 506004

ACKNOWLEDGMENT

Afterward, I would like to sincerely thank my supervisor, Dr. G. Naga Srinivasulu, Professor, Mechanical Engineering Department, National Institute of Technology, Warangal, for his continuous guidance, support, enthusiasm, and motivation in my Ph.D. research work.

I am grateful to Prof. Bidyadhar Subudhi, Director and Prof. N.V. Ramana Rao, former Director-NIT Warangal, who have been a constant source of inspiration for me. I thank Prof. V. Suresh Babu, Head of the Department of Mechanical Engineering, for his help and continuous encouragement to complete this work. I sincerely thank Prof. S. Srinivasa Rao, Prof. K. Kiran Kumar (Mechanical Engineering Department), and Prof. R. Satish Babu (Bio-Technology Department), learned members of my Doctoral Scrutiny Committee for being helpful and generous during the entire course of this work.

My sincere thanks also go to Prof. N. Selva Raj and Prof. A. Kumar, former HODs, Department of Mechanical Engineering, National Institute of Technology, Warangal, for encouragement and for providing access to the laboratory and research facilities. Without their precious support, conducting this research would not be possible.

I want to thank my family: my wife, Sai Sudha Rani; my children (Srivatsa and Sriharsha); my parents (Sri Late Subbaiah and Smt. Sarojini Devi); and my best friends I Hari Prasad, B Koti Reddy and K Sandeep for supporting me throughout writing this thesis and my life in general.

Last but not least, I sincerely express my deepest gratitude to my fellow scholars for their help and exciting discussions in the previous four years.

Nelaturi V Raghavaiah
Roll No.719059
Research Scholar
Department of Mechanical Engineering
National Institute of Technology Warangal- 506004

ABSTRACT

To attract and get a major share of the Passive Direct Methanol Fuel Cell (PDMFC) in the global market, optimization of the influencing factors like system durability, effectiveness of MEA, compatibility of current collectors in methanol environment and scavenging of reaction products are to be balanced for achieving the excellent performance of cell for electricity generation and charging portable electronic devices.

Current collectors play one of the key components of the fabricated assembly of cell hardware components. The objective of the present research is to enhance the performance of Passive Direct Methanol Fuel Cell by using different current collectors with taper cylindrical openings. Therefore, the selection of suitable materials and their novel design are the most important characteristics that ultimately affect fuel cell performance. The required characteristics of the materials of current collectors are better electrical conductivity and good corrosion resistance having chemical compatibility in methanol solution. Experimental examination of Nickel-201 and Brass current collectors at various concentrations of methanol solution are compared with the Austenitic Stainless Steel-316L current collector having the same geometry, aspect ratio, and effective opening area. From the experimental results it is observed that the best power density obtained among these current collectors is 10.416 $mW.cm^{-2}$ using uniform cylindrical openings on Nickel-201 current collectors at a 5-molar concentration. The corrosion compatibility on current collector materials with a short-term cell operation of 12 hours duration test result also inferred Nickel-201 as better material.

Analysis of buoyancy effect on evaluating CO_2 gas from Passive Direct Methanol Fuel cell current collectors' openings is carried out. The analysis shows that buoyancy is more effective in taper cylindrical openings due to the accommodation of a larger bubble volume compare to the uniform cylindrical opening. When the cell is in operation, it is observed that the CO_2 bubbles expelled more easily. The best power density obtained using taper cylindrical openings with Nickel-201 at a methanol concentration of 3M is 14.054 $mW.cm^{-2}$, whereas it is 8.092 $mW.cm^{-2}$ in the case of uniform cylindrical openings at the same 3M methanol concentration. Hence the taper cylindrical openings are found to perform better than uniform cylindrical openings by 34.92% at its best power density point and further, the weight of the current collectors is also reduced leading to gravitational power density improvement by 27.8%.

The analysis is extended with different combination of anode and cathode current collector materials in PDMFC. Among the anode-cathode combinations, the combination using Nickel-201 as anode and Stainless Steel as cathode at 3M solution using taper cylindrical openings on current collectors, produced a maximum power density of 11.776 $mW.cm^{-2}$ and corresponding maximum current density of 97.6 $mA.cm^{-2}$, whereas the SS-Brass combination showed the least performance with the power density of 6.144 $mW.cm^{-2}$ and current density of 60.8 $mA.cm^{-2}$.

The performance of Passive Direct Methanol Fuel Cell is analysed by using various Membrane Electrode Assembly (MEA) shapes such as square, rectangle, rhombus, and circle with equal areas and equal perimeters. The variation in MEA shape/size is achieved by altering gasket openings in the dynamic regions. The novelty of this research work is instead of fabricating various shapes and sizes of highly expensive MEAs, the desired shapes and sizes of the MEA are accomplished by altering gasket openings over dynamic regions to find out the highest power density of the cell. In the equal areas of MEA shapes, gasket opening areas of 1963.5 mm^2 are used. In the equal perimeters of shapes, gasket opening perimeters of 157.1 mm are used. In the equal areas, among the shapes that are chosen for investigation, the square shape opening consisting of a perimeter of 177.2 mm has developed a maximum power density of 6.344 $mW.cm^{-2}$. Similarly, in equal perimeters, the rhombus shape opening with an area of 1400 mm^2 has developed a maximum power density of 7.714 $mW.cm^{-2}$.

Fuel cell components performance and their durability are affected by methanol solution, its concentration, evaporative conditions of water, carbon dioxide evaluation, heat generation, and its sealing components. Non-Destructive Tests such as Visual Testing, Liquid Penetrant Testing, Ultrasonic Thickness measurement, hardness measurement, and metallographic examination are used to identify direct or indirect means to find the size and to locate surface and subsurface discontinuities in the materials and components. From the compatibility of current collectors' experiments, Ni-201 is found better corrosion resistant (about $1/8^{th}$ of SS corrosion rate). From this research it is observed that the PDMFC with square shaped MEA using Nickel-201 (which is introduced in this research) current collector with taper cylindrical openings on anode and cathode sides, generates maximum power density of 14.054 $mW.cm^{-2}$ at 3M methanol concentration.

TABLE OF CONTENTS

LIST OF FIGURES

LIST OF TABLES

NOMENCLATURE

ABBREVIATIONS

ABDMFC	: Air-Breathing Direct Methanol Fuel Cell
ADMFC	: Active Direct Methanol Fuel Cell
ASME	: American Society of Mechanical Engineers
CC	: Current Collector
CD	: Current Density
DL	: Diffusion Layer
DMFC	: Direct Methanol Fuel Cell
FC	: Fuel Cell
PD	: Power Density
PDMFC	: Passive Direct Methanol Fuel Cell
PEM	: Proton Exchange Membrane
PEMFC	: Proton Exchange Membrane Fuel Cell
PT	: Penetrant Testing
PTFE	: Poly Tetra Fluoro Ethylene
MEA	: Membrane Electrode Assembly
NDT	: Non-Destructive Testing
Ni-201	: Nickel grade 201
OCV	: Open Circuit Voltage
SS-316L	: Stainless Steel grade 316L
SEM	: Scanning Electron Microscope
TEM	: Transmission Electron Microscope
VT	: Visual Testing
UT	: Ultrasonic Testing

Chapter 1

Introduction

As the necessity for electric power is growing up day by day across the world for societal and industrial requirements, among alternative energy resources available in the present scenario, 'Fuel Cell Technology' has evolved as one of the efficient and cleaner energy resources for replacing other renewable and conventional fuels, Hayre et al, [1]. Fuel cell is similar to electrical converter, such as battery. It transforms the chemical energy of fuel and other reactants into electrical energy, Narayanan et al, [2]. A fuel cell produces uninterrupted electricity if fuel and oxidant are available for the cell reaction. These cells use ion exchange membranes, compatible with fuel and oxidant. Other features of the cells are: no moving components, noise-free operation, clear reactants, free from the release of oxides of Sulphur & nitrogen, readiness to cater needs of power demands, and system fluctuations.

1.1 History of Fuel Cells

In the year 1839, a systematic investigation on fuel cells was carried out by Sir William Grove and explains the basic principle of the cell to the scientific society. Further in the year 1842, he has developed a multi-stack cell and called it by the name "gaseous voltaic battery". Further to this invention, F.T. Bacon developed a stack of 6000 W by the end of 1950. Thereafter, in 1960s, Proton Exchange Membrane (PEM) Fuel Cell (FC) was used in the Gemini and Apollo space programs to generate electricity to power the communication facility. As the cost of these FCs were high, these systems were limited to space and military applications. In 1990s, Ballard Power Systems produced FC powered buses using low price membrane materials and with newer fabrication methods. In the year 1993, Energy Partners established the first passenger car working on PEM Fuel Cells. By the end of the 20th century, most of the car manufacturers had built the Fuel Cell powered vehicles, Barbir, [3]. The timeline of Fuel Cells development history is shown in figure 1.1.

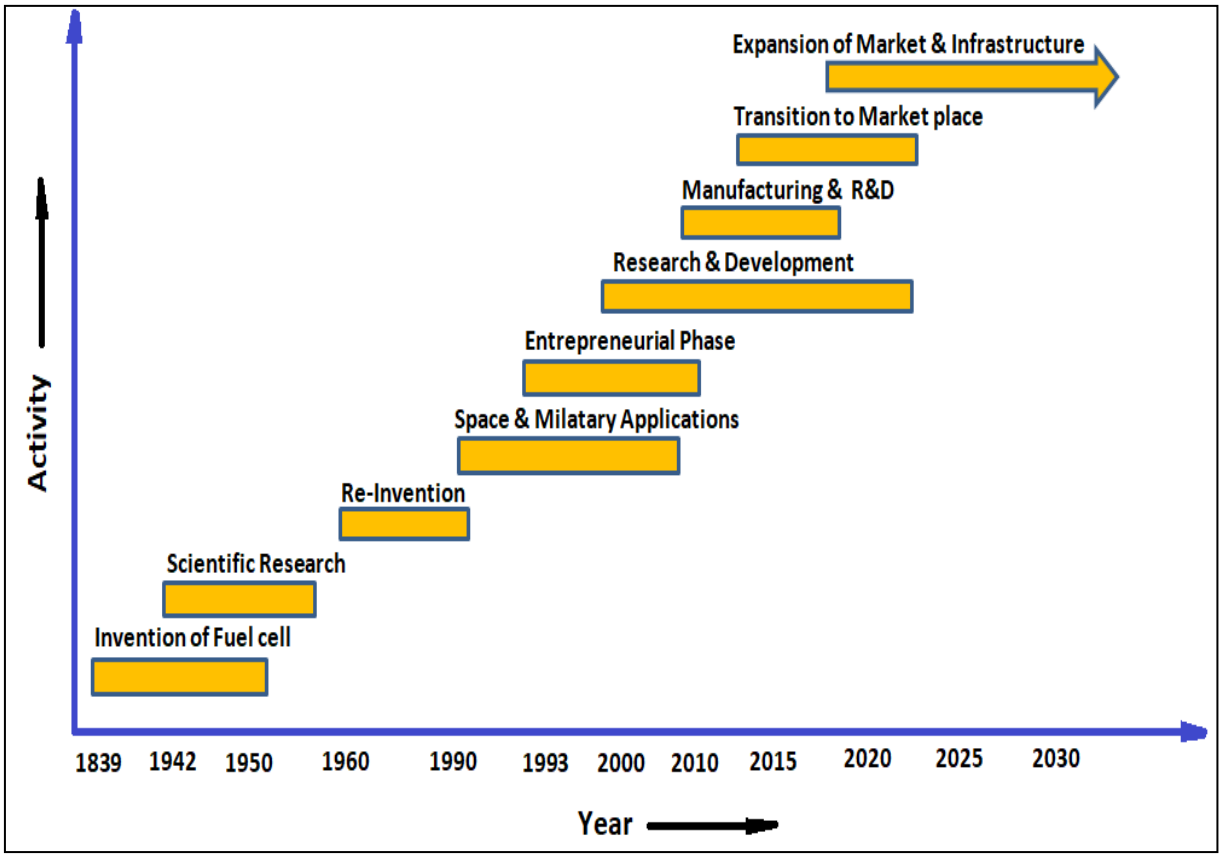

Figure 1.1 Timeline history of the evolution of fuel cells

1.2 Types of Fuel Cells

Fuel cells are classified mostly based on the type of membrane used for transfer of protons or ions through it, Barbir, [3]. Some of these popular fuel cells are:

a) PEMFC : Proton Exchange (polymer electrolyte) Membrane Fuel Cell
b) DMFC : Direct Methanol Fuel Cell
c) AFC : Alkaline Fuel Cell
d) PAFC : Phosphoric Acid Fuel Cell
e) MCFC : Molten Carbonate Fuel Cell
f) SOFC : Solid Oxide Fuel Cell

Different types of cells and their salient features such as type of electrolyte, anode, cathode, charge carrier in MEA, working temperature, construction, operation, type of fuel, catalysts used, trim parts, power rating and application of the fuel cells are tabulated in table 1.1.

Table 1.1 Types of Fuel Cells and their salient features

Description	**Type of Fuel Cell**					
	PEMFC	**DMFC**	**AFC**	**PAFC**	**MCFC**	**SOFC**
Type of electrolyte used.	Polymer based membrane	Polymer based membrane	Liquid KOH	Liquid H_3PO_3	Molten Carbonate salts	Ceramic based Y_2O_3/ZrO_2 Stabilized
Anode	Pt/C+ PTFE	Pt/Ru/C+ PTFE	Pt/Pd + PTFE	Pt/C + PTFE	Ni / Cr	NiO-YSZ
Cathode	Pt/C+ PTFE	Pt/C+ PTFE	Pt/Pd+ PTFE	Pt/C+ PTFE	NiO	Sr-Doped $LaMnO_3$
Charge Carrier	H^+	H^+	OH^-	H^+	CO_3^{-2}	O^{-2}
Working Temperature, ^OC	80	50-120	60-220	200	650	600-1000
Fuel	Hydrogen	Methanol	Hydrogen	Hydrogen	Hydrogen, methane	Hydrogen, Carbon dioxide, methane
Cell trims	Carbon based	Carbon based	Carbon based	Carbon based	Stainless steel based	Ceramic based
Catalyst used	Platinum	Platinum, Ruthenium	Platinum	Platinum	Nickel	Perovskites
Power range	Up to 250 kW	Up to 1 kW	Up to 5kW	Up to 200 kW	Up to 1MW	Up to 1MW
Applications	Auto-mobile, portable, and stationary	Portable, electronic chargers	Space, defence, and military	Integrated power and heat generation	Integrated heat with power product-ion and stand alone	Integrated heat with power production and stand alone

The present research work deals with Direct Methanol Fuel Cell (DMFC), which is a sub-class of the Proton Exchange Membrane Fuel Cell (PEMFC). The particulars of the PEMFC and DMFC are discussed in the following sections.

1.3 Proton Exchange Membrane Fuel Cell (PEMFC)

PEMFC uses PTFE based membrane *Nafion* (developed by DUPONT company) for cell reactions. It uses Hydrogen as fuel and Oxygen as oxidant. When compared to other types of fuel cells, PEMFC operates at lower operating temperature, has simple structural design and light weight. As the working temperature of the cell is about 80^{o}C, it takes lesser time for start-up. PEMFC design is appropriate for usage in automobiles and other power applications.

The major difficulty with respect to PEMFC is humidification of the membrane and water management. Water, produced as a by-product of the reaction is to be eliminated from the system for effective functioning of the cell. Else, the cell gets flooded with water and become inoperative. Further, at higher flow rates of reactants and higher current density regions of MEA, the generation of heat is also high. As the *Nafion* membrane cannot withstand high temperature, humidified reactants should be supplied on anode and cathode side to avoid drying up of MEA. This humidification process increases the complexity of the system. The energy density of PEMFC is less and therefore, higher capacity tanks are required for storing Hydrogen in order to operate the cell for longer hours. Hydrogen fuel is stored in composite cylinders at high pressure and low temperature.

1.4 Direct Methanol Fuel Cell (DMFC)

DMFC is a subcategory of the PEMFC, which converts the chemical energy of methanol fuel directly into electricity. Humidification of *Nafion* membrane is not a problem due to the use of liquid methanol at the anode side. Methanol is produced by destructive distillation of wood or naturally by anaerobic metabolism of bacteria. Thus, methanol fuel is a renewable energy. The merits of the methanol fuel are their ease of storage at room temperature and atmospheric pressure compared to hydrogen fuel. Volumetric energy density of the methanol (17.64 MJ/L) fuel is much higher than that of hydrogen (1.75 MJ/L) fuel at 20 MPa. It uses a proton exchange membrane, compatible with liquid methanol fuel and ambient air emerges as an electrical power source, Braz et al, [4] for the requirement of handy electronic gadgets such as cell phones, walk-man, mini-computers, mini-toys, mini-laptops, emergency illuminations, stereo players, handy phones, and as a power source for application of space and antenna features. Further, Methanol in liquid form is easy for transportation, re-fueling, facilitates better storage, Raghavaiah et al, [5], abundant availability, inexpensive and has high specific energy

density. Important features of the PDMFC are: it can be operated even at low to ambient temperatures, Braz et al, [6], atmospheric pressure to higher pressures, and no supplementary fluid electrolyte is required. Other features of the cell are: doesn't have moving components, noise-free operation, clear reactants, free from the release of oxides of Sulphur & Nitrogen, readiness to cater the needs of power demands, and system fluctuations. DMFC has fast charging capacity of devices, which is compatible with the conventional batteries like Li-ion, Ni-Cd batteries.

Direct methanol fuel cells are categorized into the following three types:

- Active direct methanol fuel cells (ADMFC)
- Air-Breathing direct methanol fuel cells (ABDMFC), and
- Passive direct methanol fuel cells (PDMFC)

Over the past few decades, a lot of research is carried out on the ADMFC. Whereas the operation of the ADMFC require fuel pump, air pump and a control system for controlling reactants. The amalgamation of the equipment to portable power charging appliances is very difficult. Another drawback is consumption of additional power by the reactant pumps, which in turn reduce net output power. These difficulties are making it less attractive for portable charging appliances.

ABDMFC is a popularly known as semi-active DMFC. In this ABDMFC, the methanol solution is delivered by external pump at the anode end. Whereas, at the cathode end, oxygen is served from the ambient air by natural convection. The whole system resembles to ADMFC except the cathode end. The drawback with the system is consumption of additional power by the fuel pump, which in turn reduces net output power. These difficulties make it less attractive for portable charging appliances during the operation of ABDMFC

These drawbacks in ADMFC and ABDMFC are tackled by developing a simple fuel cell, called the Passive direct methanol fuel cells (PDMFC) that suits for handy and portable power appliances.

In the PDMFC, the reactants are supplied in passive condition, i.e., methanol fuel by passive supply by gravity from inbuilt anode reservoir and air from atmosphere by natural

convection. The present work focuses on the PDMFC system. The detail of the cell and its working principle is described in subsequent sections.

1.5 Principle of operation of Passive Direct Methanol Fuel Cell

A schematic illustration of PDMFC has been shown in figure 1.2. The cell consists of an electrolyte membrane sandwiched between the anode and the cathode (MEA). Catalysts are used for controlling and for effective kinetics of the chemical reaction of PDMFC.

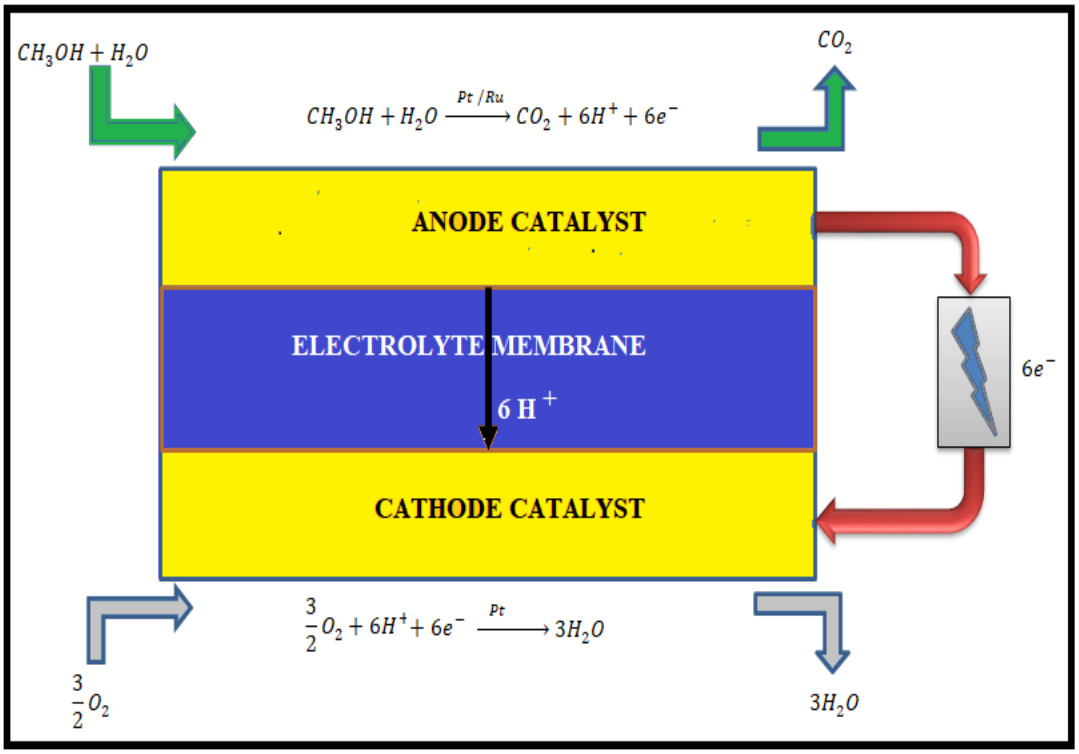

Figure 1.2 Schematic illustration of PDMFC

At the anodic end of the membrane, platinum and ruthenium on carbon are used as catalysts for liberating electrons, protons, and carbon dioxide which are shown in the chemical equation (1.1). Whereas at the cathodic end of the membrane, only platinum on carbon is used for combining oxygen, protons, and electrons and for the formation of water which is shown in the chemical equation (1.2). In this process, the electrons that are liberated at the anode flow in an exterior path to the cathode after performing useful work before reaching the cathode. The overall chemical process is shown in the reaction equation (1.3).

Anode End Reaction:

$$CH_3OH + H_2O \xrightarrow{\frac{Pt}{Ru}} CO_2 + 6H^+ + 6e^- \qquad (1.1)$$

Cathode End Reaction:

$$\frac{3}{2}O_2 + 6H^+ + 6e^- \xrightarrow{Pt} 3H_2O \quad (1.2)$$

Overall Fuel Cell Reaction:

$$CH_3OH + \frac{3}{2}O_2 \rightarrow CO_2 + 2H_2O \quad (1.3)$$

The power produced by the cell is mainly depends on methanol concentration, operating temperature of the cell, size of the MEA, material of the current collectors, and openings on the current collectors.

1.6 Construction of the passive DMFC

Figure 1.3 shows the schematic of the passive DMFC. The main components of the passive DMFC are anode & cathode end covers, membrane, current collectors and Teflon gaskets. The details of these components are discussed in the following sections.

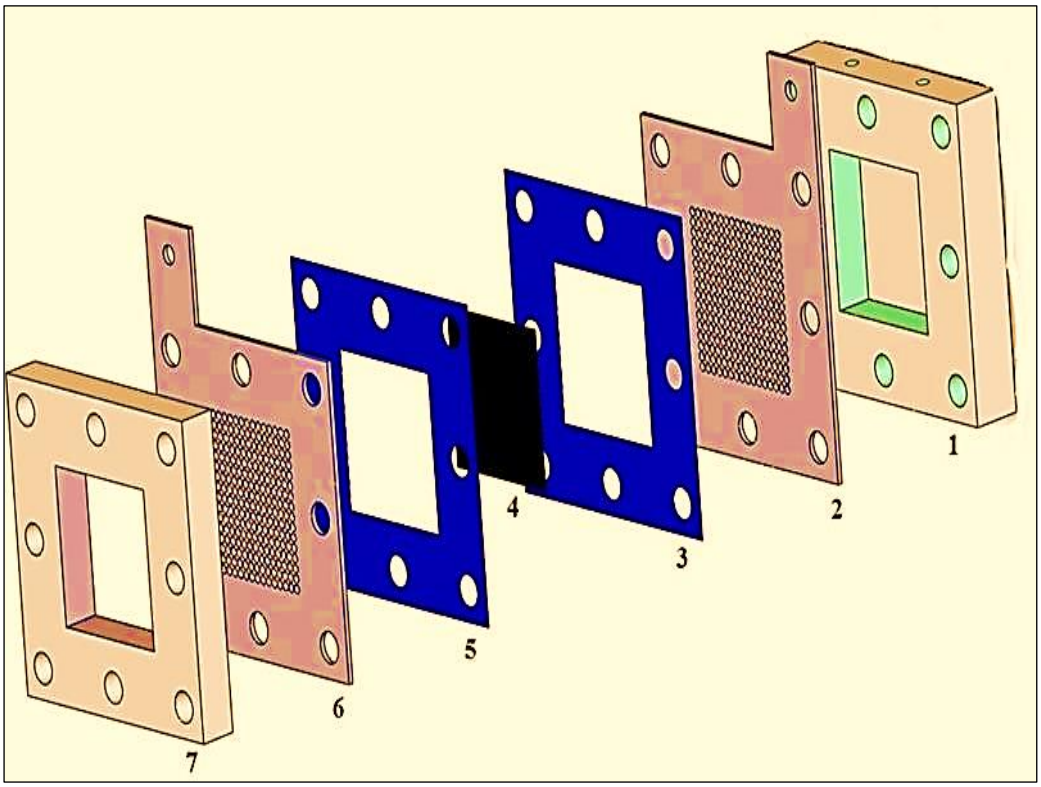

1. Anode end cover (methanol reservoir)
2. Anode current collector
3. PTFE gasket for anode side
4. MEA
5. PTFE gasket for cathode side
6. Cathode current collector
7. Cathode end plate

Figure 1.3 Schematic of the passive DMFC

1.6.1 Membrane (PEM)

The ion-conducting membrane is the heart of the cell. Through this cell membrane, the liberated ions are transported from the anode to cathode. The desirable properties of the membrane are chemical & mechanical stability in methanol environment and high proton conductivity between the electrodes. As hydrated membrane can transport the ions efficiently, it is crucial to keep the membrane always in humidified condition. For DMFC applications, membranes having per-fluoro-sulfonic-acid functional group linked with tetra-fluoro-ethylene-based polymers are used.

1.6.2 Catalyst Layer (CL)

In PDMFC, opposite faces of the membrane consist of two different catalyst layers. Catalyst layer thickness requires greater attention in the performance of oxidation and reduction reactions. Thin layers are designed for better diffusion and thicker ones for high catalyst loading. Layer optimization balances between catalyst activity, mass transportation and mechanical strength.Mostly on the anode side, Platinum (Pt) and Ruthenium (Ru) are preferred as the catalyst because of its high reactivity and stability. Whereas, on cathode side Pt is preferred as it is free from carbon monoxide. In general, these catalyst materials in particle form are impregnated on carbon to provide large surface area. A catalyst layer on Carbon with Platinum, Das et al, [7] is given in figure 1.4.

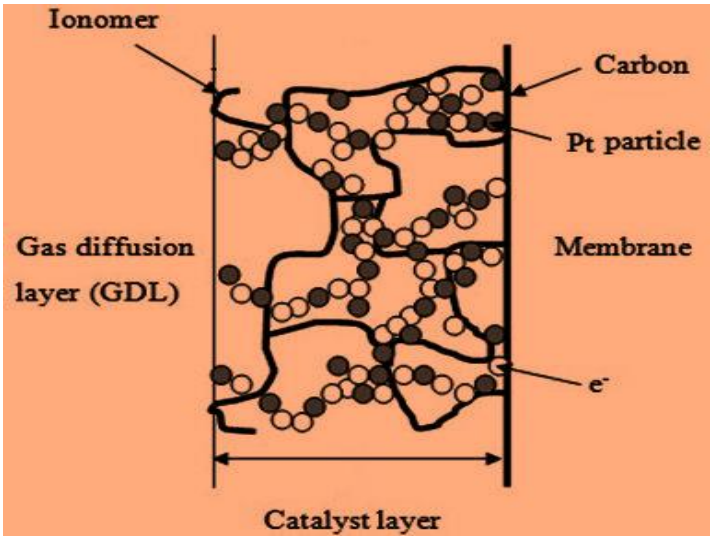

Figure 1.4 Catalyst layer

1.6.3 Diffusion Layer (DL)

Diffusion layers are attached to catalyst layers on anode and cathode ends. A substrate, i.e., a hydrophobic carbon-fiber cloth or paper is used as DL. A micro-porous hydrophobic layer, i.e., Poly Tetra-Fluoro Ethylene (PTFE) is applied to the substrate on catalyst side. The microscopic images of carbon fiber cloth and paper are shown in figure 1.5, Lim et al, [8]. The key functions of the DL are: it works as a passageway for transport of the reactants and evacuation of products, function as a heat conductor and conducts electrons from CL to CC. The amalgamated membrane with CL and DL is called as membrane electrode assembly (MEA).

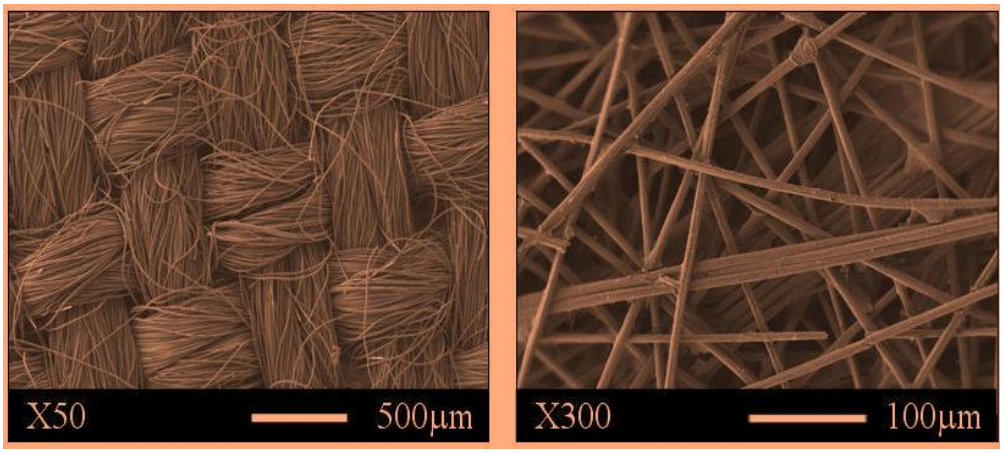

Figure 1.5 DL material: carbon cloth (left) and carbon paper (right)

1.6.4 Current collectors (CC) and gaskets

In the passive DMFC, the purpose of anode & cathode current collectors can be distinguished based on their functioning; however, there are a few collective features such as even distribution of reactants, providing cell assembly support compactness, discarding of products of chemical reaction, maintaining end-to-end electrical continuity of individual cells to facilitate stacking of several cells. Over the anodic end, CC permits transporting of diluted methanol solution and ease of scavenging of carbon dioxide through its openings. Also, it gathers electric current from membrane electrode assembly and conducts it through an external circuit.

Whereas at the cathode side, it allows oxygen from the atmosphere. Also enables conveyance of reaction products such as water and heat of reaction. Further it also acts as a path to close the external circuit through which electrons flow from anode end of the cell.

Gaskets are provided in between the current collector and the MEA. They maintain proper sealing between the current collectors and the MEA. The thickness of the gaskets also influences the fuel cell performance. Lesser the thickness of gasket, lower the impedance of the fuel cell.

1.6.5 End Plates

In the PDMFC, cathode and anode end plates are made up of Poly-methyl-meth-acrylate (PMMA). As the heat of reaction is less during the cell operation, these acrylic plates are capable to withstand the amount of heat generated. Further, the transparent acrylic plates allow for visual observation of CO_2 bubbles that are formed at anode. In the PDMFC, the anode end-cover functions as methanol reservoir. It has two openings at the top. Out of these two, one serves for filling of fuel and the other for venting of CO_2 gas. Cathode side acrylate plate has a square shaped window opening, with the area same as the active area of the cell for oxygen intake. Both these end covers have holes drilled, to facilitate assembling of the cell components with fasteners.

1.7 Fuel Cell Performance

The fuel cell performance can be compared with an ideal or thermodynamically inferred voltage against actual voltage generated. The generated voltage is always lower due to the losses which are inevitable. The major losses are predominantly from active region, ohmic region and mass transfer regions of the cell, leading to activation losses, ohmic losses and concentration losses respectively, Barbir, [3]. The causes for these losses are mentioned in table 1.2.

Table 1.2 Fuel cell losses

Type of losses	Cause
Activation losses	Attributable to electrochemical reactions.
Ohmic losses	Attributable to electrical, ionic, and electrolytic transmission.
Concentration losses	Attributable to mass transformation of reactants and products.

The schematic fuel cell characteristic curve plotted with Voltage on Y-axis and Current Density (current per unit area) on X-axis (also known as *polarisation curve*) is shown in figure 1.6.

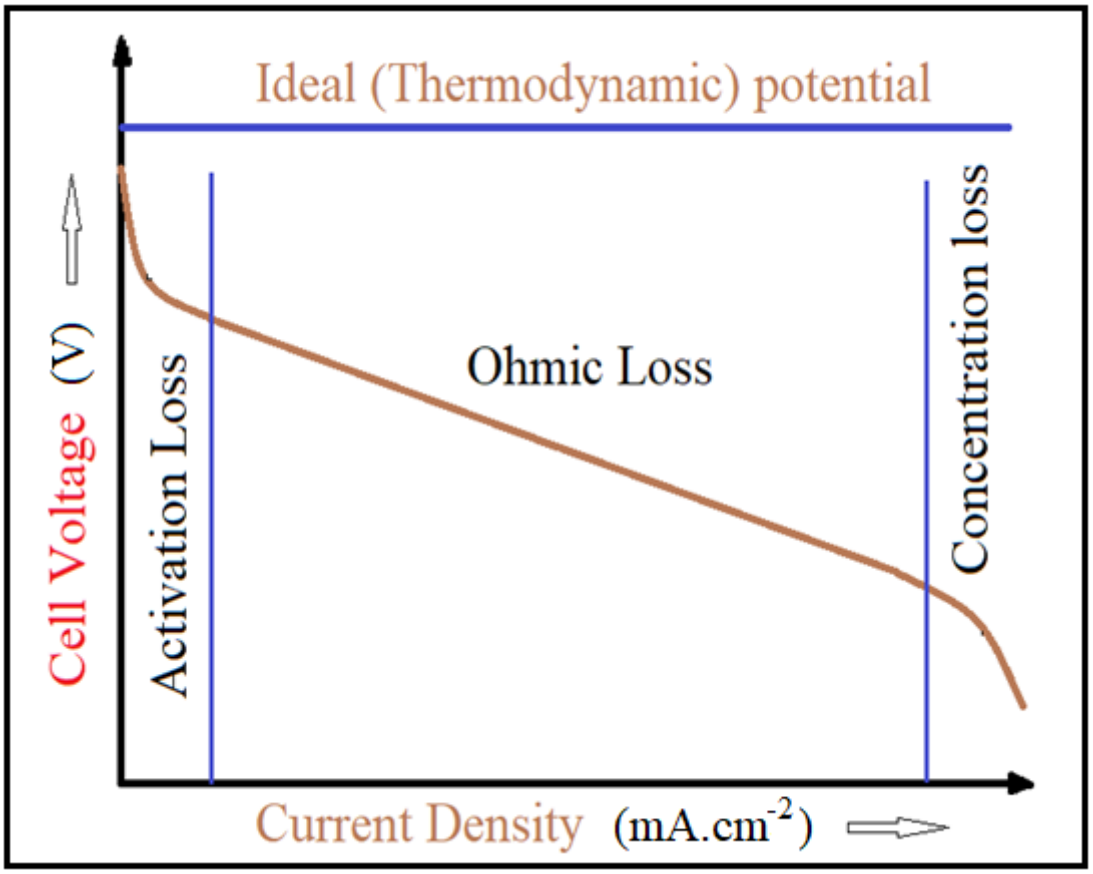

Figure1.6 Voltage against Current density curve representing various regions of losses.

After considering the losses, the real voltage generated from the cell may be estimated from the equation 1.4.

$$V_{real} = E - E_{act} - E_{ohmic} - E_{conc} \qquad (1.4)$$

Here,

V_{real} = Real voltage output of cell (V)

E = Thermodynamic cell voltage (V)

E_{act} = Activation loss due to reaction kinetics (V)

E_{ohmic} = Ohmic loss due to electric and ohmic resistance (V)

E_{conc} = Loss due to mass transportation (V)

These losses affect Fuel cell (FC) performance. The output voltage drop at lower current density of the polarization curve is mostly affected by the activation losses. In mid region of the curve, the voltage drop is mostly influenced by the ohmic losses. Finally, the mass transport losses are highly effective in the higher current density region.

1.7.1 Fuel cell power density

The output power (P) generated by cell is given by the product of voltage generated (V) and the corresponding current (I).

$$P = V * I \qquad (1.5)$$

The power density (power per unit area) curve follows parabolic trend. As the current density increases, the fuel cell power density raises from zero to a maximum value and then decreases. Hence these cells are designed, made and developed to function at maximum power density region. When the operating conditions of the cell are below the maximum or peak power density point, then the power density falls but voltage efficiency improves. Whereas, when the operating conditions are above the peak power density, both the power density and voltage efficiency fall. Schematic power density with polarisation curve (i-v curve) plotted in the figure 1.7.

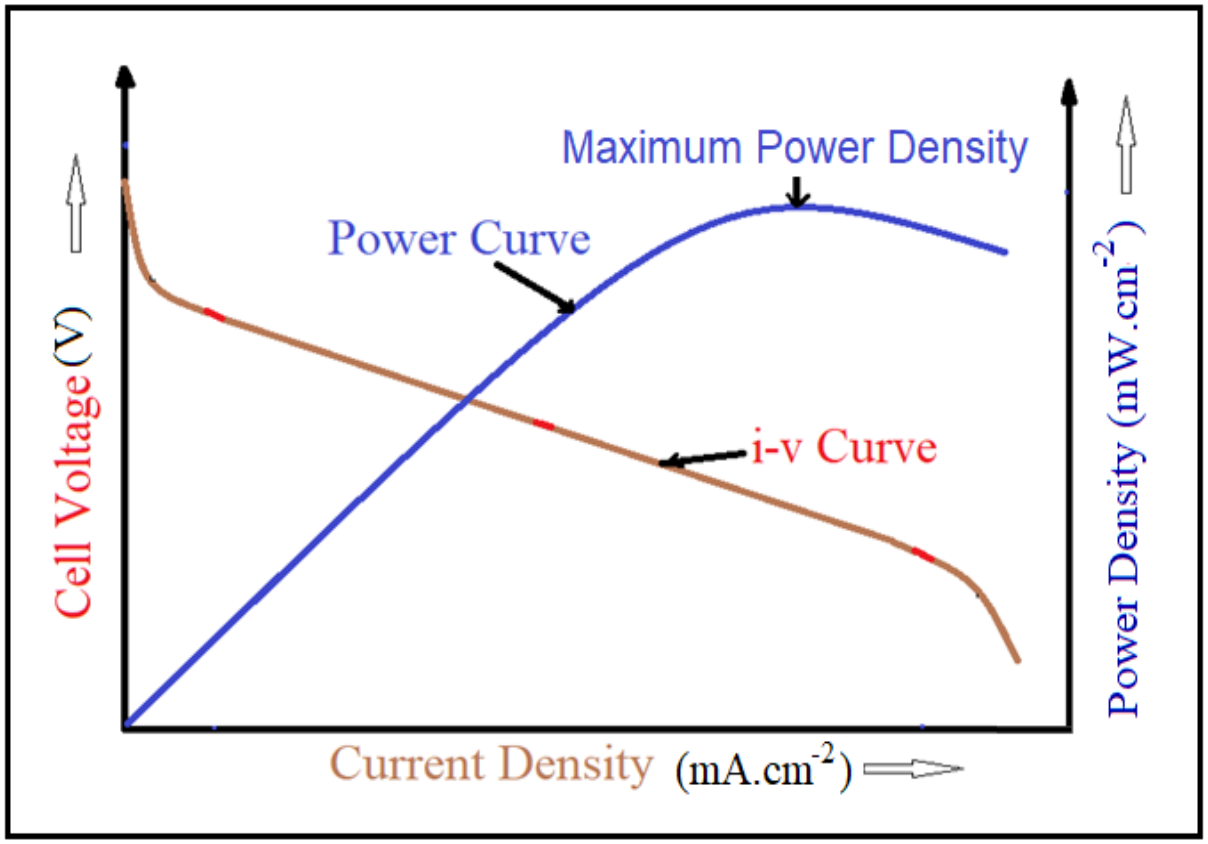

Figure 1.7 Schematic power density and polarisation curves

1.8 Organization of the thesis

This thesis comprises of five chapters. Chapter 1 outlines a short introduction of fuel cells, various types of fuel cells, briefing on principle of operation of passive DMFC, its construction, performance, and organization of the thesis.

Chapter 2 presents the literature review on the PDMFC, focusing on current collectors and their openings, MEA shapes and cell component degradations. The gaps observed from the literature and the thesis objectives are also presented in this chapter.

Chapter 3 explains experimental methodology on passive DMFC. The description of the experimental setup and components of the passive DMFC are discussed in this chapter.

Chapter 4 infers the experimental investigations of the research objectives including results and discussions.

In chapter 5, the conclusions drawn out of this research, novelty of research and recommendations for future scope of research are given.

Details of References, Publications, Conferences attended and Appendix are provided at the end.

Chapter 2

Literature Review

The passive direct methanol fuel cell was invented and demonstrated in the 1990s by NASA and the jet propulsion laboratory, Narayanan, [9]. The performance and power produced by the PDMFC is mostly influenced by the methanol solution concentration, operating temperature, size and shape of the MEA, material of the current collectors, and openings on the current collectors. Significant research on these parameters has been carried out by experimentation to understand and predict the performance of PDMFC. Hence literature review has been carried out on current collector materials, openings, MEA shapes and their sizes, and service degradation of cell components.

2.1 Studies on PDMFC Current Collector Materials

Braz et al, [10] had considered various materials of current collectors for optimization of passive direct methanol fuel cell performance. For developing the cell applications commercially, it is desirable to have optimum balance among attributes such as durability, cost, and competence. Materials of these collectors alone contributed to 75% of the cell weight and hence various materials having different specific gravity are tested to optimize their weight and cost, Boni et al, [11]. Fuel cell effectiveness, durability, and performance are carried out using polarisation characteristics. The importance of this study on fuel cells is quantification and innovative representation of performance characteristics. In the experiment, Titanium and Stainless-Steel materials as anode and cathode are used. The highest power density developed with this setup is 5.23 $mW.cm^{-2}$ at 7M methanol solution concentration. In the durability experiment, the test results showed a lifespan of around 200 h with a drop in performance of cells by 41% from the initial measurement.

Mallick et al, [12] had performed a thorough assessment of passive direct methanol fuel cell current collectors. In their experiments, higher open ratio current collectors were used for ease of transportation of methanol solution and expelling CO_2 from the anode. With this, the overall output of the fuel cell got enhanced. Even though the opening sizes of the bipolar plates are the most important characteristic that directly influence the liquid feed fuel cells, Boni et al, [13], some of the research about opening sizes of the bipolar plates showed diverse results. A few researchers have kept small opening sizes on the anodic end and large opening sizes at the

cathodic end and vice versa. Very little work has been carried out regarding the reduction of weight of the passive DMFC current collectors. The material and fabrication with varying opening ratios of the current collectors mainly contribute to the passive DMFC weight and it also affects the gravimetric power density of the fuel cell.

Yuan et al, [14] investigate the influence of opening sizes of the anodic end bipolar plates. In this study, they fabricated two types of anode bipolar plates with circular perforations having opening ratios of 28.3% and 38.5%. This study has identified that a smaller opening ratio is ideal for reducing the methanol cross-over from anodic end to cathodic end, while a larger opening ratio is favored for hassle-free transport of methanol solution and scavenging of carbon dioxide from the anodic end which improved the cell performance. Further, it is identified that, on higher opening sizes of anodic end bipolar plates, the effective contact surface with anode diffusion layer got decreased and contact resistance of interfacial surfaces got increased.

Esquivel et al, [15] fabricated anodic end bipolar plates having three different opening ratios of 40%, 23% & 10% for investigating the influence over the performance of DMFC. In this study, with 2 M methanol solutions, the peak power densities 11.7×10^{-3} Wcm^{-2}, 9.0×10^{-3} Wcm^{-2}& 8.5×10^{-3} Wcm^{-2} were obtained with anodic end opening ratios of 40%, 23% and 10% respectively. This decrease in the power density is due to the reduction in area of exposure of electrode to methanol solution followed by low mass transportation. However, at higher concentrations such as at 4 M methanol concentrations, at 40% opening ratio, peak power density got dropped down to 8.0×10^{-3} Wcm^{-2} due to more methanol cross over, but the peak power density performance of other current collectors with 23% and 10 % improved to 10×10^{-3} Wcm^{-2}.

Gholami et al, [16] have examined the influence of non-uniform parallel channels on passive direct methanol fuel cell performance. In their investigation, the effect of current collectors on the performance of passive DMFC and expelling of carbon dioxide was taken up. A simple DMFC using two different setups of bipolar plates on anodic and cathodic sides was constructed. In the 1st setup, non-uniform parallel flow channel was used at anodic end and a perforated flow field was used at cathodic end. In 2nd set of construction, uniform parallel flow channels with equal opening ratio had been used at both anodic and cathodic ends. These experiments have revealed that with the collectors having non-uniform parallel flow

channelling paths were most efficient in expelling carbon dioxide than other types of parallel flow channelling paths.

Yuan et al [17] had published “corrosion behaviour of Porous Metal Fiber-Sintered Felt in both Simulated and Practical Environments of DMFC”. The usage of metals for manufacturing current collectors in PEMFC is recognized as an efficient alternative to substitute graphite for maintaining lightweight, less price, and ease of fabrication. However, several technical issues are still to be addressed over the proposed metals that are being used in large fuel cell systems, having setbacks due to complex properties connected with acidic fuels, oxidants, humidity & heat generated. If the materials being used are corroded, the liberated ions may degrade the fuel cell performance by poisoning the catalyst and thereby contaminating the membrane.

Tabbi et al [18] have identified that recent automobile trends are encouraging the usage of metallic current-conducting bipolar plates with smaller thickness resulting reduction in the weight of the fuel cell. These conductors are chosen with better conductivity having superior electrical and thermal characteristics. Stainless steel current collectors are proven to be relatively inexpensive. However, the surface protective passive layer of oxides of chromium that lead to higher electric resistance are still to be addressed for their use in PDMFC.

Seema et al, [19] have reviewed the use of advanced materials in direct methanol fuel cells. This review has made prominence on various aspects such as durability, effective performance, compatibility, stability and cost. Fuel Cell sub-assemblies and characteristics of the materials used in their components are reported in this review. This paper also investigated passive DMFC components and their materials of construction, which might make the cell more compact and make it a possible power source of the future.

Mallick et al, [20] have performed an important analysis on bipolar plates used in PDMFC that accent the significant features like materials of construction, size, shape, and profile of the current collectors. Several bipolar plates have been chosen and reviewed systematically to study PDMFC performance. But very small investigation work is performed to reduce the heaviness of the plates which contribute significantly to the total weight of the cell. It also influences the gravimetric density of the cell.

Boni et al, [21] have indicated that among the components of sub-assemblies, current collector of the PDMFC is a crucial part and its performance is influenced by its material of construction, innovative design, and size proportions. The weight of PDMFC current collectors alone contributes about 2/3rd to 4/5th of the entire weight of the cell system. Hence its gravitational power density and reliability, Escudero et al, [22] are considerably influenced by the selected current collector material and its fabrication characteristics, Raghavaiah et al, [23]. The required characteristics of materials of the current collectors in the passive direct methanol fuel cell were indicated by several researchers. These desirable characteristics are higher electric conductivity (or) low electric resistivity over the effective working region of PDMFC, Yang et al, [24], better thermal conductivity for optimizing & for maintaining thermal steadiness during the operation of the cell, Dohle [25], essential mechanical characteristics such as flexural rigidity & working strength, Huang et al, [26], easy fabrication and machinability, Abraham et al, [27], high corrosion resistance over wide ranges of effective temperatures and various solution concentrations in a methanol environment with impermeable properties, Song et al, [28], free from corrosion and surface oxides, Das et al, [29], more durability and longer life, Cha et al, [30], less weight or low density, Kuan et al, [31], easily available at a cheaper cost, Sgroi et al, [32], minimum contact resistance with the diffusion layers, Xu et al, [33], Braz et al, [34], uniform distribution and transport area of reactants, Shrivastava et al, [35]. Further, the important contributing factors of current collectors that directly influence the cell performance are ohmic losses, Braz et al, [36], corrosion resistance [37], and contact resistance, Meenakshi et al, [38]. Power densities of the combinations of the metallic current collectors found in literature are tabulated in table 2.1.

Table 2.1 Power densities of the same combinations of the metallic current collectors

Anode CC	Cathode CC	Membrane	Anode catalyst ($mgcm^{-2}$)	Cathode Catalyst ($mgcm^{-2}$)	Methanol Concentra-tion (M)	Power Density, ($mWcm^{-2}$)	Reference
SS 316L	SS 316L	Nafion 117	3	1.3	2	3.14	[6]
Titanium	Titanium	Nafion 117	3	1.3	2	1.3	[6]
SS 316L	SS 316L	Nafion 117	3	1.3	5	3.0	[39]
SS 316L	SS 316L	Nafion 117	3	1.3	2	3.14	[40]
SS 316L	SS 316L	Nafion 117	4	4	2	3.6	[41]
SS 316L	SS 316L	Nafion 117	4	2	3	3.3	[42]
SS 316L	SS 316L	Nafion 117	4	2	4	4.4	[43]
SS 316L	SS 316L	Nafion 117	5	8	5	8.6	[44]

2.2 Studies on PDMFC Current Collector Openings

Ranjan et al, [20] had carried out a critical review on the current collectors of passive direct methanol fuel cells. In their experiment, a higher opening ratio current collector was used for ease of transportation of methanol solution and expelling of CO_2 from the anode side. With this, the overall output of the fuel cell is enhanced. Even though the opening sizes of the bipolar plates are the most important characteristic that directly influences the liquid feed fuel cells, some research about opening sizes of the bipolar plates, showed diverse results. A few researchers have experimented with small opening sizes on the anodic end and large opening sizes at the cathodic end while some researchers have experimented with large opening sizes at the anodic end and small opening sizes at the cathodic end. Very little work has been carried out regarding the reduction of weight of the passive DMFC current collectors. The material and fabrication with varying opening ratios of the current collectors is the key contribution to the weight of the passive DMFC and affects the gravimetric power density of the fuel cell. In their publication, it is indicated that the experimental performance of SS-316L circular perforated current collectors of 3 mm thickness having 121 openings with Nafion-115 membrane, produced 5.771 $mW.cm^{-2}$ power density.

Braz et al, [6] has indicated that current collectors of passive direct methanol fuel cells play as a key component and the performance of the fuel cell depends on its material of construction, dimensions, novel design with shape factors. The weight of the current collectors contributes almost 3/4 of the total weight of the cell. Hence the gravitational power density is significantly affected by the selection of current collector materials and their design aspects. The required characteristics of materials of the current collectors in PDMFC are good electrical conductivity or very low electrical resistivity at the operating zone of the Direct Liquid Feed Methanol cell, high thermal conductivity to optimize and maintain the thermal stability of cells during operation, desirable mechanical properties like high tensile strength and flexural rigidity of materials, better fabrication and machinability of materials, corrosion resistance in methanol environment at various concentrations and wide range of operating temperatures, longer durability and life, low density of materials, easily availability at cheaper cost, less contact resistance with the diffusion layers, uniform distribution and transportation area for reactants.

Yuan et al, [17] investigated the influence of opening sizes of the anodic end bipolar plates. In this study, they fabricated two types of anode bipolar plates with round perforations

having opening ratios of 28.3% and 38.5%. This study identified that a smaller opening ratio is ideal for reducing the methanol cross-over from anodic end to cathodic end, while a larger opening ratio is favored for hassle-free transport of methanol solution and scavenging of carbon dioxide from the anodic end which improved the cell performance. Further, it is identified that, on higher opening sizes of anodic end bipolar plates, it decreases the effective mating surface with anode diffusion layer. This also enhances contact resistance of interfacial surfaces. The authors had indicated that the experimental performance of SS-316L circular perforated current collectors of 1 mm thickness having 144 openings on the anode side and rectangular channel having 7 openings of 3mm width x 27mm length on cathode side with GEFC-10N membrane, produces 5.6 $mW.cm^{-2}$ power density.

Esquivel et al, [15] have performed experiments with anode CCs with various opening sizes. At higher methanol concentrations, the cell performance got reduced. This indicates higher opening ratios on anode CC led to more methanol cross-over from anode to cathode. The reduction in fuel cell performance can be attributed to the blockage of cathode sites caused by the cross-over of methanol. For a fuel cell configuration of a 40% opening ratio on the anode side and a 10% open ratio on the cathode side produces the maximum power density value of 6 $mW.cm^{-2}$ at 4 M methanol concentration.

Gholami et al, [45] have examined the influence of non-uniform parallel channels on passive direct methanol fuel cell performance. In their investigation, the effect of current collectors on the performance of passive DMFC and expelling of carbon dioxide was taken up. A simple DMFC using two different setups of bipolar plates on anodic and cathodic sides were constructed. In 1^{st} construction, non-uniform parallel flow channels were used in the anodic end and a perforated flow field was used in the cathodic end. In 2^{nd} construction, uniform parallel flow channels with equal open ratio had been used in both anodic and cathodic ends. It was revealed through these experiments that the collectors having non-uniform flow parallel channelling paths were most efficient in expelling carbon dioxide than other types of parallel flow channelling paths.

Argyropoulos et al, [46] have also studied gas evolution and its effect on performance of direct methanol fuel cells. The gas evolution and flow patterns observed were significantly different in small and large cell designs. In small cells, the gas flow was inhibited by the manifold design which cannot accommodate large proportions of gas without experiencing

operational problems at low liquid flow rates. In their study, it was revealed that a properly designed flow system with comparatively higher opening ratios could be more advantageous in terms of gas management. A range of parameters were investigated for large cells and there was little evidence for the formation of gas slugs even at high current densities; very small, rapid moving gas bubbles were produced.

Shing et al, [47] described that the current collectors of direct methanol fuel cell are important components of the cell and play a key role in the performance of the cell. Further, the performance also depends on the material of construction, dimensions, novel design with shape factors of the current collectors. The weight of the current collectors contributes to about 75% to 85% of the entire weight of the fuel cell system. Hence gravitational power density is significantly affected by the selection of current collector materials and their design aspects. The required characteristics of materials of the current collectors in PDMFC are low electrical resistivity at the operating zones of the cell, high thermal conductivity to optimize and maintain the thermal stability of cells during operation, desirable mechanical properties such as high tensile strength and flexural rigidity, easy fabrication and machinability, high corrosion resistance in methanol environment at various concentrations and a wide range of operating temperatures with impermeable properties, more durability in the system, lower density, material availability at a low price, Sgroi et al, [48], minimum contact resistance with the diffusion layers, uniform distribution and transport to the area of reactants, Argyropoulos et al, [49].

2.3 Studies on DMFC anode/cathode dissimilar materials

Braz et al [6] has studied the optimization process of passive direct methanol fuel cells with various current collector materials. It is indicated that to ascertain the commercial usage of DMFC, an optimum balance between its price, competence, and durability should be achieved. Current collectors are accountable for about 70-80% of the system weight and different current collector materials were tested to balance price and weight reduction. The performance of the fuel cell and its duration were identified using polarization measurements. A notable novelty of this study is the use of innovative identification and quantification of performance. A peak power density of 5.23 $mW.cm^{-2}$ was achieved using Titanium as anode current collector and Stainless Steel as cathode current collector at a methanol concentration of 7M. The durability tests showed a lifetime of about 200 hours and a reduction in efficiency of the fuel cell by 41% from the original value.

Tabbi et al, [18] in their investigation, identified that the automobile industry is encouraging the use of metals as current collector plates as metals have small thickness and therefore less weight as well as good conductivity, both thermal and electrical. Using stainless steel would reduce the cost, but non–coated SS, the material used in this investigation still have challenges with respect to surface–insulating layer of chromium oxide (Cr_2O_3).

Seema et al, [19] have done a comprehensive review on recent material development of passive direct methanol fuel cells, with an emphasis on performance, cost, durability, and stability aspects. Each component with its material development along with basic desirable characteristics is reported in this paper. This paper has also reviewed all possible materials of passive DMFC components, which might make the passive DMFC compact and feasible energy source in the future.

Mallick et al, [20] in their study on critical review of current collectors for passive direct methanol fuel cells has emphasized on the important aspects such as the profile of the current collectors including materials of construction. Several current collectors of passive DMFC have been selected and reviewed thoroughly. However, very little research works have been found concerning to decrease in the weight of the current collectors as the current collector majorly contribute to the total weight of passive DMFC and affects the gravimetric energy density of the fuel cell. Power densities of a few combinations of metallic current collectors from the literature are tabulated in table 2.2.

Table 2.2 Power densities with different combinations of metallic current collectors

Anode CC	**Cathode CC**	**Membr-ane**	**Anode catalyst ($mg.cm^{-2}$)**	**Cathode Catalyst ($mg.cm^{-2}$)**	**Methanol Concent-ration (M)**	**Power Density, ($mWcm^{-2}$)**	**Reference**
Au on SS	SS 316L	Nafion 117	3	1.3	3	3.41	[6]
Titanium	SS 316L	Nafion 117	3	1.3	3	3.54	[6]
Titanium	Au on SS	Nafion 117	3	1.3	3	2.3	[6]
Titanium	SS 316L	Nafion 117	3	1.3	7	5.23	[6]

2.4 Studies on MEA dynamic shapes

Yong et al, [50] investigated the influence of structural characteristics on the performance of a passive air-breathing direct methanol fuel cell is studied. The hot-pressed diffusion layer can reduce the permeation of methanol, but the non-bonded one can increase reaction outputs with special congregation techniques of the dispersion sheet.

Govindarasu et al, [51] in their publication on "Recent evolutions in modeling of direct methanol fuel cell", stated that direct methanol fuel cells prove to be one of the better potential substitutes for non-renewable energy sources. He also opined that, with legitimate modelling and simulation, the performance of the cell can be improved to a great extant. The significance and the requirement for the modelling of a DMFC were discussed in detail. The modelling of the key segments, for example, the dispersion layer, MEA, stream dissemination and impetus thickness which add to the performance of the fuel cell were discussed. As the cell performance is influenced to a large extent by the characteristics of MEA, in his experiment, Nafion-117 polymer electrolyte is used. The anode side is doped with ~4 $mg.cm^{-2}$ Platinum-Ruthenium (in equal proportions) catalyst on Carbon cloth and the cathode side is doped with 2 $mg.cm^{-2}$ Platinum catalyst on Carbon cloth.

Chang et al, [52] performed "Experimental Investigation of a Direct Methanol Fuel Cell with Hilbert Fractal Current Collectors" and fractal current collectors were fabricated with current collectors of various free opening perimeters and opening ratios. In their investigation, the performance of PDMFC was observed as a function of the opening perimeter and free opening ratio of conducting bipolar plates. However, these current collectors could not show better performance.

In the analysis of membranes for direct methanol fuel cell applications, Vasco et al, [53] emphasized on characterization, experimentation, and modelling. A significant investigation was carried out on essential characteristics of the PDMFC system that focuses primarily on the membrane. The work focused on the PEM performance with an outline of research advancement.

Hashemi et al, [54] studied the effect of the active area, shape and methanol consumption on performance of cell. They have observed that the cell performance increased with increase in the size of the active area. Over the large dynamic zones, as current density is less when

compared to the smaller dynamic zones, fuel is absorbed gradually. Hence, the local fuel concentration over the polymer membrane is more, resulting in further fuel crossover. The permeated methanol and oxygen at the cathode lead to higher temperatures due to exothermic reaction, resulting in better electrochemical kinetics of oxidation and reduction reactions. The shape factor results showed that square shape active area performance is found to be better due to less distance between the edge of the active area and to bolting system resulting in adequate compressive strength over the dynamic zone causing less contact resistance and leading to improved performance. This infers that a higher active area alone is not the solution for better performance of the cell. Hence optimization of area, size, and shape of the dynamic zone are to be considered while designing the cell.

Govindarasu et al, [55] has mentioned that direct methanol fuel cell emerges as a reliable alternative for the substitution of petroleum derivative-based systems. A fuel cell with an effective MEA region of 4500 $mm^2$and a Pt-Ru/C impetus amalgamation at the anodic side is taken for investigation and further to conducting tests. Using this cell, the experiment is performed at various cell operating temperatures. However, further experiments are not carried out at room temperature conditions to optimize the better shape and sizes of dynamic zones of MEA.

2.5 Studies on Service Oriented Degradations using Non-Destructive Testing

Claycomb et al, [56] reported on electric and magnetic Non-Destructive Testing of Proton Exchange Membrane (PEM) fuel cells to locate flaws in the PEM from measured magnetic field maps. They explored several NDT techniques employing highly sensitive HTS and LTS SQUID and fluxgate magnetometers. The Magnetic fields produced by currents in the cell are investigated in spatial, frequency and time domains under several operational conditions. Frequency domain magnetic and electric signals are related to extreme operating conditions including membrane adversity. The study aimed at the membrane point of view, but not on the total components of the cell.

Frikkie [57] has presented optimization of Hydrogen Fuel Cells through NDT using Neutron Radiography. In this presentation, efficient water management for optimization of energy production from fuel cells is demonstrated by using radiation as probe.

Axenics [58] indicated that Non-Destructive examination is an important part of the component production process. The performance of the components of the three-pass heat exchanger of hydrogen fuel cells including material corrosion, welding fissures, bonding distortion, surface flaws, etc., are evaluated. Vacuum and Helium testing processes were used to ensure the components are free from leaks.

Zhou et al, [59], in the review of optimization design, indicated that NDT is used to identify direct and/or indirect means to find the size and to locate surface and subsurface discontinuities in the materials and components. The materials and components examined using NDT are interpreted for acceptance/rejection/repair and assure the safety and reliability of components, Raghavaiah et al, [60]. Various Non-Destructive Testing methods such as Visual Testing, Liquid Penetrant Testing, Ultrasonic Testing for Thickness measurement, hardness measurement, metallographic examination, etc., on Passive Direct Methanol Fuel Cell components are chosen based on the mode of failure and are considered in this analysis to ascertain their serviceability, durability, Siti et al, [61], expected life, and healthiness. The envisaged and anticipated modes of failure in PDMFC are uniform corrosion, Deng et al, [62], hydrogen attack, Kim et al, [63], compressive loading-related crack growth, PavolDlhý et al, [64], stress corrosion cracking, Prabhuraj et al, [65], and compression set, Bayerl [66].

From the ASME B&PV code section V article 9, Harold [67], Visual Testing is to be performed as a primitive examination on PDMFC components to identify surface imperfections, corrosion, de-colorization, physical distortion, thinning, and physical discontinuities if any present under daylight or using illuminating source, Dwivedi et al, [68]. The required illumination is met with daylight and inspection is carried out as standard visual examination procedure for identifying the discontinuities.

As per ASME B&PV code section V article 6, Zillmann [69], Penetrant Testing is capable of detecting discontinuities that are open to the surface of the non-porous component under test, Dalalana et al, [70]. The penetrant method is very reliable in the detection of pitting and cracks which occur during the service life of a material. The complete surface of the component can be tested relatively quickly. PT cannot detect subsurface discontinuities, defects filled with oxides, and defects covered by paint films. The cleaned components of the PDMFC being examined are applied with a chemical solution (Penetrant) that contains a visible dye. Excess penetrant is then wiped off from the surface of the component except that entered in

surface-breaking openings. A developer is then applied uniformly to draw the penetrant out of the discontinuities, thus allowing imperfections to be readily seen providing contrast between penetrant and surface being checked. The total procedure consists of surface preparation, penetrant application, holding the component for penetrant dwell, excess penetrant removal, developer application, indication development (if present), inspection, and cleaning of the surface. The dwell time allowed after the penetrant application is 10 minutes. The evaluation is started immediately after the developer's application with an inspection time of 15 minutes for identification of indications, if present any on the surface. The required illumination is met with daylight and inspection is carried out as a standard liquid penetrant examination procedure as per ASME B&PV code section V article 6.

ISO standard no: 16809-2017, Tesfaye et al, [71] stipulates the procedure for ultrasonic thickness measurement based on the time of flight of ultrasonic pulsations on metallic & non-metallic materials by direct contact method. The thickness of the DMFC components has been carried out using Ultrasonic Testing (UT) which uses high-frequency sound energy to conduct examinations and to make measurements. In ultrasonic testing, high-frequency sound waves are transmitted into the component using the pulse-echo technique, whereby sound is introduced into the test object and reflections (echoes) from the geometrical back surface are returned to a receiver. The time of flight of sound waves is a measure of the thickness of the given material, Sharma et al, [72].

ASTM D2240, Qi et al, [73] standard is used for measuring hardness for soft materials and polymers. The hardness of rubber and plastics is generally tested in Shore scales. Shore hardness uses a spring-loaded needle-like indenter to measure the resistance of the material to penetration. *Shore A* scale is preferred for checking rubbers and soft polymers. The harder polymer materials are mostly tested with the *Shore D* scale. Durometer is a testing instrument for measuring Shore hardness. Durometer employs a spring with an indenter and the hardness is measured by the depth of penetration. The softer material corresponds to the least Shore hardness and the harder material corresponds to highest shore hardness, Zhao et al, [74].

ASTM E407 standard [75] is used for metallic components exposed to the methanol environment that undergo gradual degradation by the way of changes occurring in microstructure during service, which will indicate degradation in the mechanical properties of materials. For metallic materials, the component surface is metallographically prepared by

using grinding, polishing, and electro-polishing units. The microstructure is examined on the prepared spot using a microscope which will reveal the microstructure. These values are compared with the values of virgin materials of the same composition and this data is used as input parameters for component life assessment, Tcr et al, [76]. Scanning Electron Microscope (SEM) [77], Matsuyama et al, [78] pictures reveal the sample's topography with elemental composition. It is capable to capture 3D black-and-white images of samples. The sample dimensions are limited by the chamber size of the electron microscope. Transmission Electron Microscope (TEM) [79], Mast et al, [80] is a kind of electron microscope that uses wide-spreading rays of electrons to produce an internal structure image of the sample. An electron beam spread through the sample produces an image that contains crystal structure, composition, and morphology, Nicole [81].

Materials and their properties are essentially considered while selecting the passive direct methanol fuel cell components for their suitability in the methanol environment, Tsen [82], with cell reaction temperatures, reaction chemical products, components thermal stability, and durability, Awang et al, [83]. Some of the important material properties that need to be considered while selecting the cell components are tabulated in table 2.3.

Table 2.3 Material Properties of Fuel Cell Components

Material of the PDMFC component	**Properties of materials**	**Reference**
Acrylic (for anode and cathode end covers)	• Excellent resistance to UV (ultraviolet) light • Excellent resistance to weathering and methanol. • Good dimensional stability • Good rigidity • Moderate strength • Scratch resistant	[84][85]
PTFE (for gaskets)	• Electrical insulator • Excellent chemical resistance to methanol • High thermal stability and flame resistance • No embrittlement or aging • Non-stick • Non-wetting • Sealability	[86][87]

Stainless Steel (for current collectors)	• Corrosion Resistance • Ease of Fabrication • Heat Resistance • Machinability	[88][89]
Nickel (for the current collectors)	• Corrosion Resistance • Ductile metal. • Good conductor of heat and electricity • Malleable	[90][91]
Brass (for the current collectors)	• Corrosion-resistance in water • Easily machinable • Good conductor of heat and electricity • Malleable	[92]
Teflon coated woven cloth(for gaskets)	• Temperature resistance. • Tensile strength. • Outstanding electrical properties. • Superior chemical resistance. • Sealability	[93][94]
Nafion-117 (for membranes)	• High operating temperature, up to 190 °C • Highly conductive to ions • Highly permeable • Resists chemical attacks. • Less suitable for dry gases	[95][96] [97][98] [99]
VITON (for gaskets)	• Abrasion Resistance. • Resistance to aging with weather/ sunlight. • Solvent Resistance. • Tear Resistance.	[100][101]
MS (for fasteners)	• High impact strength. • High tensile strength.	[102]
Bakelite (for wrapping on fasteners)	• Mouldings of smooth surface. • Resistant to electricity. • Resistant to heat. • Resistant to scratches. • Retains shape	[103]

Czichos [104] has indicated the role of materials and their testing while choosing them for a specific purpose. The most susceptible and envisaged degradation of cell components is due to the methanol environment, interaction of reaction by-products, temperature, heat dissipation, and ambient conditions. Hence the materials and their testing have become critical in the analysis.

Liu et al, [105] have studied the performance degradation of the cell focusing on membrane electrode assembly consisting of the anode loaded with Platinum-Ruthenium as a catalyst, cathode loaded with Platinum as a catalyst and a proton-conducting membrane in between anode and cathode. From the literature, it is observed that the initial power density of PDMFC is lost by about 30% after a test period of 75 hours. This is due to an increase in resistance because of de-bonding of electrodes with MEA and swelling of membrane and electrodes.

Ermilova et al, [106] have studied the stability of structured materials against failures. From the PDMFC, it is observed that the cathode end current collectors are getting corroded slower than that at the anode side. The reason behind the cathode end CC corrosion is attributed to methanol cross-over and the formation of water at the cathode. Therefore, these collectors are free from distortion.

2.6 Summary of Literature Review

- Current collectors and their material properties play a significant role in the performance of fuel cells.
- Current collectors with larger openings on the anode side provide ease of Carbon dioxide scavenging. The lower limit is starvation, and the higher limit is flooding with respect to methanol fuel.
- Geometry and dimensions of active region (MEA) of the cell influence the cell performance.
- Performance and power density of cell vary with the size of active dynamic areas of membrane.
- PDMFC components undergo degradation during the service and can be identified using various Non-Destructive Testing methods.

2.7 Gaps identified from the Literature Review

- In the literature, most of the authors concentrated on SS current collectors in PDMFC. It is observed that not much research is found on other materials of current collectors like Nickel, Brass, etc., for high electrical conductivity with compatibility in dilute methanol solution.
- From the literature, cell performance with uniform-shaped opening ratios is available. Current collectors opening modification with taper cylindrical shape for better performance and ease of CO_2 scavenging keeping the contact area same at MEA side is not available.
- Very few authors considered the analysis of the best performance and the highest power density among the square, rectangular and circular active areas. However, from the literature, cell performance studies with the size and shape of active zones with equal areas and equal perimeters are not available.
- A little literature is available on NDT evaluation on PEM Fuel cell components. But there is no literature on DMFC components for identifying the service-induced imperfections, flaws, and defects using various Non-Destructive Testing methods like VT, PT, UT, Metallography, and hardness testing methods.

2.8 Objectives of the proposed research work

The following objectives are framed from the literature research gaps identified for the proposed research work.

- To evaluate the performance of PDMFC current collectors by using Ni-201 and Brass materials and comparing them with SS-316L material.
- To analyse the performance of current collectors by providing taper cylindrical openings for better CO_2 scavenging.
- To examine the performance of PDMFC current collectors with the combination of different anode and cathode materials among SS-316L, Nickel-201, and Brass materials.
- To investigate the maximum power produced by PDMFC by various shapes and sizes of active regions with equal area and equal perimeter geometries.
- To evaluate service-oriented degradation of PDMFC components using various Non-Destructive Testing methods.

2.9 Novelty of the Research

Novelty of present work can be found in the methods employed to improve the overall performance of Passive Direct Methanol Fuel Cell and these are:

- Introduction of new and better material (Ni-201) for fabrication of current collectors, compatible with the methanol solution leading to higher and durable performance of PDMFC.
- The modification of current collector openings from conventional uniform cylindrical openings to taper cylindrical openings, leading to a clear-cut improvement in the performance of PDMFC.
- Non-Destructive Testing methods are employed to better understand the service-oriented degradations of the fuel cell components, thereby improving the durability and reliability of the PDMFC system.

Chapter 3

Experimental Methodology

3.1 Introduction

In this chapter, details of research methodology, experimental setup including fabrication details and operating procedure of the passive direct methanol fuel cell are described. Fabricated components of the passive direct methanol fuel cell are assembled in the laboratory of Fuel Cells, NIT, Warangal. The effective dynamic area (MEA active region) of the cell is 2500 mm^2 (50 mm X 50 mm).

3.2 Cell description

The major components of the fuel cell are anode side acrylic end cover, anode-side current collector, membrane electrode assembly, cathode-side current collector, cathode side acrylic end cover, gaskets, and fasteners with electrical isolators. Assembled passive DMFC with schematic diagram is shown in figure 3.1.

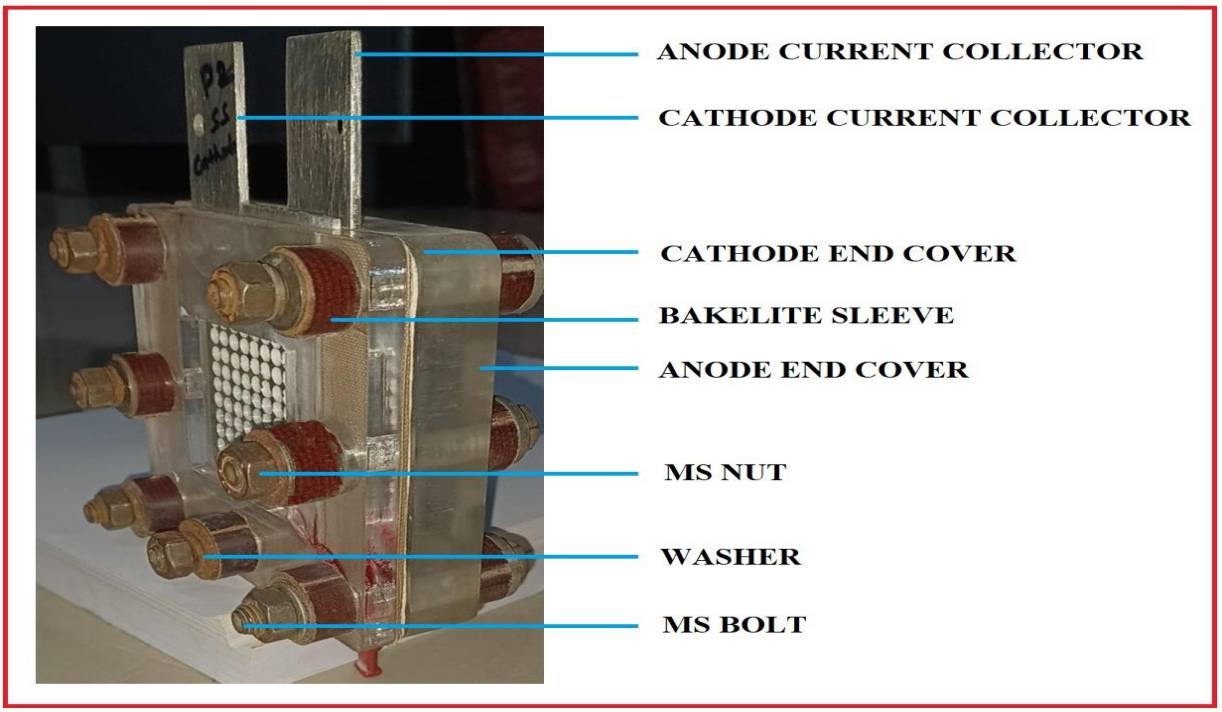

Figure 3.1 Assembled Passive Direct Methanol Fuel Cell

3.3 Experimental Methodology

3.3.1 Identification of best current collector material

To evaluate the performance of the various current collector materials in methanol environment, a comparison study on the required characteristics of the materials is performed. Based on the required characteristics, prospective materials are arranged in the order of decreasing electrical conductivity. The other desired properties of the chosen materials are gathered from literature and the values are tabulated in table 3.1 [37][107].

Table 3.1 Materials suitability and comparison study

Material/ Characteristics	**Silver**	**Copper**	**Gold**	**Aluminium**	**Zinc**	**Brass**	**Nickel**	**Titanium**	**Stainless Steel**
Electrical conductivity, 10^6S/m	62.1	58.7	44.2	36.9	16.6	15.9	14.3	2.4	1.32
Methanol compatibility (1)(2)(3)	X	X	√	X	X	√	√	~	√
Durability (1)(2)(3)	X	X	√	X	X	~	√	~	√
Density, g/cc	10.51	8.91	19.3	2.64	7.13	8.55	8.89	4.5	7.9
Price, $/kg	708	8.02	60360	2.29	3.25	3.52	15.8	80	5.57

Note: (1) X Not compatible with methanol
(2)√ Compatible with methanol
(3) ~ Limited application in methanol solution

From the above table, it can be inferred that Silver, Copper, Aluminium and Zinc are not compatible with methanol. Hence, these materials not considered for cell current collectors. Although Gold is compatible, its high density and cost make it less attractive for the current research. Titanium is compatible in the limited range (2%-10% v/v) of methanol solution but its high cost makes it not suitable for current collectors. Nickel, Brass, and stainless steel are compatible in methanol.

The other factors influencing the performance of current collectors are ohmic losses, corrosion resistance, and contact resistance. These factors are studied for Ni-201, Brass, and SS-316L current collector materials and relative comparative observations are tabulated in table 3.2 [37][38][108].

Table 3.2 Factors influencing the performance of current collectors

Contributing Factors	**Materials**		
	Ni-201	**Brass**	**SS-316L**
Ohmic losses	Less (High electrical conductivity)	Less (High electrical conductivity)	Moderate (Relatively less electrical conductivity)
Rate of Corrosion	Least (<0.002 inch/year)	High (0.02 to 0.05 inch/year)	Moderate (<0.02 inch/year)
Contact resistance	Least	High (Oxides and Hydroxides of zinc and copper).	Moderate (Oxides of Chromium).

The particulars of composition of these materials are shown in table 3.3, and relevant data of the materials is shown in table 3.4.

Table 3.3 Composition of Materials [108]

Element in the composition	**Material Composition, % w/w.**		
	Ni-201	**Brass**	**SS-316L**
C, Carbon	0.02 maximum	----	0.03 maximum
Mn, Manganese	0.35 maximum	----	2.00 maximum
Si, Silicon	0.35 maximum	----	0.75 maximum
P, Phosphorus	----	----	0.045 maximum
S, Sulphur	0.01 maximum	----	0.030 maximum
Cr, Chromium	----	----	16-18
Ni, Nickel	99.00 minimum	About 0.05	10-14
Cu, Copper	0.25 maximum	65-70	----
Zn, Zinc	----	30-35	----
N, Nitrogen	----	----	0.1 maximum
Fe, Iron	0.40 maximum	About 0.4	Remaining

Table 3.4 Relevant Data of the Current Collector Materials [107]

Material of construction	Rate of Corrosion in pure methanol, (mm/year)	Specific Weight, (kg/m^3)	Resistivity (Electrical) of material at 20 ^{O}C, ($x10^{-7}$ Ωm)	Electrical Conductivity of material at 20 ^{O}C, ($x10^{6}$ S/m)	Cost, ($/kg)
SS-316L	0.5	7900	7.4	1.351	5.57
Ni-201	0.05	8890	0.68	14.705	15.80
Brass	1.25	8500	0.62	16.129	3.52

With due consideration to required characteristics of current collectors, experimental investigation of PDMFC for identifying best material among Stainless-Steel (ASTM-A240 Grade 316L, UNS S31603), Nickel (Grade 201 ASTM-B162, UNS N02201), and Brass (ASTM-B36, UNS C26800) in dilute methanol solution is carried out.

3.3.2 Taper and uniform cylindrical openings in current collectors

In the fuel cell, the methanol flows from reservoir to the reaction site through the CC openings and the liberated CO_2 flows back to the reservoir. To investigate the performance of PDMFC, the existing design of uniform cylindrical openings in current collectors is modified to taper cylindrical openings. Schematic of uniform and taper cylindrical openings are shown in figure 3.2.

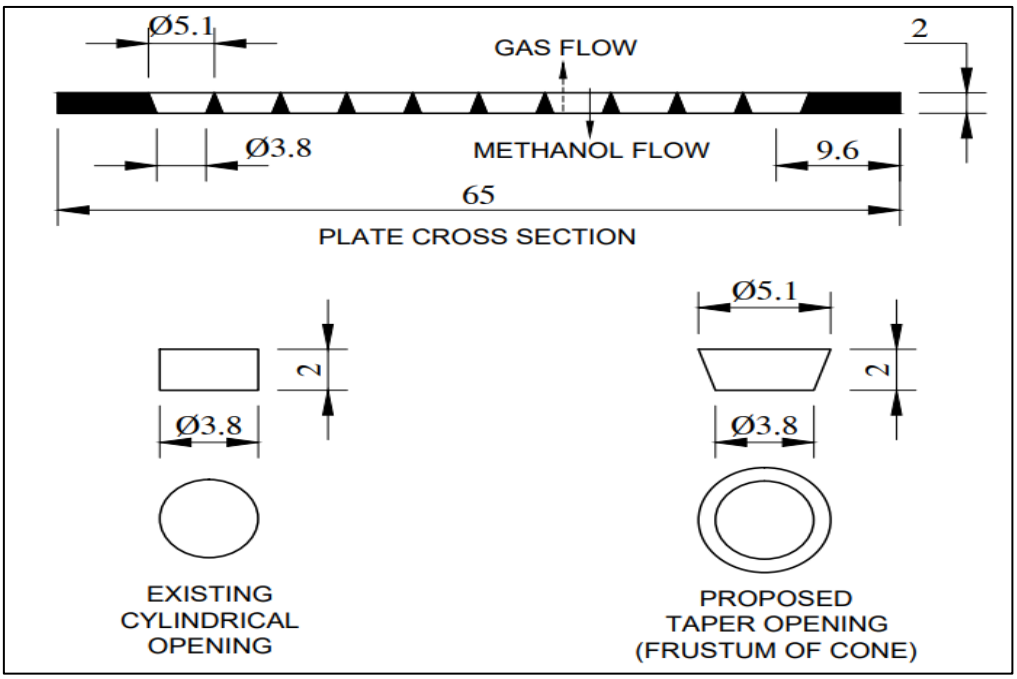

Figure 3.2 Uniform and Conical Openings

The taper cone angle of the opening in the current collector influences the buoyancy of carbon dioxide bubbles moving through the conical opening and also influence on the electrical charge density distribution. Buoyancy on the CO_2 bubble in methanol solution through the CC opening is a function of density of methanol solution, acceleration due to gravity of the location and volume of the bubble.

Hence,

Buoyancy (F_{byo}) $\propto$ Density of the methanol solution (ρ_l)

$\propto$ Local acceleration due to gravity (g_l)

$\propto$ Volume of the CO_2 bubble (V_o)

Implies, $F_{byo} \propto \rho_l g_l V_o$

$$F_{byo} = k_b \rho_l g_l V_o \quad (3.1)$$

(where k_b is a constant of proportionality ~ 1)

In a given set up of passive direct methanol cell, the values of the ρ_l and g_l are practically constant. Hence buoyancy on the carbon dioxide bubble in the current collector is the function of its volume. Therefore, as the volume of the bubble increases, the buoyancy also increases. To study buoyancy effect, the conical opening considered in the material of the current collector as shown in figure. 3.3.

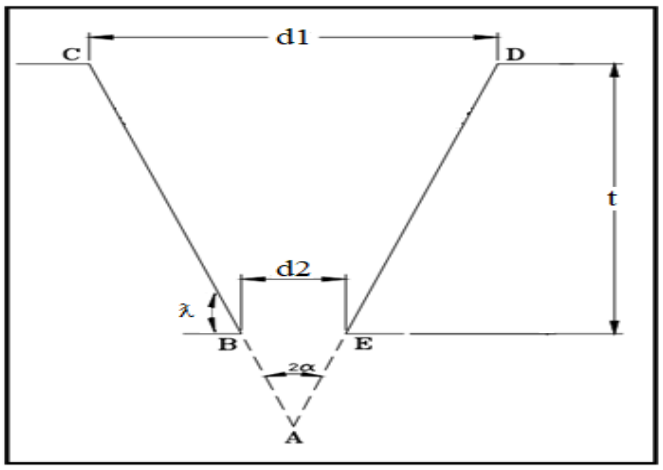

Figure 3.3 Details of conical opening on the current collector

Volume of uniform opening = $\frac{\pi}{4}(d2)^2\, t$ (3.2)

Volume of conical opening=$\frac{\pi}{12}[(d2)^2 + (d1)^2 + d1d2]t$ (3.3)

Half angle of the cone is, $\propto = \tan^{-1}[(d1 - d2)/2t]$ (3.4)

As the existing current collectors with uniform cylindrical openings are drilled with 3.8 mm holes in 2 mm thick plate, the same thickness is considered for taper cylindrical openings CC, keeping the base diameter of the hole 3.8 mm at the bottom side and analysed for the different cone angles of 0.0, 8.6, 17.1, 25.4, 33.4, 36.0 degrees. The maximum cone angle obtained is 36.0 degrees. At this angle, the top circles of the adjacent openings are meeting each other i.e., the sum of the radii of adjacent openings is approaching the pitch distance. The buoyancy on CO_2 bubble in taper cylindrical opening (using equation 3.1) and the buoyancy ratio, i.e., volume of taper cylindrical opening to the volume of uniform opening, (equation 3.2 divided by equation 3.3) are calculated and tabulated in the table 3.5.

Table 3.5 Effect of Cone angle on Buoyancy

Thickness of current collector, mm	**Bottom Diameter of opening, mm**	**Top diameter of opening, mm**	**Cone Angle ($2\propto$), degree**	**Buoyancy, N**	**Buoyancy Ratio of conical opening to uniform opening**
2	3.8	3.8	0.0	222.51	1.00
2	3.8	4.1	8.6	240.54	1.08
2	3.8	4.4	17.1	259.50	1.17
2	3.8	4.7	25.4	279.37	1.26
2	3.8	5.0	33.4	300.18	1.35
2	3.8	5.1	36.0	307.32	1.38

As the cone angle increases, the buoyancy and buoyancy ratio are also increasing proportionally. The effect of Cone angle on buoyancy force and buoyancy ratio is graphically represented in figure 3.4.

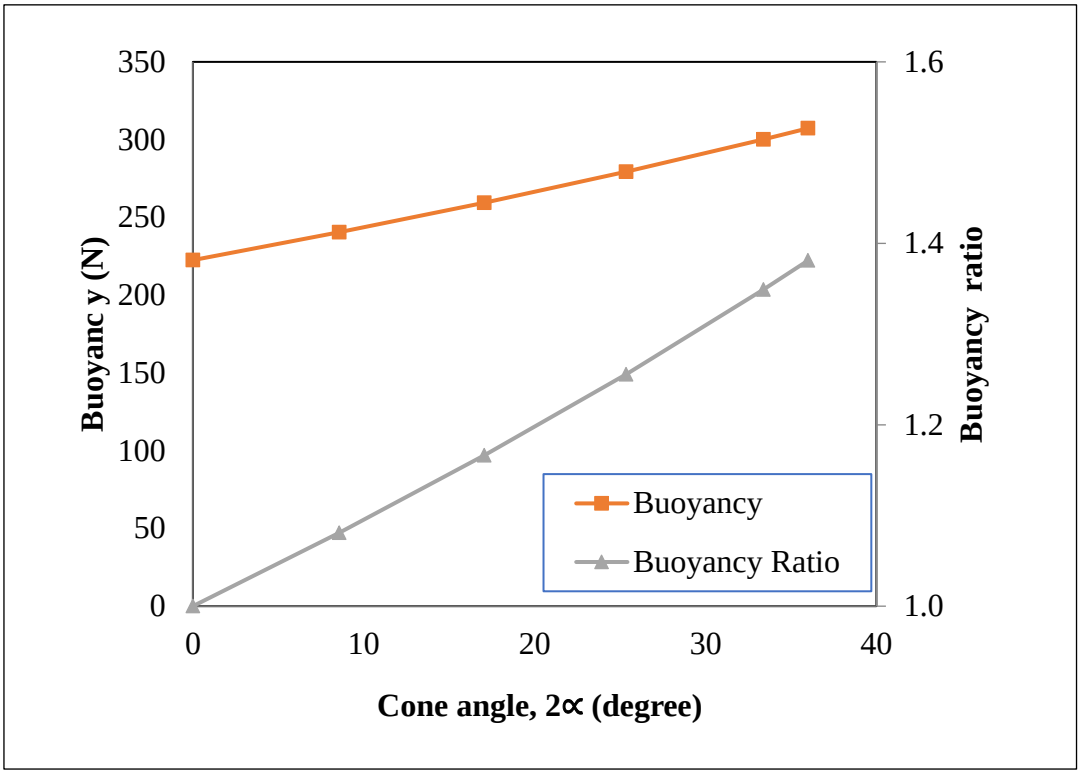

Figure 3.4 Effect of Cone angle on buoyancy force and buoyancy ratio

Two types of current collectors are fabricated, the first CC with a taper cylindrical cross-section having openings of 5.10 mm at the top & 3.80 mm at the bottom with a taper angle of 36^{o}, and the second CC of uniform cylindrical cross-section openings with a diameter of 3.80 mm each. The number of openings in CC is 100, in 10 x 10 matrix pattern. The images of current collectors fabricated with uniform cylindrical openings and taper cylindrical openings are shown in figure 3.5.

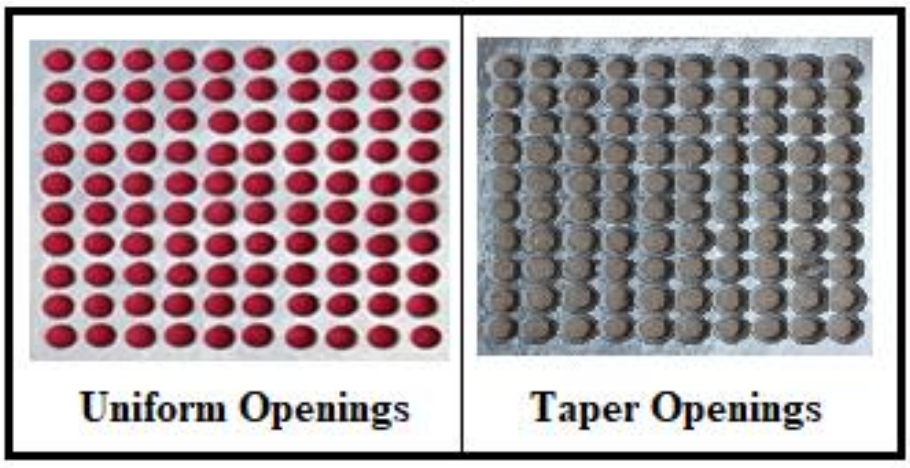

Figure 3.5 Images of uniform openings and taper openings

3.3.3 Various shapes and sizes of MEA active regions

To investigate the performance of Passive Direct Methanol Fuel Cell with different sizes and shapes of active regions, gaskets of different geometries having Equal Areas and Equal Perimeters are used. PTFE gaskets of 0.11 mm thickness are chosen for fabrication of desired shapes and sizes of effective flow path area over MEA of the cell.

The controlling shape of MEA dynamic zone, i.e., a circular opening in both equal areas and equal perimeters is chosen as a reference. The maximum circular shape size with a diameter of 50mm is cut in the PTFE gasket to accommodate in 50 mm side square area of MEA. This opened circular shape has an effective area of 1963.5 mm^2 and a perimeter of 177.2 mm. Using this area and perimeter as constant, dimensions of the other shapes such as square, rectangle, and rhombus are fixed. The same sets of gaskets are used on either side of MEA for achieving desired dynamic MEA region. Ni-201 current collector is used in the PDMFC as it has good electrical conductivity and better compatibility with methanol solution. Methanol solution of 5Mis used to perform the experiment.

Conceptual drawings of the gasket openings, with equal area geometry such as circle having diameter 50 mm, rectangle of length 50 mm & breadth 39.27 mm, square with 44.31 mm side and rhombus with 44.95 mm side and the same in equal perimeter geometry such as circle having diameter 50 mm, rectangle length 50 mm X breadth 28.54 mm, square with 39.27 mm side and rhombus with 39.27 mm side are shown in figure 3.6.

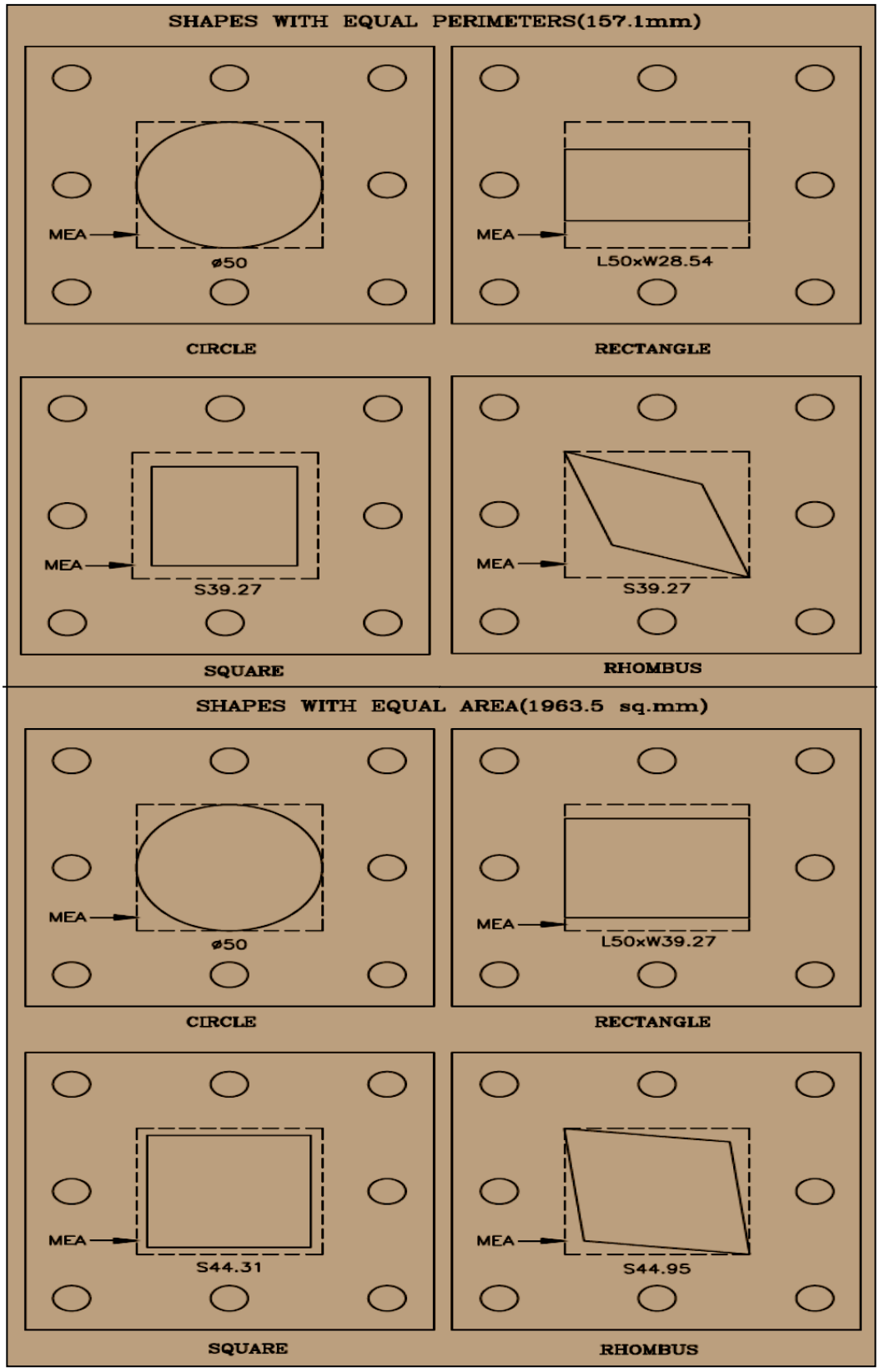

Figure 3.6 Details of the gasket dynamic openings with equal areas and perimeters

Drawings of the gasket openings over current collectors in equal area and equal perimeter geometries are shown in figure 3.7.

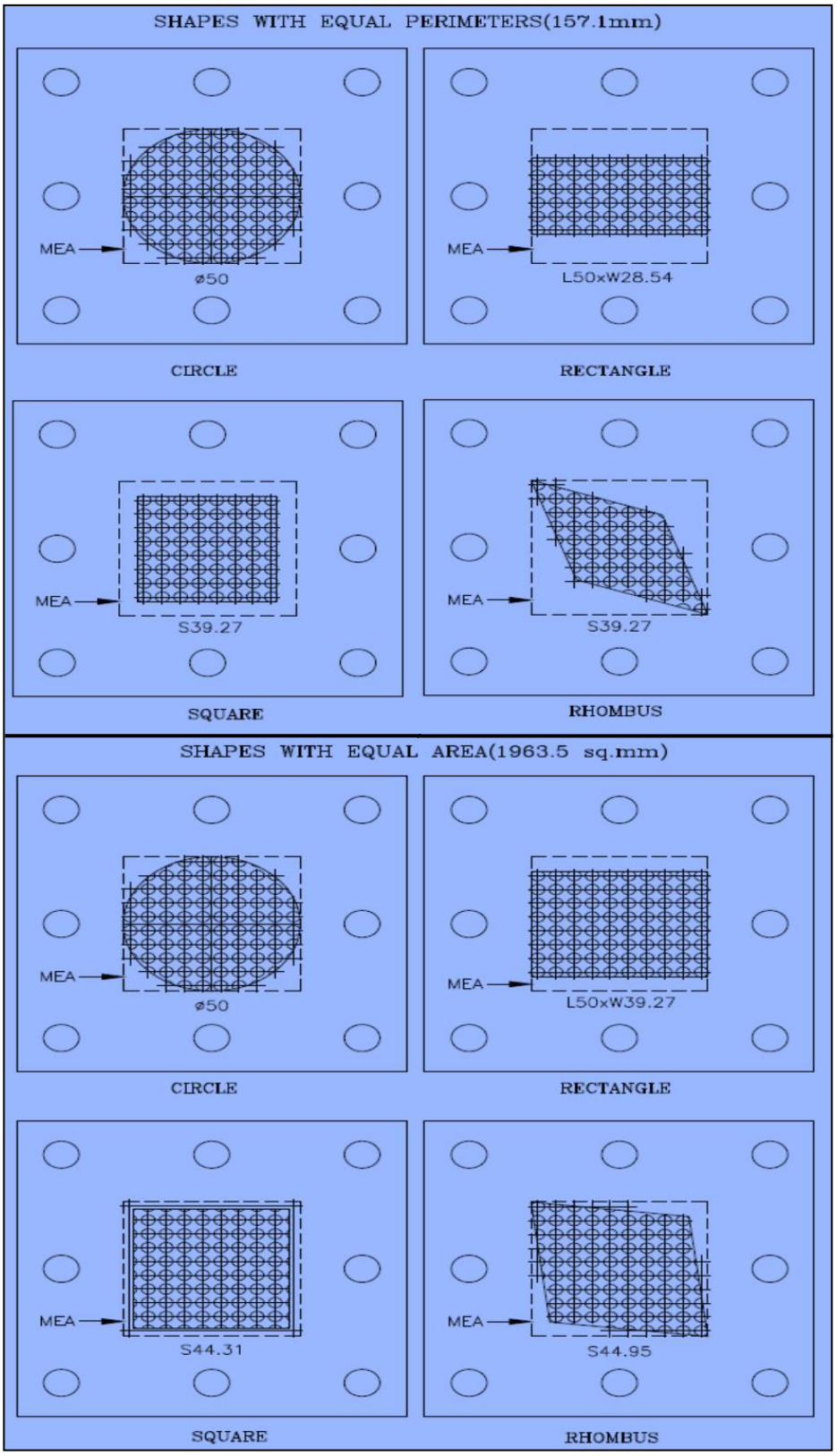

Figure 3.7 Details of the gasket dynamic openings over the current collector with equal areas and perimeters.

3.3.4 Service-oriented degradation of PDMFC components using various Non-Destructive Testing methods

Fuel cell components and their durability are affected by methanol, its solution concentration, evaporative conditions of water, carbon dioxide evolution, heat generation, and its sealing components. Hence it is necessary to know and identify the In-Service developed degradations of Passive Direct Methanol Fuel Cell Components for ascertaining the integrity of cell components. One of the best tools for the identification of degradations is by using Non-Destructive Testing (NDT) Methods. NDT is a technique for analyzing and testing to evaluate discontinuities, defects, properties of components, characteristics of structures, etc., without causing damage to the intended service of the components. The PDMFC components' degradation that are envisaged, components material of construction (MOC) and quantity used with the cell are tabulated in table 3.6.

Table 3.6 Most susceptible degradation mechanisms of PDMFC components

Name of the component	MOC	Qty	Envisaged Degradation Mechanism
Anode End Cover	Acrylic	1	Brittle Cracks under aging and bolt loading
Gasket between anode end cover & anode	Viton	1	Compression Set Lack of softness
Anode Current Collector	SS, Nickel, Brass	1	Uniform Corrosion Corrosion Erosion in openings Surface cracks
Gasket between anode and MEA	Teflon coated woven cloth	2	Compression Set Lack of softness
MEA	Nafion-117	1	Reduction of Exchange Performance with time
Gasket between MEA and cathode	Teflon coated woven cloth	2	Compression Set Lack of softness
Cathode Current Collector	SS, Nickel, Brass	1	Uniform Corrosion
Gasket between cathode end cover & cathode	PTFE Viton	1	Compression Set Lack of softness
Cathode end cover	Acrylic	1	Brittle Cracks
Fasteners (bolts, nuts, washers)	MS, SS	7	Uniform Corrosion
Wrapping on fasteners	Bakelite	7	Cracks under compression Methanol Tolerance Swelling

Non-Destructive Examination uses various methods such as visual examination (VT)for identification of surface discontinuities, leaks, distortion, de-colorization, surface corrosion, etc.; Ultrasonic Testing (UT) for thickness inspection, identification of internal cracks, laminations in plates and structures; Liquid Penetrate Testing (PT) for identification of surface discontinuities which are opened the surface on non-porous materials; Hardness testing to identify changes in metallographic structures, and hardness; metallurgical studies using Scanning Electronic Microscope (SEM) and Transmission Electron Microscope (TEM) are extensively used to evaluate and identify the In-Service generated degradations. The methods of various NDT for identifying the envisaged degradation mechanisms of PDMFC components and their record of results for interpretation are tabulated in table 3.7.

Table 3.7 NDT methods for PDMFC Components

PDMFC component	Degradation Mechanisms	Examination Methods	Record for interpretation
Anode End Cover	Brittle Cracks under aging and bolt loading	Visual Examination Surface Examination with Penetrant Testing	VT-Image, PT-Image.
Gasket between anode end cover & anode Current Collector	Compression Set, Lack of softness.	Visual Examination, Thickness Testing, Hardness Testing.	VT-Images, Thickness- measurement for compression set, Hardness-Shore A value.
Anode Current Collector	Uniform Corrosion, Corrosion Erosion in openings, Surface cracks.	Visual Examination, Thickness Testing, Loss of weight in a given time.	VT-Images, PT- Images, Corrosion- Images& Weight loss calculations.
Gasket between anode Current Collector and MEA	Compression Set, Lack of softness.	Thickness Testing, Hardness Testing.	VT-Image (for new and used gaskets), Thickness- measurement for compression set, Hardness-Shore A value.
MEA	Reduction of Performance	Durability	SEM and TEM images
Gasket between MEA and cathode CC	Compression Set, Lack of softness.	Thickness Testing, Hardness Testing.	VT-Images, Thickness-Compression, Hardness-Shore A.
Cathode Current Collector	Uniform Corrosion	Visual Examination, Surface Examination with Penetrant Testing, Thickness Testing.	VT-Image for SS, Ni, Brass; PT- Image, Corrosion- Images.

Gasket between cathode cover & cathode Current Collector	Compression Set, Lack of softness.	Thickness Testing, Hardness Testing.	VT-Images, Thickness- measurement for compression set, Hardness-Shore A value.
Cathode end cover	Brittle Cracks	Visual Examination Surface Examination	VT-Image, PT-Image
Fasteners (bolts, nuts, washers)	Uniform Corrosion	Visual Examination	VT-Image, Corrosion-weight loss calculations
Wrapping on fasteners	Cracks under compression, Methanol Tolerance Swelling	Visual Examination	VT-Image (new & used)

3.4 Experimental Setup

3.4.1 Current collector materials

For the experimentation, identical materials of current collectors are used at anodic and cathodic ends fabricated from a 2 mm (+/- 0.02) thick sheet. Circular openings in a 10 X 10 pattern are drilled using a 3.8 mm drill bit. Fabrication drawing details of CC are shown in figure 3.8(a). Fabricated current collectors from Ni-201, Brass and SS-316L sheets are shown in figures 3.8(b), 3.8(c), and 3.8(d) respectively.

To avoid leakage of methanol solution, Poly Tetra Fluoro Ethylene (PTFE) gaskets are used for assembling the components of the cell. The effective dynamic area of MEA in the fuel cell is 50 mm x 50 mm. Various concentrations of methanol solution viz., 1M, 2M, 3M, 4M, 5M, and 6M are prepared for use in these experiments. Weights of the current collectors are noted before starting the experiment. The necessary tightening of cell components is done using M8 bolts & nuts and uniform fixing of bolting system is confirmed with a pre-set torque wrench, with torque value fixed at 5 N-m.

In this experiment, the current collectors Ni-201, Brass, and SS-316L with an opening ratio of 45.3% are used. The experiment is carried out by choosing identical current collectors on anode and cathode ends.

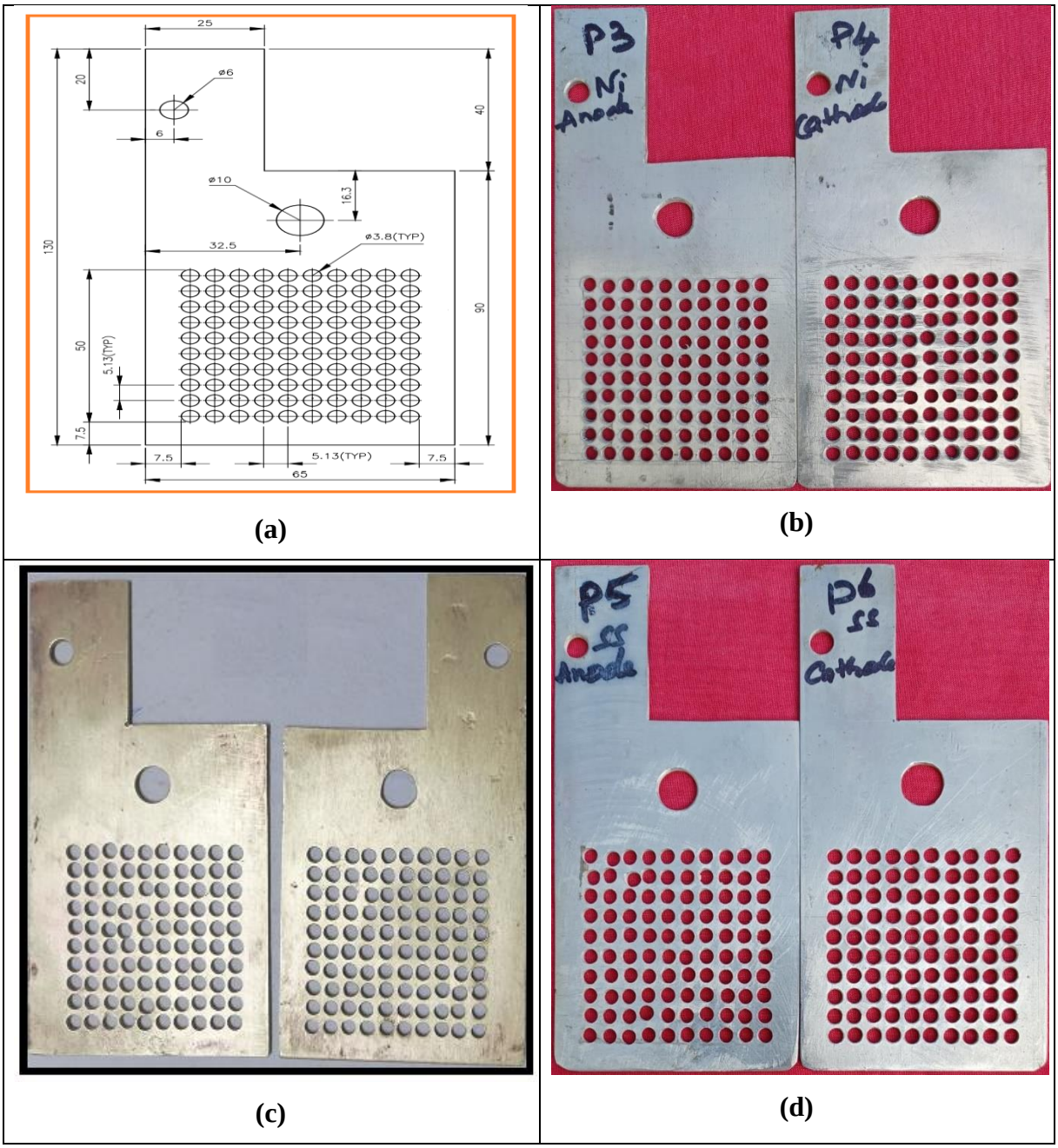

(a). Drawing details of 2 mm thick current collector.
(b). Fabricated Nickel current collectors.
(c). Fabricated Brass current collectors.
(d). Fabricated SS-316L current collectors.

Figure 3.8 Current Collectors Fabrication details

The experimental arrangement of PDMFC is shown in figure 3.9. The passive DMFC hardware setup used in this experiment consists of acrylic end plates for providing mechanical support, isolating gaskets, current collectors, Membrane Electrode Assembly (MEA), and fasteners.

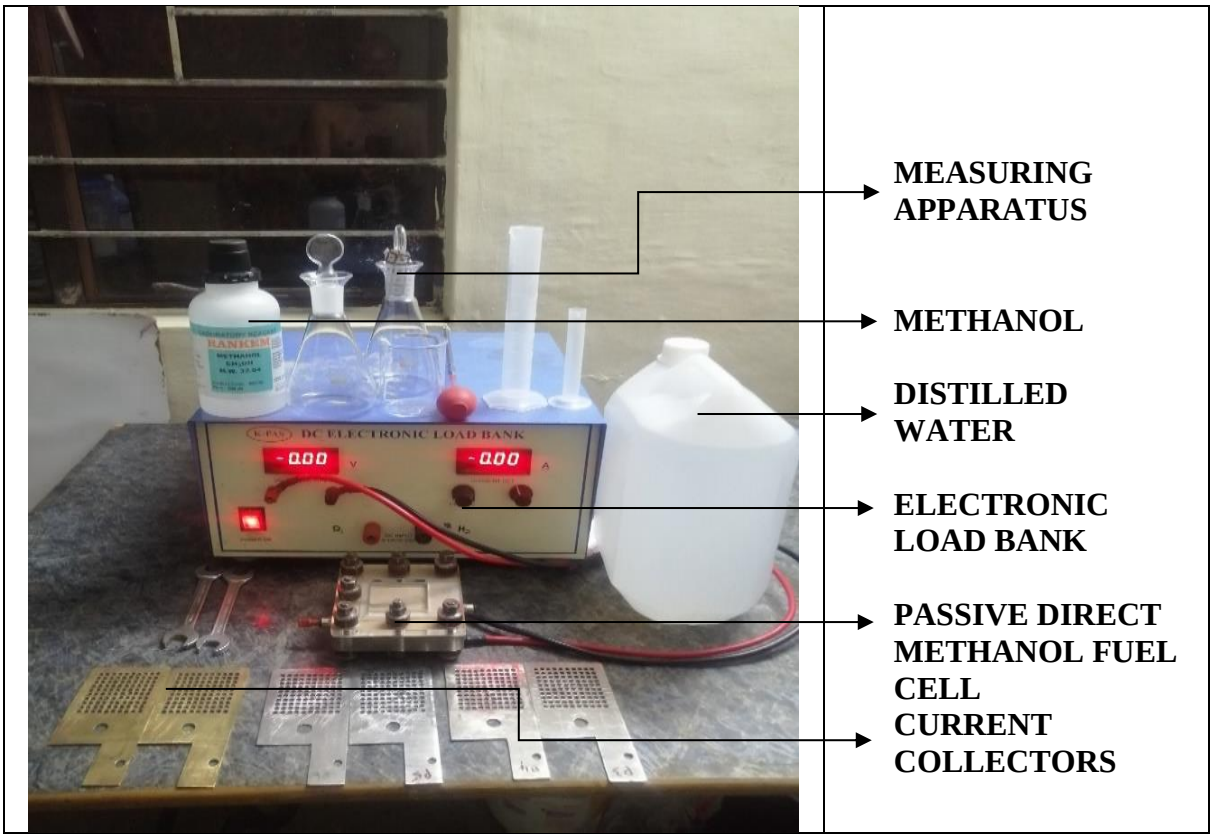

Figure 3.9 Experimental Setup of PDMFC

Anode side of cell: The anode endplate has 110 x 110 x 18 mm dimensions with an in-built fuel reservoir of 50 x 50 x 10 mm size including two ports for filling and draining of methanol solution. The capacity of the fuel reservoir is 25 cm^3 to accommodate the methanol solution. The methanol solution reaches the MEA through current collector openings and initiates the reactions. The generated H^+ ions are conducted through the membrane; the by-product CO_2 passes back to the reservoir and the liberated electrons are conducted by the current collector.

cathode side of the cell: The cathode end acrylic plate has 110 x 110 x 8 mm dimensions with a square shaped window opening of 50 mm side, for allowing oxygen from the ambient air. This air passes through the cathode-side current collector to the reaction zone at MEA. The oxygen in the air joins with H^+ ions and electrons at the cathode end to form H_2O as a by-product.

The DC Programmable Electronic Load Bank is used to measure the voltage and current produced by PDMFC in all the experiments along with the setup.

3.4.2 Taper cylindrical openings current collectors

Drawing details of uniform and taper cylindrical opening current collectors is shown in figure 3.10. The images of fabricated current collectors having uniform cylindrical openings are shown in figures 3.11 & 3.12 and taper cylindrical opening current collectors are shown in figure 3.13. A Nafion-117 is used as permeable membrane in MEA. To prevent the leakage of methanol solution, sealing gaskets are provided in between the components of the cell. Keeping the active area of the cell as 50 mm x 50 mm, various concentrations of methanol solution viz., 1M, 2M, 3M, 4M, 5M, and 6M are prepared for use in this experiment. Weights of these current collectors are measured before starting the experiment.

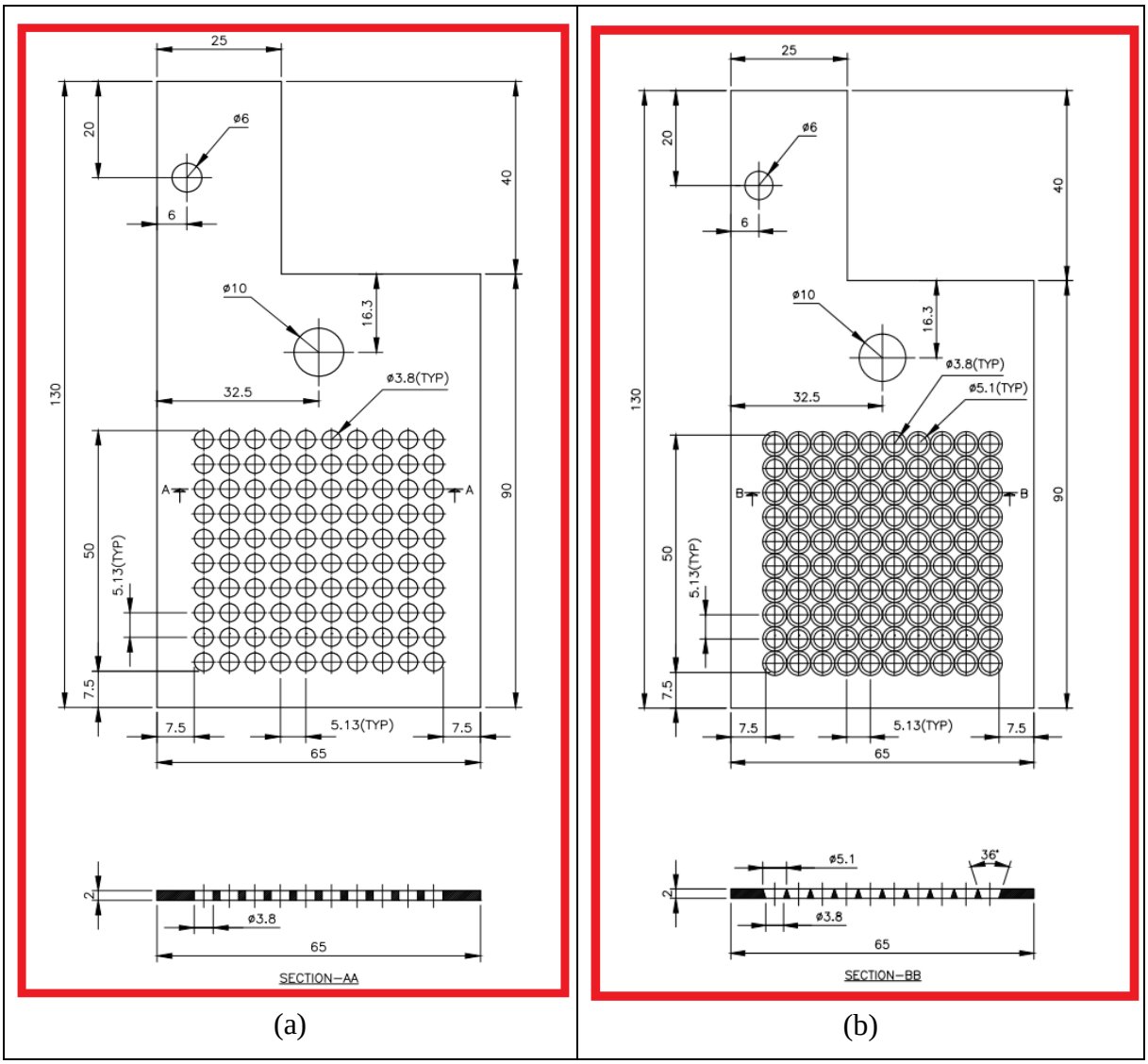

(a)Uniform cylindrical openings on current collectors

(b) Taper cylindrical openings on current collectors

Figure 3.10 Drawing details of current collectors

Figure 3.11 Details of SS-316L material and Fabrication of uniform cylindrical openings on current collectors

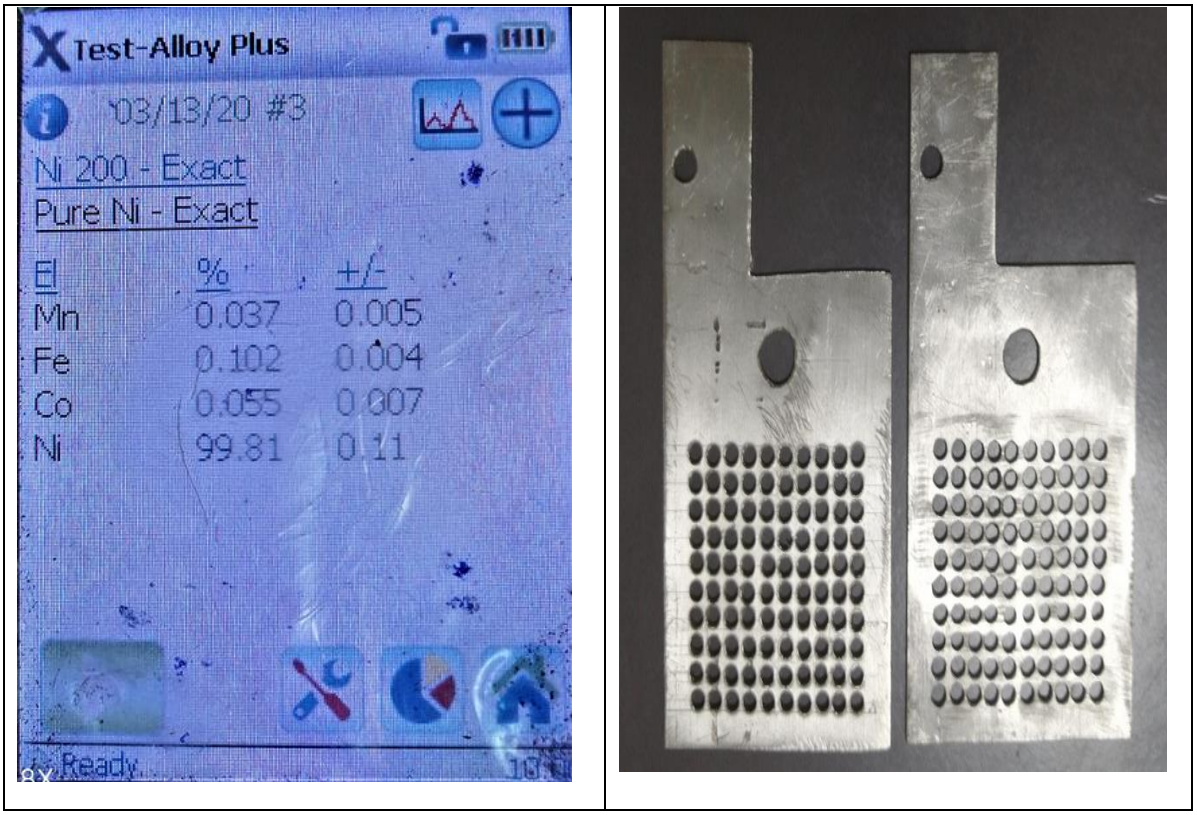

Figure 3.12 Details of Ni-201 material and Fabrication of uniform cylindrical openings on current collectors

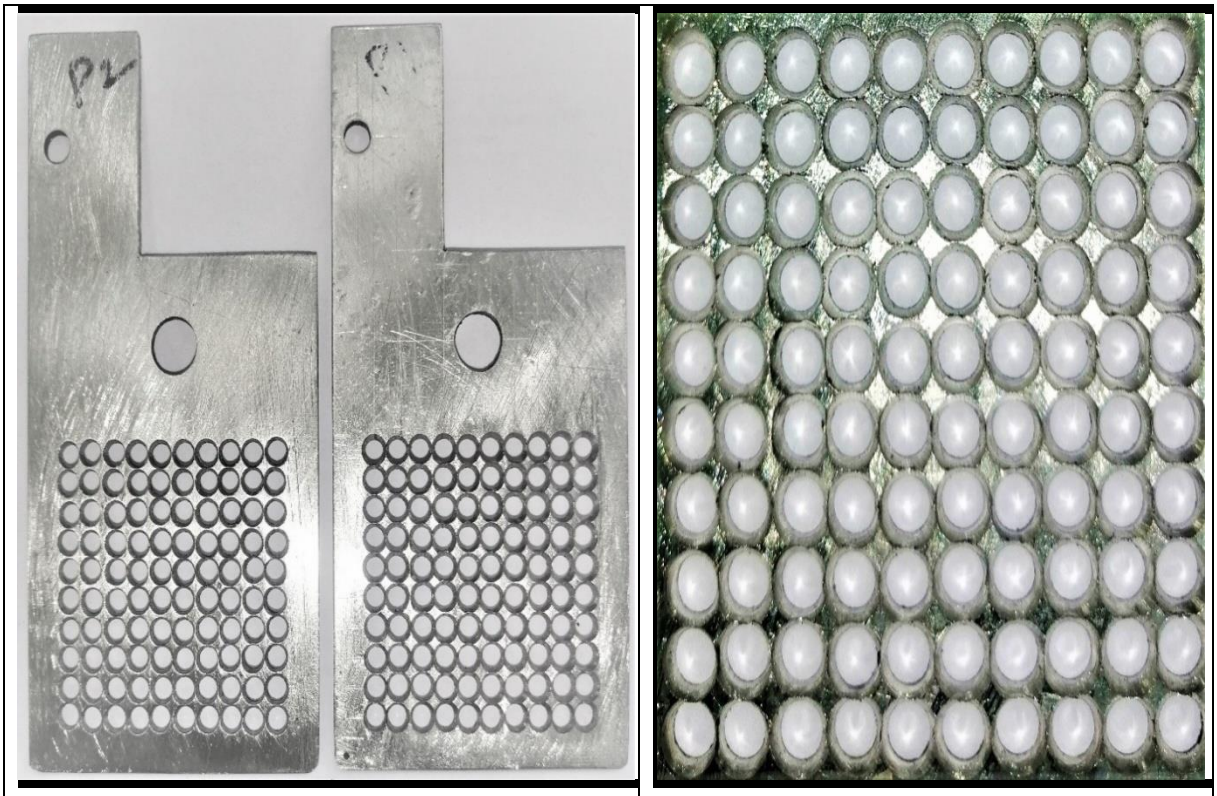

(a) (b)

(a) with taper cylindrical openings, (b) magnified view of openings

Figure 3.13 Images of fabricated current collectors of PDMFC

For investigating the performance of cell with current collectors of uniform cylindrical openings and taper cylindrical openings, two setups are used shown in table 3.8.

Table 3.8 Combinations of current collectors

Experimental Setup	Anode	Cathode
Setup-1	Uniform cylindrical openings	Uniform cylindrical openings
Setup-2	Taper cylindrical openings (Converging towards MEA side)	Taper cylindrical openings (Converging towards MEA side)

3.4.3 Various shapes and sizes of MEA active regions

The setup of the gasket opening shapes such as circular, rectangular, rhombus and square over the anode-side current collector and over MEA are shown in figure 3.14 and figure 3.15 respectively.

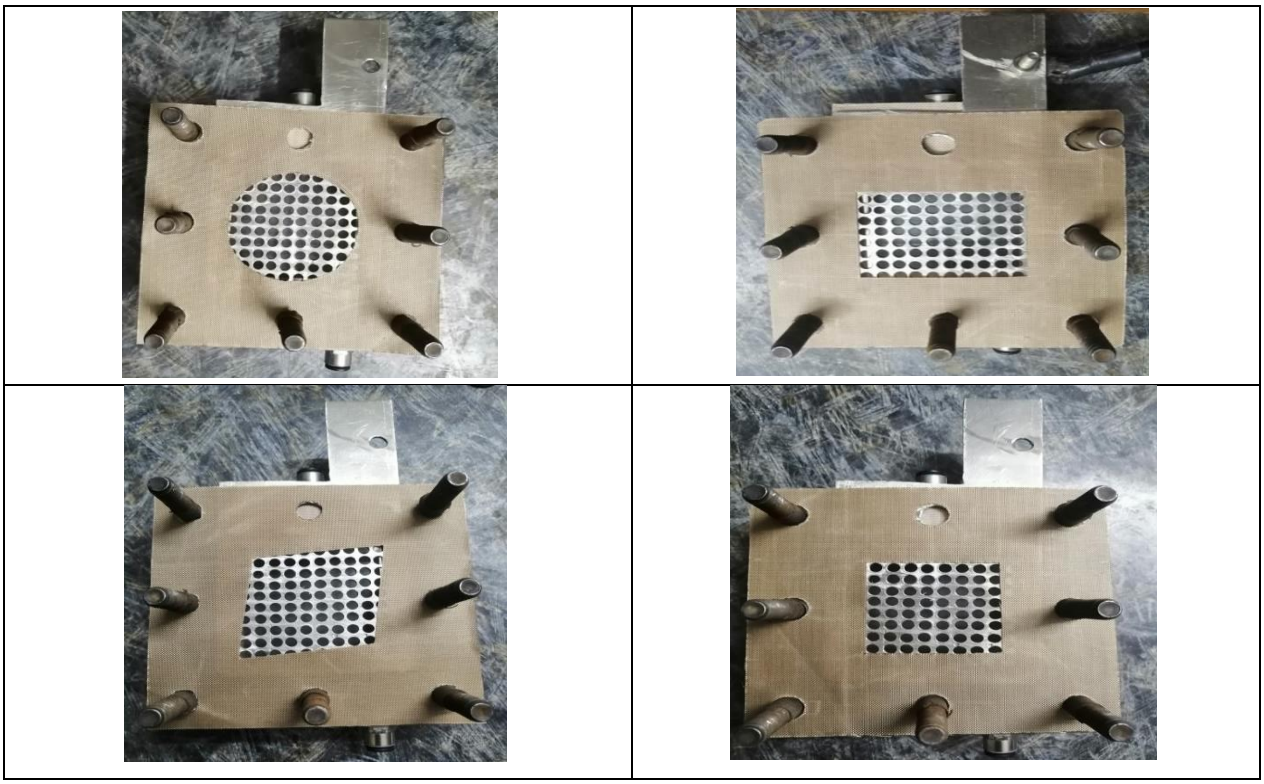

Figure 3.14 Setup of the gasket over the anode-side current collector

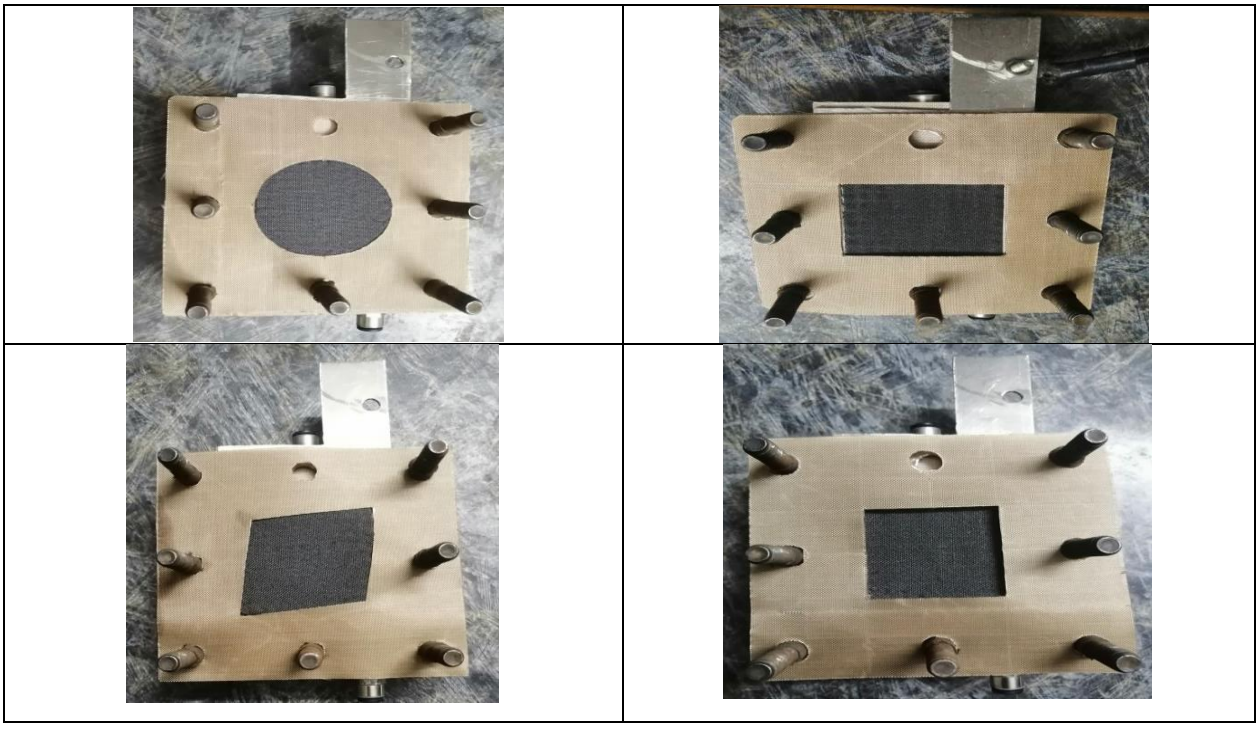

Figure 3.15 Setup of the gasket over MEA

3.5 Experimental Procedure

The procedure for the experiment of PDMFC is as follows:

- Identical current collectors at anode and cathode sides are placed in the cell.
- The new MEA being used in the cell must require initial activation before proceeding for further experimentation.
- To activate the MEA, 1M methanol solution is used in the cell under constant electrical load for a period about12 hours.
- Methanol solutions (diluted with distilled water) of various concentrations are prepared ranging from 1M to 6M.
- The anode side reservoir is filled with the prepared methanol solution with the help of pipette.
- The cell assembly is inspected for leakages of methanol solution (fuel).
- All the experiments are carried out at ambient conditions. The cell is kept in horizontal position, with anode side facing top.
- The electrode terminals of the fuel cell are connected to a DC electronic load bank.
- The experimental set-up is kept in switched-on for 15 minutes at open circuit voltage to attain steady state conditions before taking the readings.
- By varying current values (under constant current characteristics) in equal increments of 0.04A, the respective voltage readings are noted down starting from OCV to the minimum achievable value.
- The voltage reading for each current set value is recorded after obtaining steady state conditions starting from 1M to higher concentrations till the performance of the cell is found maximum.
- Polarization (V-I) curves and power density (PD) curves at different methanol concentrations are drawn to analyse the performance of the cell.
- All these experiments have been repeated thrice to get consistency, repeatability, reproducibility & reliability in the interpretations of the obtained results and to investigate the PDMFC intrinsic characteristics.

3.5.1 Operating Conditions

For the above procedure, the experiments with the passive direct methanol fuel cell are carried out with the operating conditions given in table 3.9.

Table 3.9 Operating Conditions

Parameter	**Operating range**
New MEA activation period	12 hours, using 1M methanol solution.
Voltage set during activation	0.25 V (+/- 0.01V)
Relative humidity	60% -75%
Temperature, during experimentation	Room temperature (20 ℃ - 28 ℃).
Pressure, during experimentation	Atmospheric pressure.
Methanol solution	1M to 6M concentration.
Cell orientation	Horizontal, Anode side facing top.

3.5.2 Uncertainty

The DC electronic load bank inherent uncertainty specified by the manufacturer is given in table 3.10.

Table 3.10 Uncertainty in the results

Electrical Characteristics	**Range of instrument**	**Uncertainty Value**
Voltage (V)	0.00-9.99	0.28%
Current (A)	0.00-9.99	0.15%
Power (W)	---	0.31%

The uncertainty in experimental results is calculated (Appendix A) and found within the permitted uncertainty limits of above specified values.

3.5.3 Assumptions considered during the experimentation

The following assumptions are considered during the experimentation.

a. Catalyst distribution is uniform and retain its chemical properties in the MEA
b. Water and methanol solution is homogeneous in nature
c. Membrane performance is not getting deteriorated during the experimentation.
d. Methanol solution concentration is not getting altered in the reservoir till the completion of experiment.
e. Cell trim parts are compatible with methanol solution.

3.5.4 List of problems / issues arise in the experimentation

The following assumptions are considered during the experimentation.

a. Since the fuel is liquid state, leakage is identified some times.
b. Firm contact should be ensured between the current collectors and electrode wires,
c. Too much tightening of Cell assembly fasteners (exceeding 5 N-m torque) leads to membrane damage,
d. Successive experiments with different concentrations need a minimum time gap of 20 hours for getting better results.
e. Membrane should be protected from ambient air when not in use to avoid oxidation of catalysts.

Chapter4

Results and Discussions

With due consideration to required characteristics of current collectors in dilute methanol solution, experimental investigation of PDMFC performance among Stainless Steel (ASTM-A240 Grade 316L, UNS S31603), Nickel (Grade 201 ASTM-B162, UNS N02201), and Brass (ASTM-B36, UNS C26800) materials is carried out.

4.1 Effect of Current Collector materials on the performance of PDMFC

4.1.1 Nickel current collector material

PDMFC with Ni-201 current collector material is operated by varying methanol concentrations from 1M to 6M. Polarization (Voltage versus Current density) curves and power density (Power density versus Current density) curves are drawn from the experimental results. The combined polarization with superimposed power density curves is shown in figure 4.1. It is observed that fuel cells with Ni-201 current collectors produced the highest PD of 10.416 $mW.cm^{-2}$ corresponding to a CD of 49.6 $mA.cm^{-2}$ at 5M methanol concentration. The maximum current density achieved at this 5M concentration is 84.8 $mA.cm^{-2}$. As the methanol concentration increases, methanol crossover also increases. The permeated methanol and oxygen at the cathode lead to higher temperatures due to exothermic reaction, resulting in better electrochemical kinetics of oxidation and reduction reactions. This improves cell performance up to 5M. Further increase of methanol concentration beyond 5M the cell performance decreases due to evaporation of water produced by electrochemical reactions, oxidation of crossover methanol at cathode end and diffused water from anode to cathode. This evaporation of water decreases the cell temperature, leads to lowering of kinetics of chemical reactions. As the maximum current density starts to fall beyond methanol concentration of 5M, the experiments are limited to a methanol concentration of 6M.

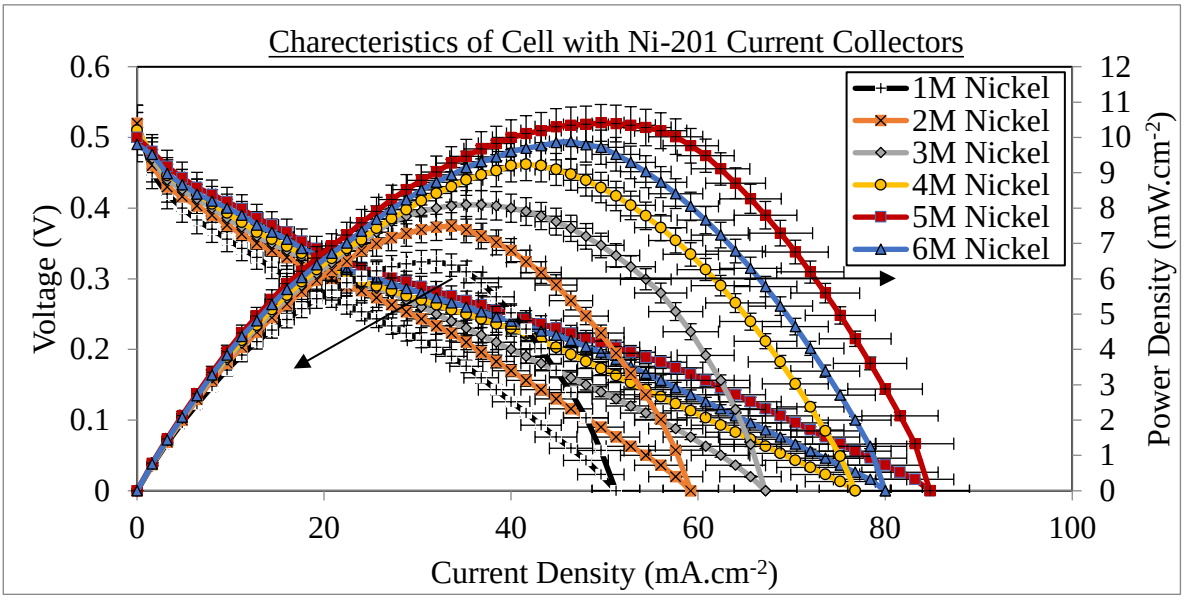

Figure 4.1 Effect of methanol concentration on combined polarization and power density characteristics of Ni-201 current collectors.

4.1.2 Brass current collector material

With Brass current collectors, the cell is tested with 1M to 4M methanol solution concentration. Polarization curves and power density curves are drawn from the experimental results. The combined polarization with superimposed power density curves is plotted and shown in figure 4.2. The cell generates the highest PD of 4.368 $mW.cm^{-2}$ corresponding to a CD of 20.8 $mA.cm^{-2}$ at 3M methanol concentration. During the experiment, the highest CD recorded is 35.2 $mA.cm^{-2}$ at 3M methanol solution. As the maximum current density starts to fall beyond a methanol concentration of 3M, the experiments are limited to a methanol concentration of 4M.

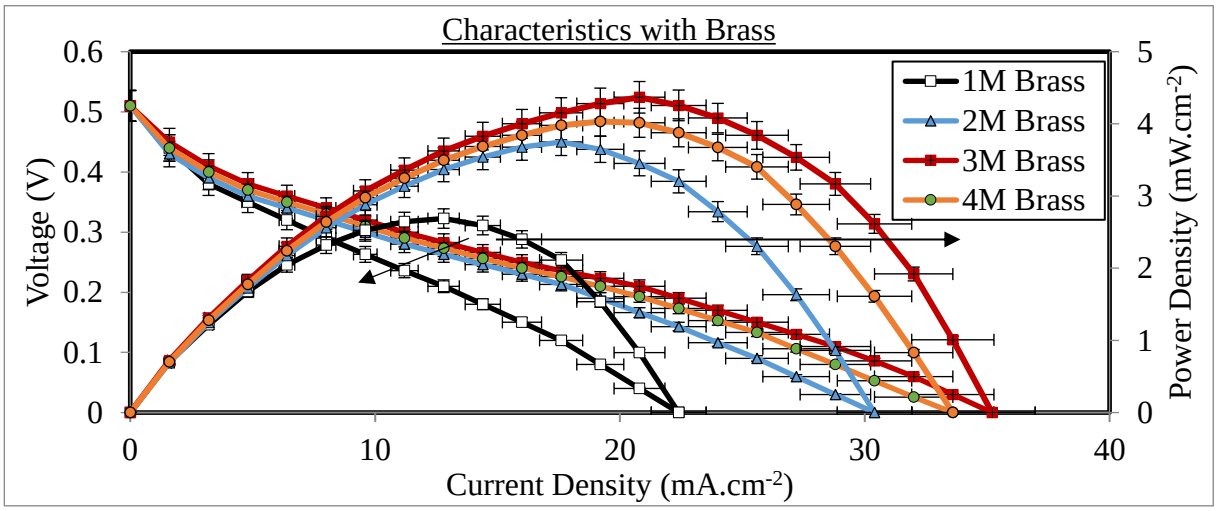

Figure 4.2 Influence of methanol concentration on combined polarization & power density characteristics of Brass current collectors

4.1.3 Stainless Steel current collector material

The PDMFC with SS-316L current collector materials is experimented with 1M to 6M methanol concentration. Polarization and power density curves are drawn from the experimental results. The combined polarization with superimposed power density curves is shown in figure 4.3. It is observed that fuel cells with SS-316L current collectors produced the peak PD of 5.712 $mW.cm^{-2}$ corresponding to a CD of 27.2 $mA.cm^{-2}$ at 5M methanol concentration. The maximum current density achieved at this 5M concentration is 56.0 $mA.cm^{-2}$. As the maximum current density starts to fall beyond a methanol concentration of 5M, the experiments are limited to a methanol concentration of 6M.

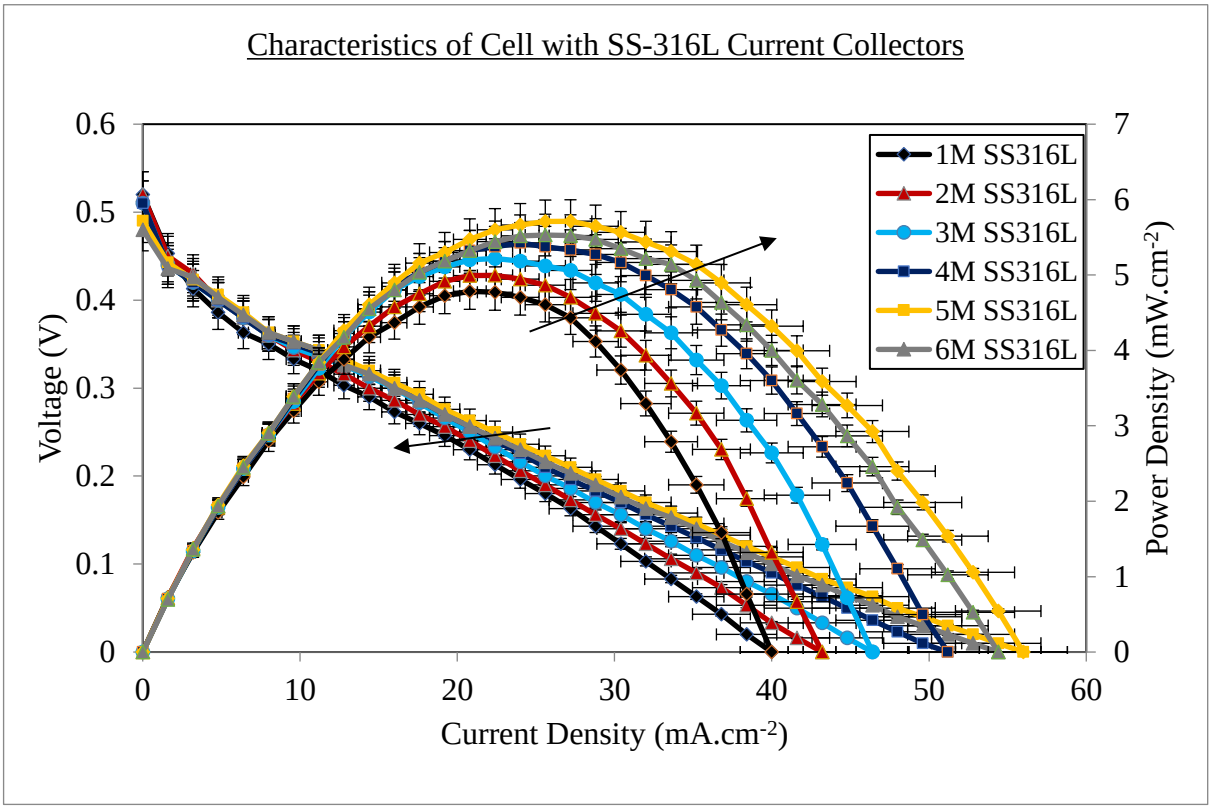

Figure 4.3 Influence of methanol concentration over combined polarization & power-density characteristics of SS-316L current collectors

Comparison of the best performance of the cell for three types of current collectors is represented in figure 4.4. From the figure, it is evident that the cell with Ni-201 current collectors is producing the highest power density and current density than Brass or SS-316L current collectors. When compared to SS-316L current collectors, cell with Ni-201 CC is producing 31.92% higher power density and cell with brass CC is producing 23.52% lower power density. The reason behind the higher power density of Ni-201 CC is attributed to low

ohmic losses due to its higher electrical conductivity along with better corrosion resistance in methanol environment and lower contact resistance as the contact surface with MEA is free from surface oxides. Brass is attacked slowly by methanol. Therefore, it is not durable in methanol environment due to the formation of metal surface oxides and hydroxides. The formed surface barriers increase the contact resistance between CC & MEA. These oxides and hydroxides are soluble in methanol. Therefore, these dissolved impurities get carried over towards MEA along with fuel and get deposited on MEA surface. This leads to the deterioration of MEA performance.

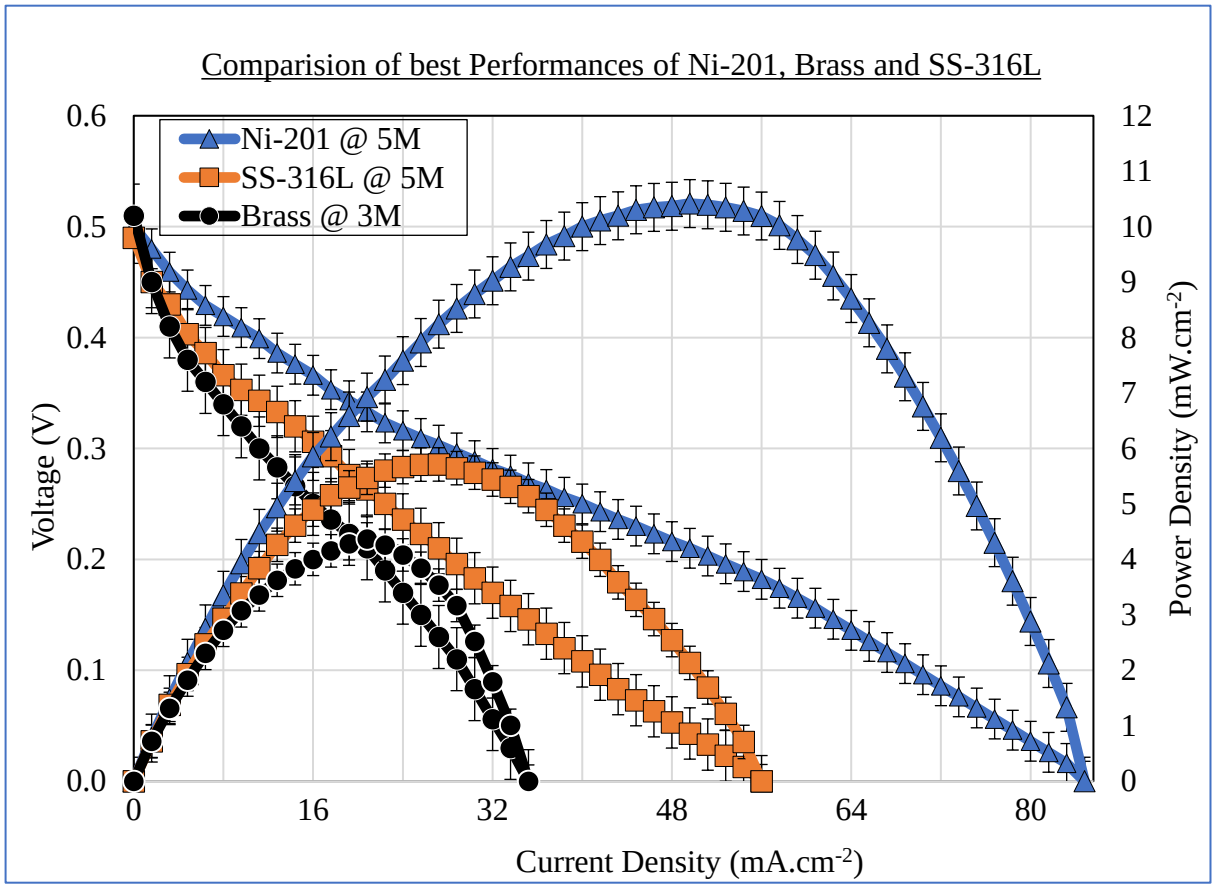

Figure 4.4 Comparison of best Performance of Nickel-201, Brass, and SS-316L current collectors

4.1.4 Effect of methanol concentration

With the experimental investigations, it is evident that Ni-201 current collectors produced a maximum OCV of 520 mV at 1M methanol solution and further this OCV falls with a rise in the concentration of methanol solution. The peak PD observed with 1M methanol is 6.496 $mW.cm^{-2}$ corresponding to a CD of 32.0 $mA.cm^{-2}$. As the methanol concentration is increased to 2M, the cell produced a maximum PD of 7.493 $mW.cm^{-2}$ against a CD of 33.6

$mA.cm^{-2}$. When the methanol concentration is further increased to 3M and 4M, the cell produced a maximum power density of 8.096 $mW.cm^{-2}$ against the CD of 35.2 $mA.cm^{-2}$ and 9.235 $mW.cm^{-2}$ corresponding to a CD of 41.6 $mA.cm^{-2}$ respectively. At 5 M methanol concentration, the cell produced its best performance of 10.416 $mW.cm^{-2}$ with respect to CD of 49.6 $mA.cm^{-2}$. At 6M methanol concentration, the performance of the cell fell and the highest PD recorded is 9.883 $mW.cm^{-2}$ corresponding to CD of 46.4 $mA.cm^{-2}$. During the series of experiments with Ni-201 current collectors, the peak CD achieved is 84.8 $mA.cm^{-2}$ at 5M Methanol concentration. The better performance of Ni-201 is due to better electrochemical kinetics of oxidation and reduction reactions at 5M concentration.

With Brass current collectors, the cell produced a maximum OCV of 510 mV at 1M methanol and further this OCV fell with a rise in the concentration of methanol solution. The peak PD observed at 1M concentration is 2.688 $mW.cm^{-2}$ corresponding to a CD of 12.8 $mA.cm^{-2}$. When the methanol concentration is increased to 2M, the cell produced a maximum PD of 3.749 $mW.cm^{-2}$ corresponding to a CD of 17.6 $mA.cm^{-2}$. At 3M methanol, the cell gave its best performance, a peak PD of 4.368 $mW.cm^{-2}$ corresponding to a CD of 20.8 $mA.cm^{-2}$. At 4M methanol, the performance of the cell fell and the peak PD recorded is 4.032 $mW.cm^{-2}$ at a CD of 19.2 $mA.cm^{-2}$. During the series of experiments with brass current collectors, the peak CD recorded is 35.2 $mA.cm^{-2}$ at 3M methanol solution.

With the experimental investigations, it is evident that SS-316L current collectors produced a maximum OCV of 510 mV at 1M methanol solution and further this OCV falls with a rise in the concentration of methanol solution. The peak PD observed with 1M methanol is 4.784 $mW.cm^{-2}$corresponding to a CD of 20.8 $mA.cm^{-2}$. As methanol concentration is raised to 2M, the cell produced a maximum PD of 4.995 $mW.cm^{-2}$against a CD of 22.4 $mA.cm^{-2}$. When the methanol concentration is further increased to 3M and 4M, the cell produced a maximum power density of 5.219 $mW.cm^{-2}$against the CD of 22.4 $mA.cm^{-2}$ and 5.424 $mW.cm^{-2}$ corresponding to a current density of 24.0 $mA.cm^{-2}$ respectively. At 5 M methanol concentration, the cell produced its best performance of 5.712 $mW.cm^{-2}$with respect to CD of 27.2 $mA.cm^{-2}$. At 6M methanol concentration, the performance of the cell fell and the highest PD recorded is 5.530 $mW.cm^{-2}$corresponding to CD of 25.6 $mA.cm^{-2}$. During the series of experiments with SS-316L current collectors, the highest CD achieved is 56.0 $mA.cm^{-2}$ at 5M methanol concentration.

Effect of methanol concentration on maximum Current Density of Ni-201, Brass, and SS-316L current collectors is shown in figure 4.5 and the effect of methanol concentration on the maximum power density of Ni-201, Brass, and SS-316L current collectors is shown in figure 4.6.

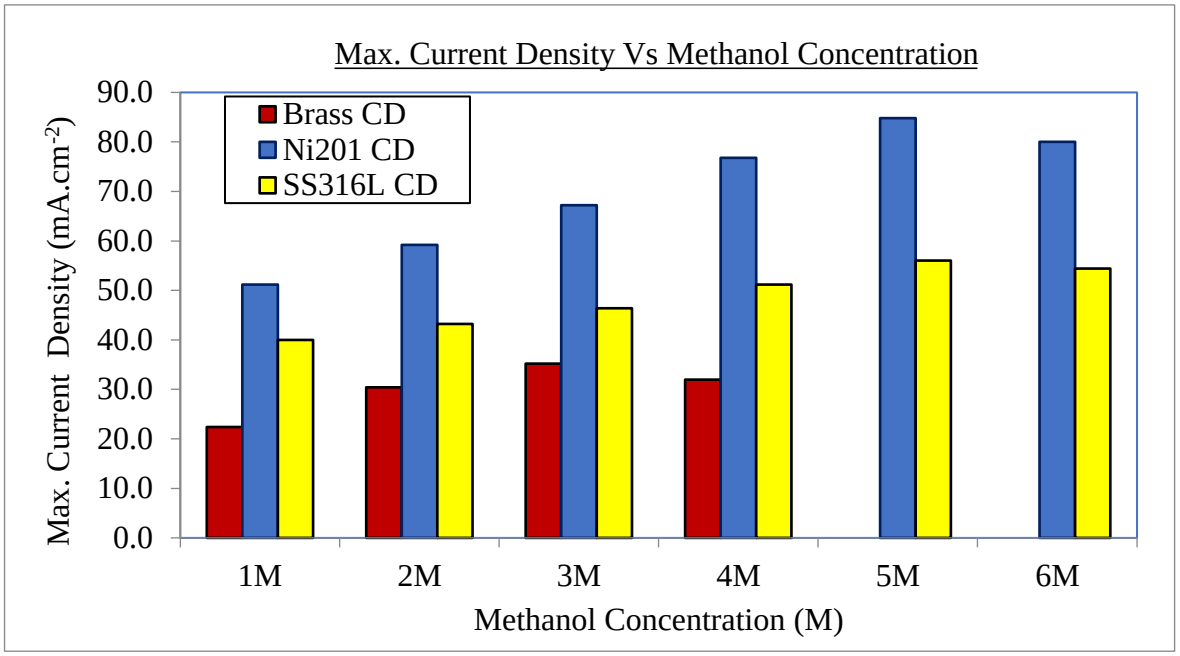

Figure 4.5 Effect of methanol concentration on maximum Current Density of Nickel-201, Brass, and SS-316L current collectors

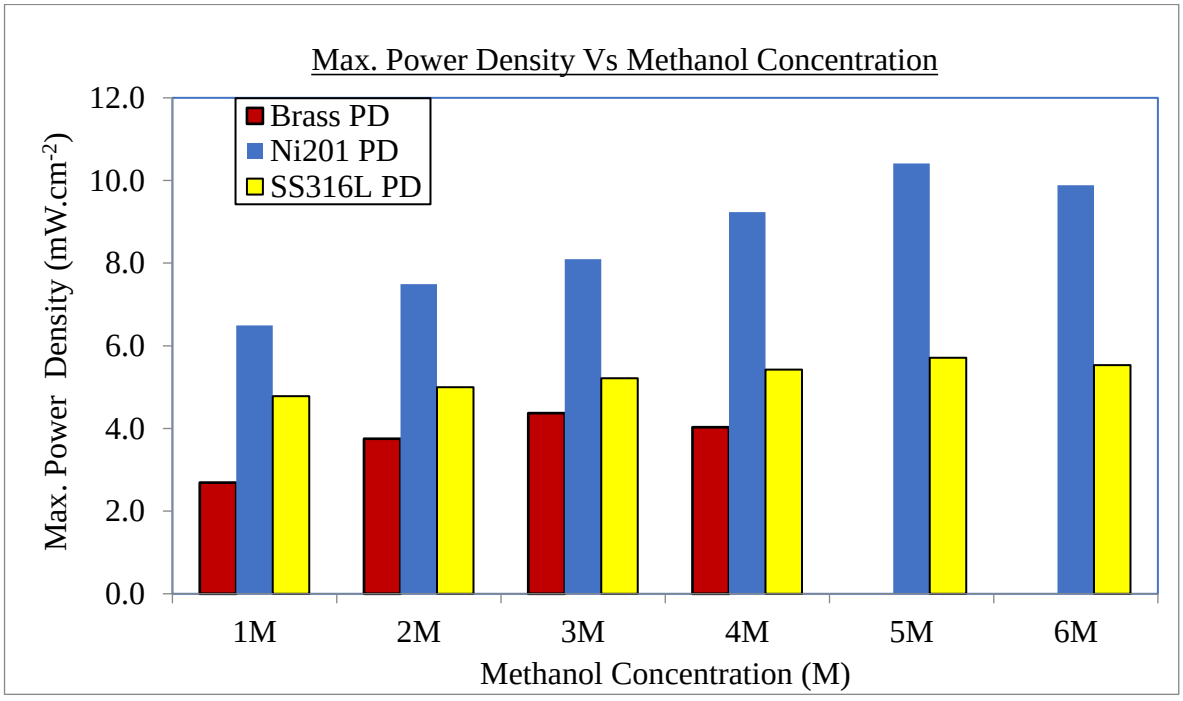

Figure 4.6 Effect of methanol concentration on the maximum power density of Ni-201, Brass, and SS-316L current collectors

4.1.5 Durability of Current Collectors

As it is observed that the current collector at anode side deteriorate quickly than that at cathode, anodic current collectors are chosen for the study of corrosion and loss of material. In dilute solutions of methanol, brass reacts and forms metal oxides. Photographs of the brass CC before start of the experiment and after exposing to methanol environment at different concentrations are shown in figures 4.7 (a) to (d).

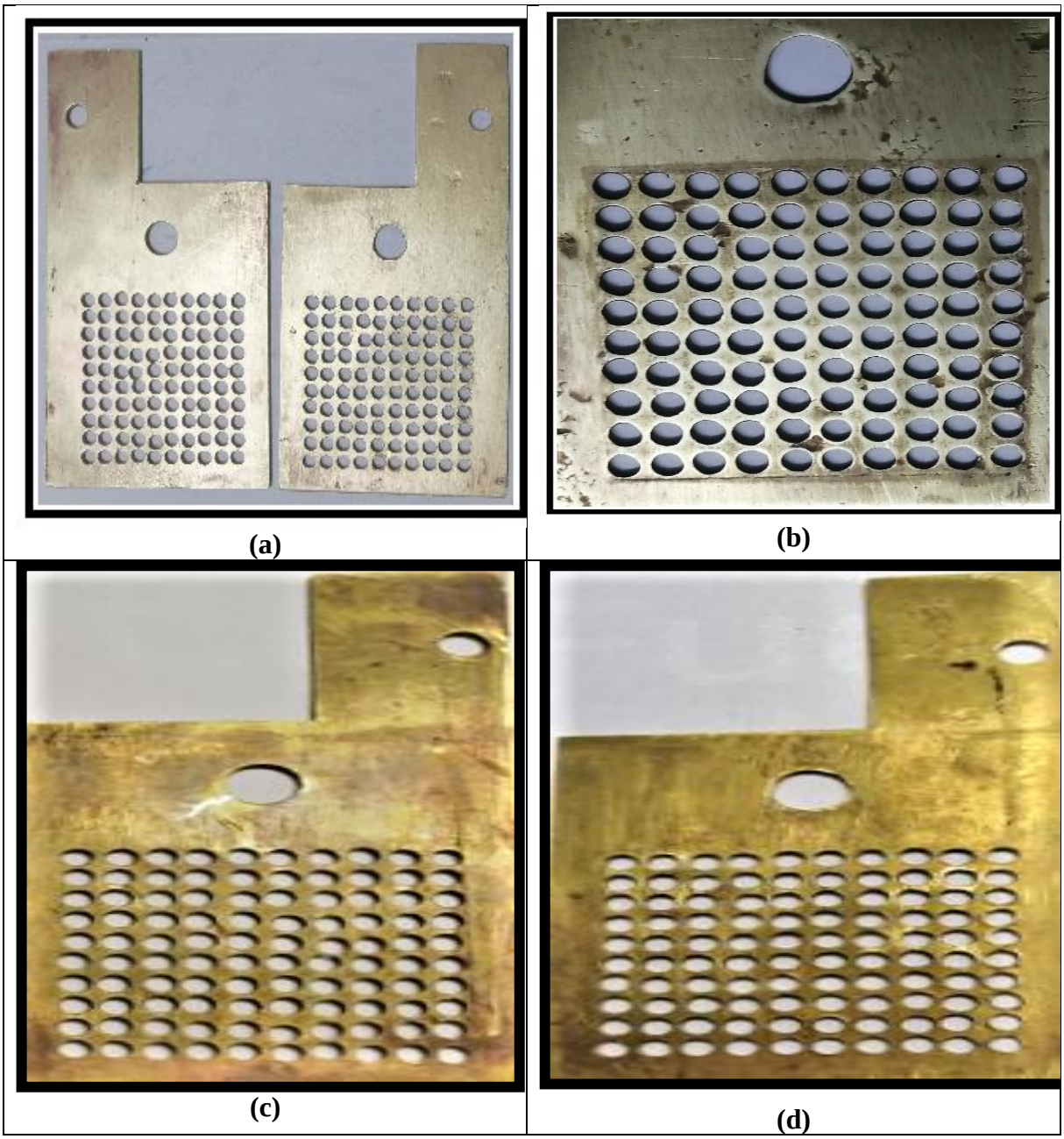

(a) Brass electrodes before the start of the experiment, (b) Brass at cathode side after exposure to 4M methanol, (c) Brass at anode side after exposure to 3M methanol, (d) Brass at anode side after exposure to 4M methanol

Figure 4.7 Brass current collectors

These oxides and corrosion products may get deposited on the membrane and also act as barrier between metallic conductors and membrane, leading to reduced performance of the cell. So, the use of brass materials especially at anodic end might not be a good choice. For short-term working, its use at cathode end may be considered.

Short term corrosion rate of the CC materials during the experiment is calculated and tabulated by taking the weights before and after the experiment. The time of exposure to methanol solution is also recorded during the test. Comparison of experimental corrosion rates with respect to SS-316L material is also calculated and tabulated in table 4.1.

Calculation details

Density of the material $= \rho$ g/cm^3

Thickness of CC $= \xi$ mm

Weight Before the experiment $= \omega 1$ g

Weight after the experiment $= \omega 2$ g

Weight Loss $= (\omega 1 - \omega 2)$ g

Duration of experiment (in hours) $= \theta$ h

Constant, $\prod$ $=3.14$

Effective surface area (Exposed surface area to methanol), A_s

$= (50*50-100*\prod/4*3.8*3.8)*2+100*\prod*3.8*\xi$ mm^2

Experimental Corrosion Rate $=[(\omega 1-\omega 2)/\theta]*[\ 1/\ (1000 * \rho * A_s)] *[24*365]$ mm/year

Table 4.1 Short-Term Corrosion Measurement Data

Data / Materials	**SS-316L**	**Nickel-201**	**Brass (66-34)**
Density of the material, ρ g/cm^3	7.90	8.89	8.50
Thickness of CC, ξ mm	2.01	1.98	1.99
Weight before the experiment, $\omega 1$ g	89.1572	97.8724	94.3231
Weight after the experiment, $\omega 2$ g	89.1546	97.8720	94.2901
Weight loss, g	0.0026	0.0004	0.0330
Duration of exposure θ h	12	12	12
Effective Surface area of the current collector, mm^2	5131.25	5095.45	5107.39
Experimental Corrosion rate in mm/year	0.047	0.006	0.555
Comparison of experimental corrosion rates with respect to SS-316L material.	100% (Assumed reference)	12.7% (~1/8thof SS corrosion rate)	1180% (11.8 times of SS corrosion rate)

4.1.6 Summary

The important contributing factors of current collectors influence the PDMFC performance are ohmic losses, corrosion resistance, and contact resistance. The metallic current collectors are prone to corrosion as the surfaces that are exposed to methanol form insulating surface oxides, resulting in contact resistance and membrane poisoning.

Experimental examination of the effect of better electrical conductivity together with corrosion resistance of Ni-201 and Brass current collectors is performed at various concentrations of methanol solution. The results are compared with stainless-steel grade 316L current collector having the same geometry, aspect ratio, and effective opening area.

It is revealed from the experimental results that:

- The cell with Ni-201 current collectors is producing the highest power density & maximum current density when compared to brass and SS-316L current collectors.
- The maximum power density of cell obtained using Ni-201 current collectors is 10.416 $mW.cm^{-2}$ at 5M methanol concentration.
- The maximum power density of cell with brass current collectors is 4.368 $mW.cm^{-2}$ at 3M concentration and with Stainless steel current collectors it is 5.712 $mW.cm^{-2}$ at 5M methanol concentration.
- Cell with Ni-201 current collectors is producing 31.92% higher power density than with SS-316L current collectors, whereas with brass current collectors it is producing 23.52% lower power density than with SS-316L current collectors.
- With respect to the effect of methanol concentration on maximum current density, the cell with Ni-201 CC is producing a higher current density of 84.8 $mA.cm^{-2}$ at 5M compared to the cell with SS-316L CC, which is producing 56.0 $mA.cm^{-2}$ at the same methanol concentration.
- The corrosion compatibility tests showed degradation of brass CC after a short-term exposure to methanol during the operation of cell for a period of 12 h.
- As Brass is identified as less durable in dilute methanol environment due to formation of surface metal oxides. Due to this, the use of brass as current collector material at anode is not a good choice, however, its use in cathode side can be considered.

4.2 Performance of Passive Direct Methanol Fuel Cell using current collectors with taper cylindrical openings for better CO_2 scavenging

At anode side of the cell, the current collector allows methanol solution and carbon dioxide to pass through it. Further, it collects the electric current from the Membrane Electrode Assembly (MEA). Whereas the cathode end current collector receives electrons and also provide transportation of products. It is observed in previous section that, the anode side current collector with uniform cylindrical openings the CO_2 evolved gas bubbles block the passage of fuel to membrane. This experimental study has been taken up by modifying the present design of uniform cylindrical openings to taper cylindrical openings with material of construction as SS-316L and Ni-201in methanol environment.

4.2.1 Performance of PDMFC using SS-316L current collectors with taper cylindrical openings

The PDMFC is operated by placing SS-316L taper cylindrical openings current collectors using 1M to 4M methanol concentrations. The performance of cell is examined by plotting Polarization and Power density curves as shown in figures 4.8 and 4.9 respectively.

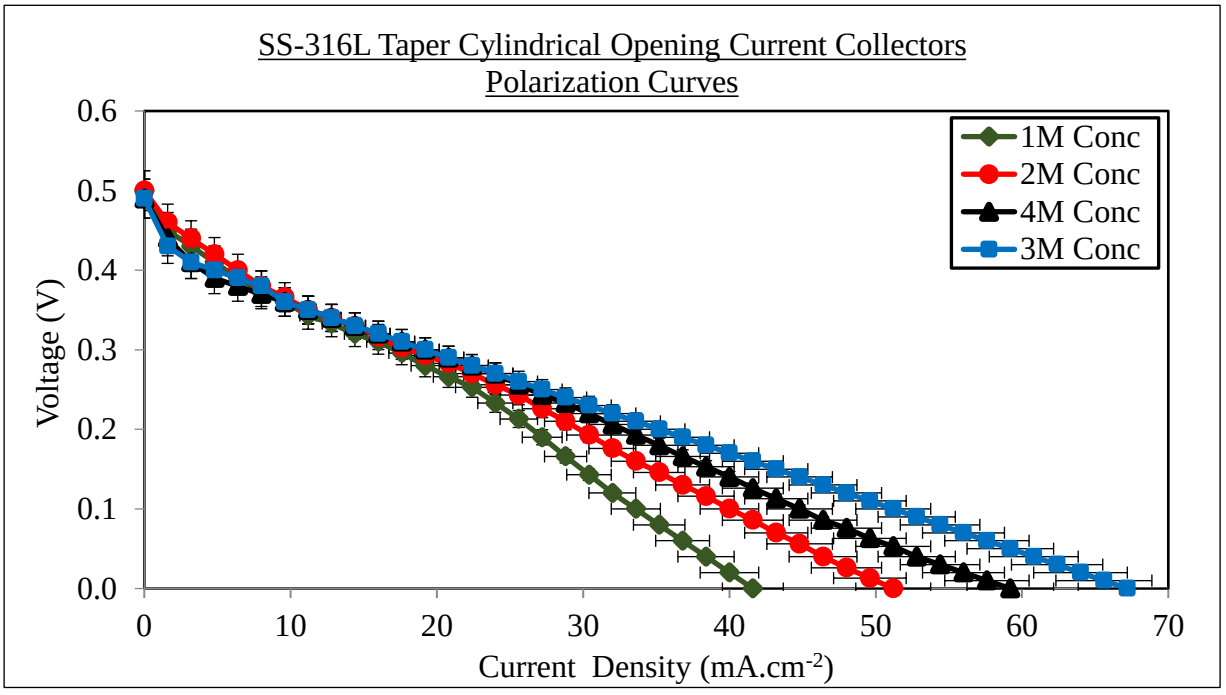

Figure 4.8 Performance of Taper cylindrical opening current collectors (polarization Curves) with SS-316L

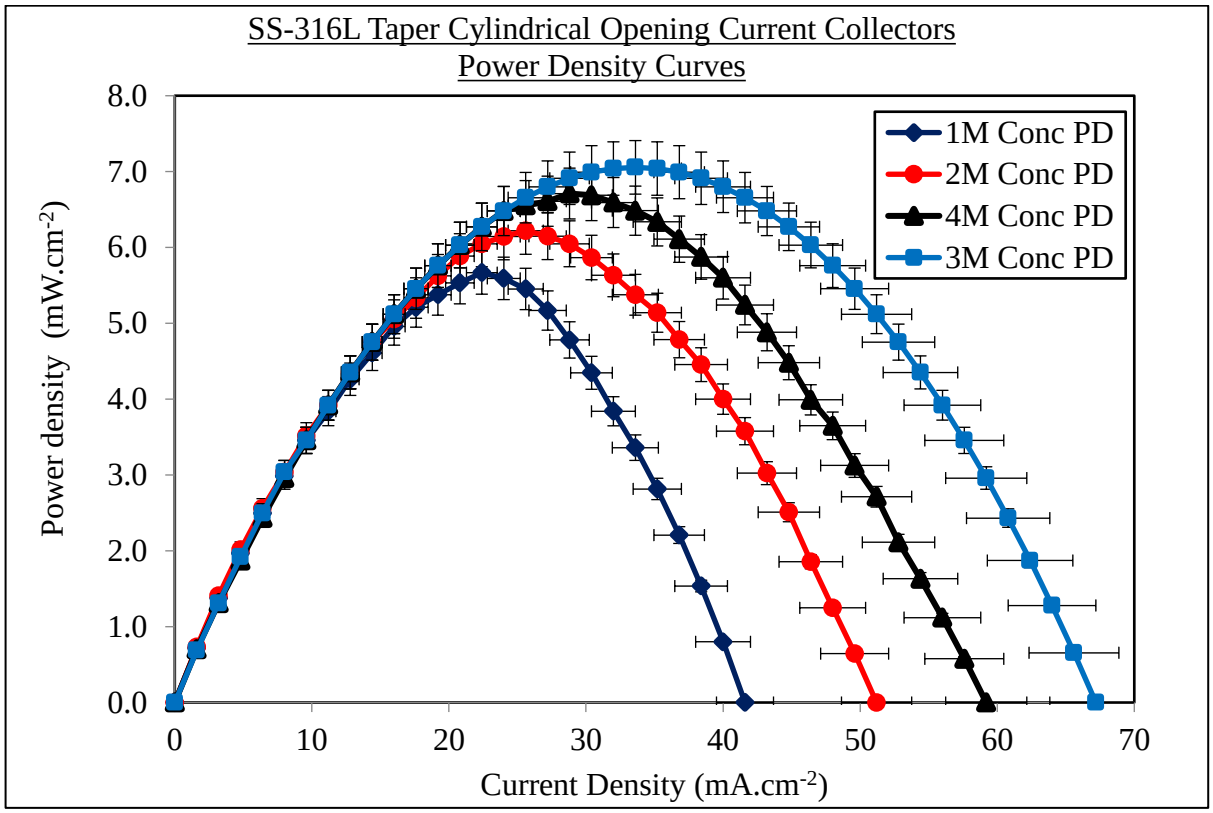

Figure 4.9 Performance of Taper cylindrical opening current collectors (Power Density Curves) with SS-316L

From the plot, it is clear that the cell highest power density is 7.056 $mW.cm^{-2}$ at 3M methanol solution concentration, corresponding to a current density of 33.6 $mA.cm^{-2}$. In this experiment, the maximum current density recorded is 67.2 $mA.cm^{-2}$.

From these curves, it is observed that the PMDFC with taper cylindrical opening current collectors perform better due to the buoyancy on CO_2 bubble is more effective in taper cylindrical openings (due to larger bubble volume accommodation than that in the case of uniform cylindrical opening).

Whereas in taper cylindrical openings, the positive slope in the tapered surface allows the methanol fuel to flow more easily to the membrane site leading to continuous chemical reaction kinetics.

The effect of methanol concentration on maximum power density and current density of PDMFC is shown in figure 4.10 for SS-316L.

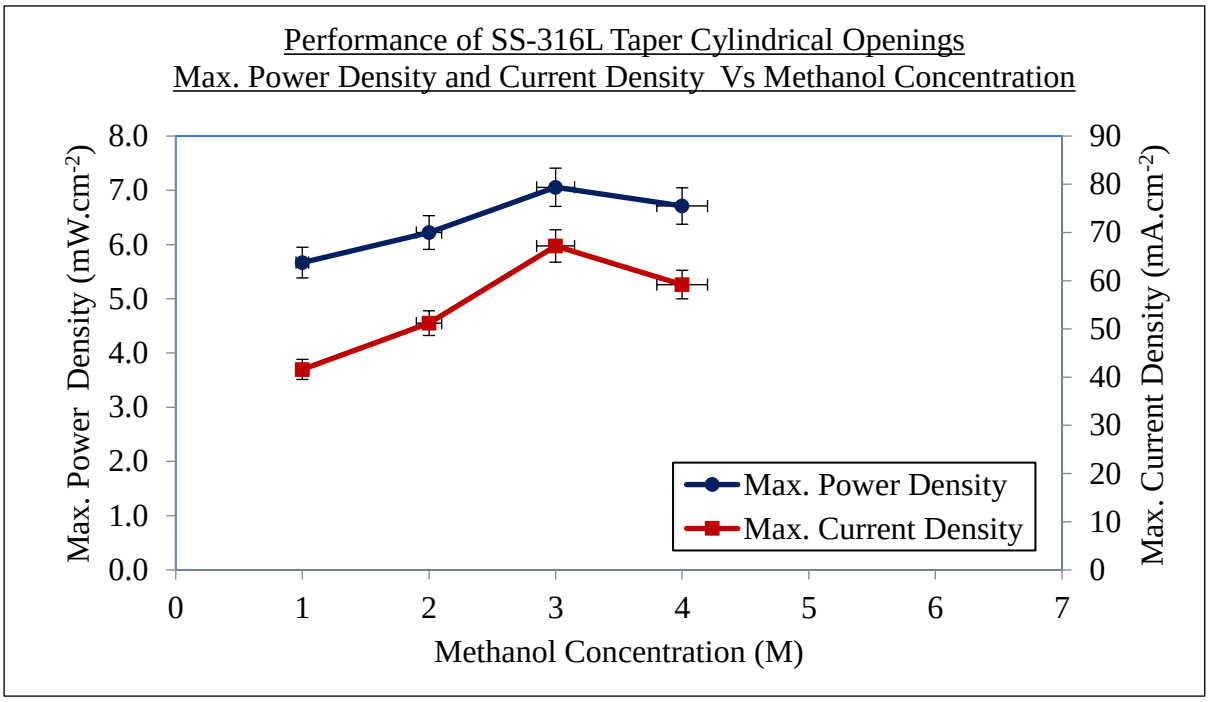

Figure 4.10 Performance of PDMFC using SS-316L CC with Taper cylindrical opening current collectors (at maximum Power Density and maximum Current Density) versus varying methanol solution concentrations.

As the methanol concentration is increased up to 3M, the current density also got increased to a value of 67.2 $mA.cm^{-2}$ and then it got reduced at methanol concentrations above 3M. The reason for the reduction of performance is predominant cross-over of methanol towards the cathode at higher concentrations. Trends of power density also follow the similar path i.e., the power density increases to a value of 7.056 $mW.cm^{-2}$ corresponding to a methanol concentration of 3M and then it starts decreasing at methanol concentrations higher than 3M.

4.2.2 Performance of PDMFC using Ni-201 current collectors with taper cylindrical openings

The PDMFC is operated by placing Ni-201 taper cylindrical openings current collectors using 1M to 4M methanol concentrations. The performance of cell is examined by plotting Polarization and Power density curves as shown in figures 4.11 and 4.12 respectively.

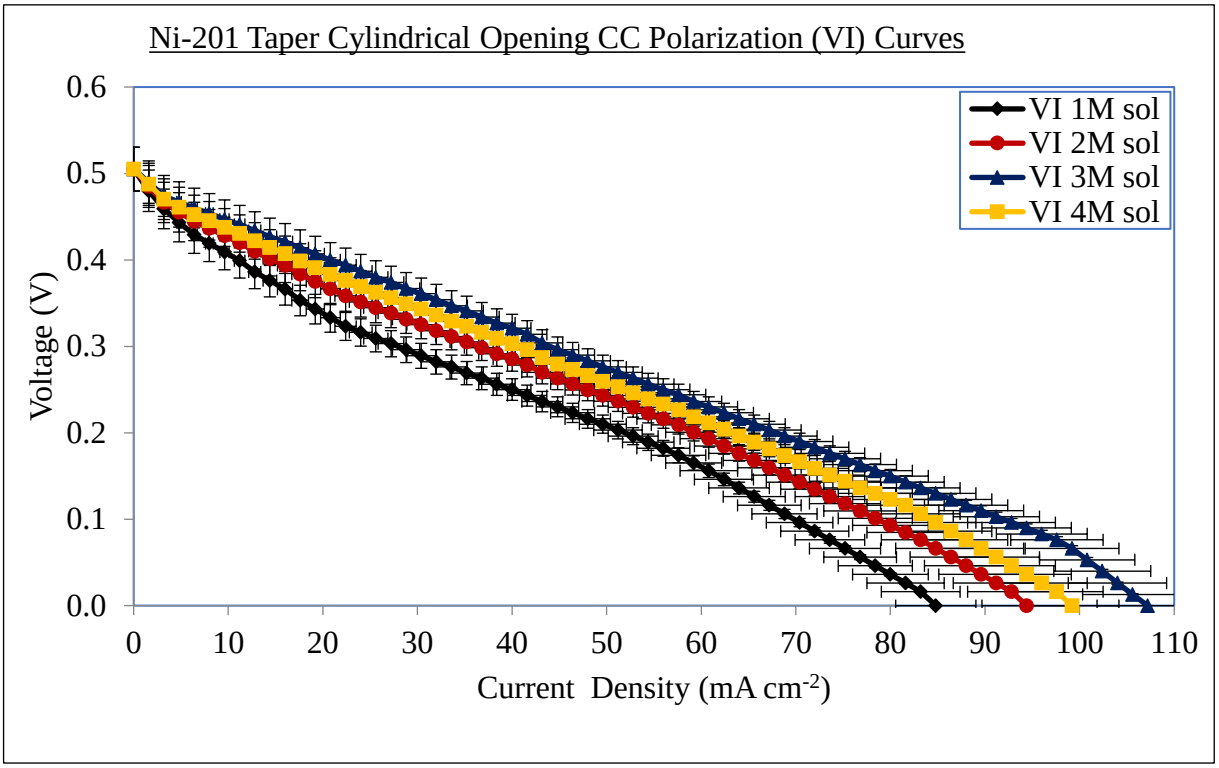

Figure 4.11 Performance of Taper cylindrical opening current collectors (Polarization curves with Ni-201)

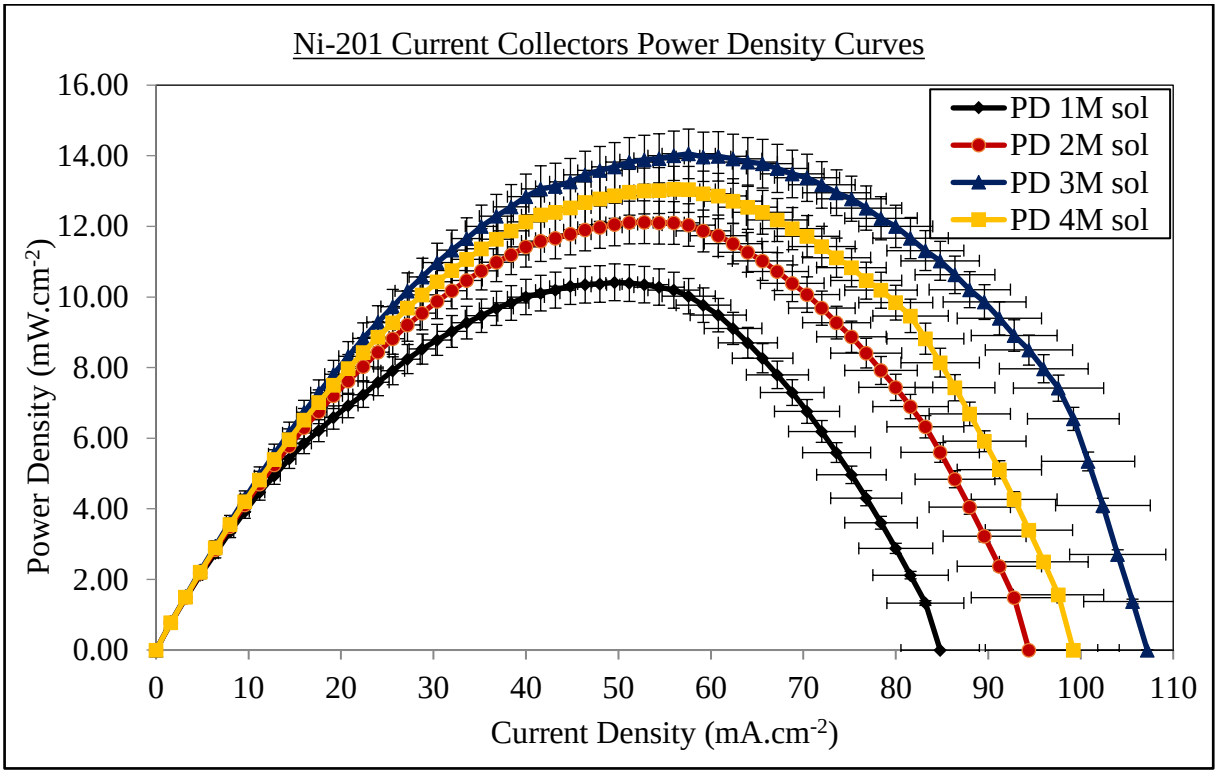

Figure 4.12 Performance of Taper cylindrical opening current collectors (Power density Curves) with Ni-201

From the plot, it is clear that the cell highest power density is 14.054 $mW.cm^{-2}$ 3M methanol solution concentration, corresponding to a current density of 57.6 $mA.cm^{-2}$. In this experiment, the maximum current density recorded is 107.2 $mA.cm^{-2}$.

The cell performance is better with Ni-201 taper cylindrical opening CCs due to higher electrical conductivity together with corrosion resistance over SS-316L CCs for the same molarity of methanol concentration.

The effect of methanol concentration on maximum power density and current density of PDMFC is shown in figure 4.13 for Ni-201.

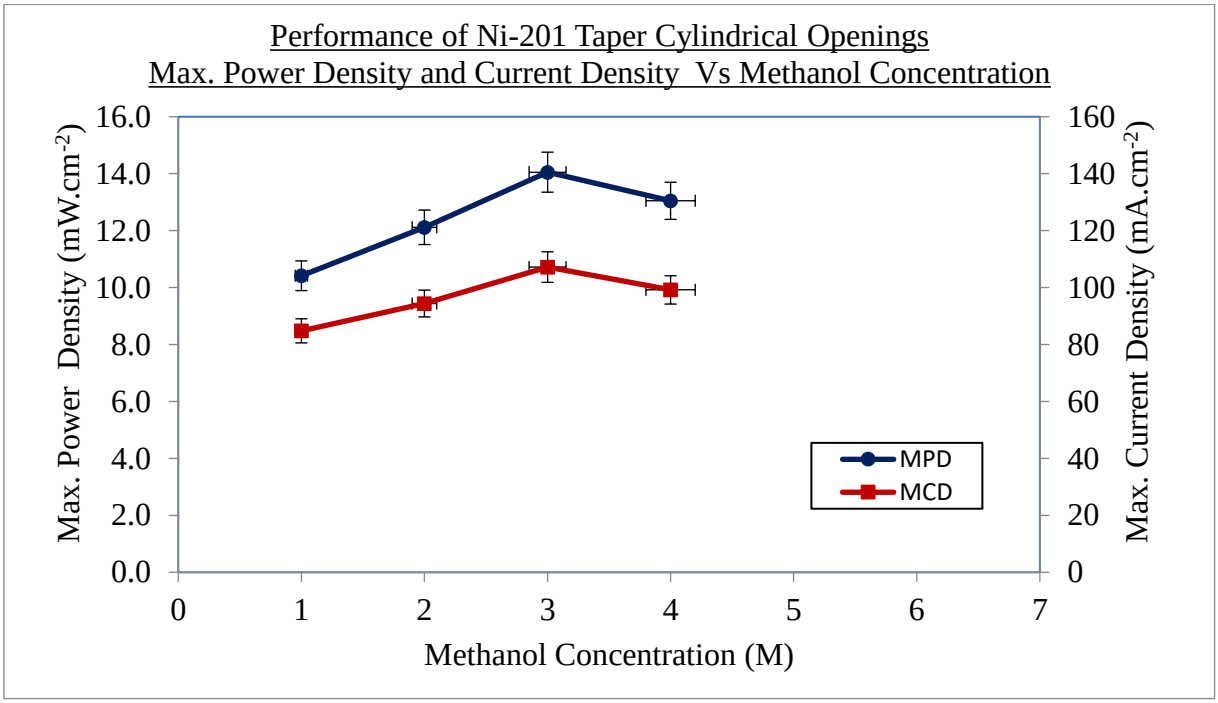

Figure 4.13 Performance PDMFC using Ni-201 CC with Taper cylindrical opening current collectors (at maximum Power Density and maximum Current Density) versus varying methanol solution concentrations.

As the methanol concentration is increased up to 3M, the current density also got increased to a value of 107.2 $mA.cm^{-2}$ and then it got reduced at methanol concentrations above 3M. The reason for the reduction of performance is predominant cross-over of methanol towards the cathode at higher concentrations. Trends of power density also follow the similar path i.e., the power density increases to a value of 14.054 $mW.cm^{-2}$ corresponding to a methanol concentration of 3M and then it starts decreasing at methanol concentrations higher than 3M.

4.2.3 Performance comparison of PDMFC with taper cylindrical opening current collectors over uniform cylindrical opening current collectors

Comparison of performance of PDMFC at 3M methanol solution,with taper cylindrical opening current collectors over uniform cylindrical opening current collectors by plotting polarization and power density curves are shown in figures 4.14 and 4.15 respectively for SS-316L materials. These performance curves using Ni-201 CC are plotted as shown in figures 4.16 and 4.17.

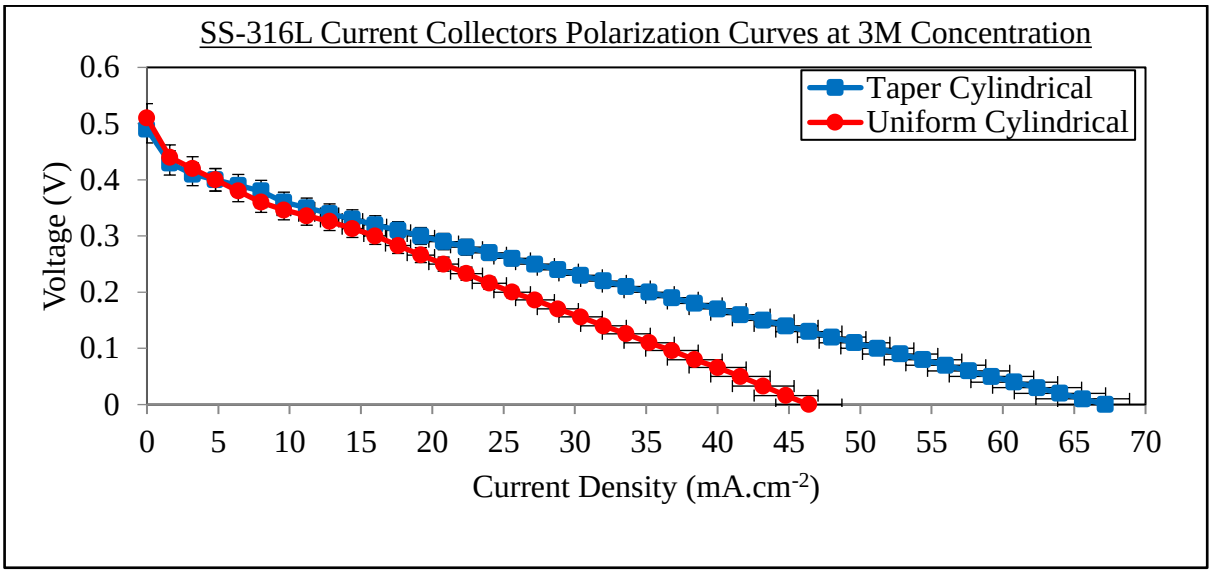

Figure 4.14 Performance of SS-316L uniform cylindrical and taper cylindrical opening current collectors (Polarization Curves) at 3M Methanol solution.

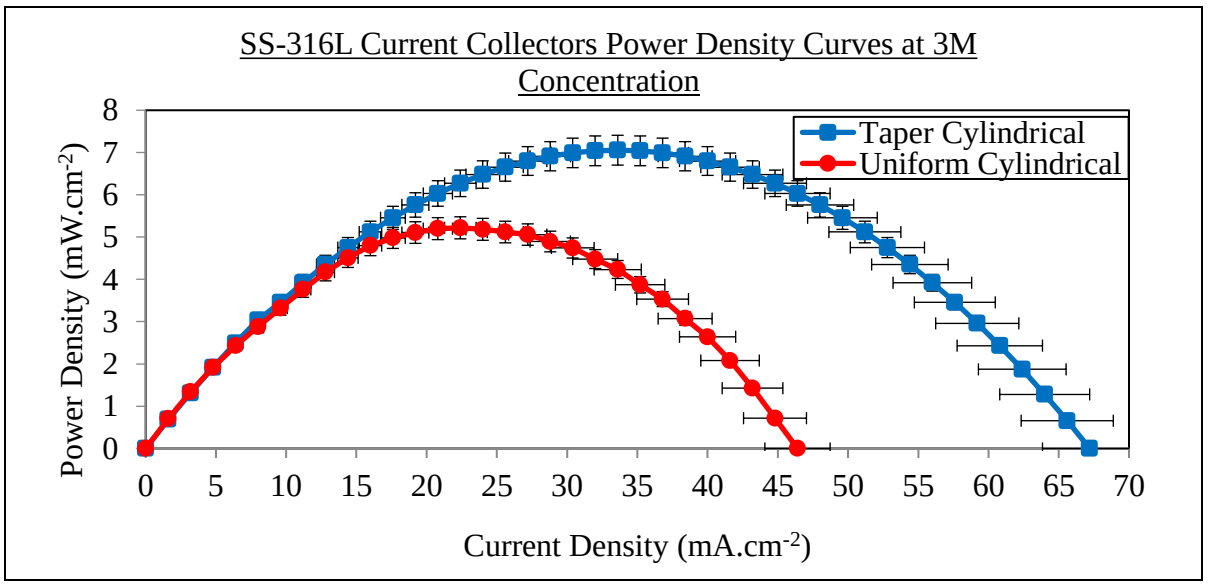

Figure 4.15 Performance of SS-316L uniform cylindrical and taper cylindrical opening current collectors (Power Density Curves) at 3M Methanol solution.

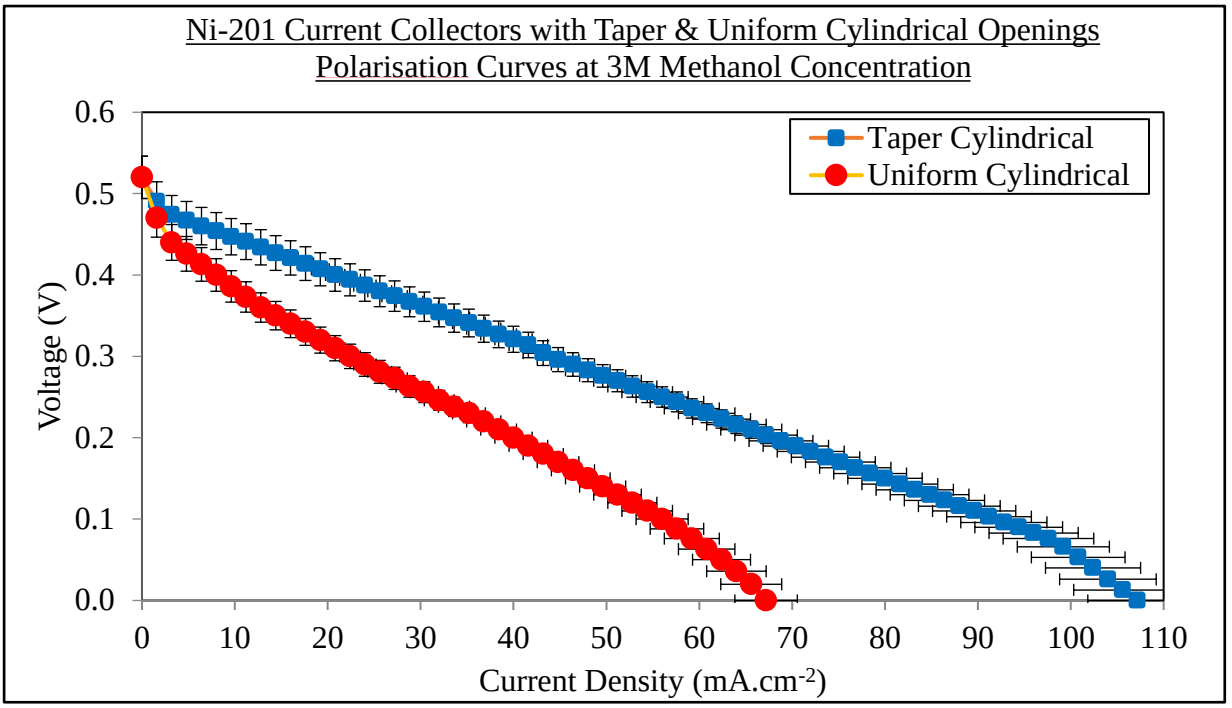

Figure 4.16 Performance of Ni-201 uniform cylindrical and taper cylindrical opening current collectors (Polarization Curves) at 3M Methanol solution.

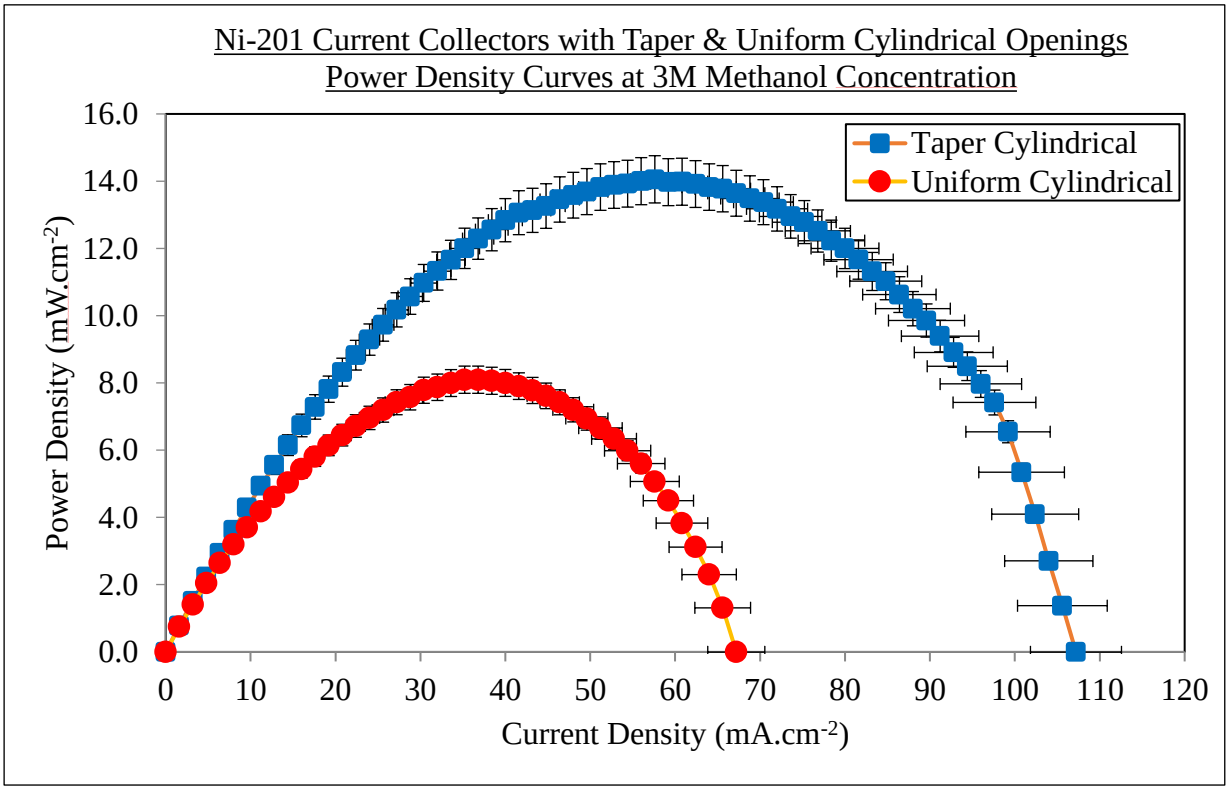

Figure 4.17 Performance of Ni-201 uniform cylindrical and taper cylindrical opening current collectors (Power Density Curves) at 3M Methanol solution.

From these curves, it is observed that the PDMFC with taper cylindrical opening current collectors perform better than uniform cylindrical opening current collectors. In uniform cylindrical openings, the evolved CO_2 gas bubble blocks the passage of fuel to membrane, resulting in starvation of fuel at the reaction site leading to cell lower performance. It is evident that buoyancy on CO_2 bubble is more effective in taper cylindrical openings due to larger bubble volume accommodation than that in the case of uniform cylindrical opening.

The PDMFC at 3M methanol solution with SS-316L as material of construction of current collector, the maximum current density recorded is 67.2 $mA.cm^{-2}$ with taper cylindrical openings whereas it is 46.4 $mA.cm^{-2}$ with uniform cylindrical openings as shown in figure 4.14. The maximum recorded power densities with taper cylindrical opening current collectors and uniform cylindrical opening current collectors are 7.056 $mW.cm^{-2}$ and 5.219 $mW.cm^{-2}$ respectively as shown in figure 4.15. This indicates that the PDMFC with taper cylindrical opening current collectors perform 1.35 times more or 35.19% higher in terms of power density when compared to uniform cylindrical opening current collectors at 3M methanol concentration.

The PDMFC at 3M methanol solution with Ni-201 as material of construction of current collector, the maximum current density recorded is 107.2 $mA.cm^{-2}$ with taper cylindrical openings whereas it is 67.2 $mA.cm^{-2}$ with uniform cylindrical openings as shown in figure 4.16. The maximum recorded power densities with taper cylindrical opening current collectors and uniform cylindrical opening current collectors are 14.054 $mW.cm^{-2}$ and 8.096 $mW.cm^{-2}$ respectively as shown in figure 4.17. This indicates that the PDMFC with taper cylindrical opening current collectors perform 1.73 times more or 73.5% higher in terms of power density when compared to uniform cylindrical opening current collectors at 3M methanol concentration.

4.2.4 Effect of Methanol concentration on Current Collectors openings

The performance characteristics of uniform cylindrical and taper cylindrical opening current collectors against varying methanol concentrations are plotted as shown in figures 4.18 & 4.19 with SS-316L CC and in figures 4.20 & 4.21 with Ni-201 CC. From these curves, it is inferred that the power and current densities of uniform cylindrical and taper cylindrical opening current collectors have an increasing trend up to 5M and 3M methanol concentrations

respectively. At methanol concentrations beyond the above said values, cell is showing reduction in performance due to methanol cross over towards cathode.

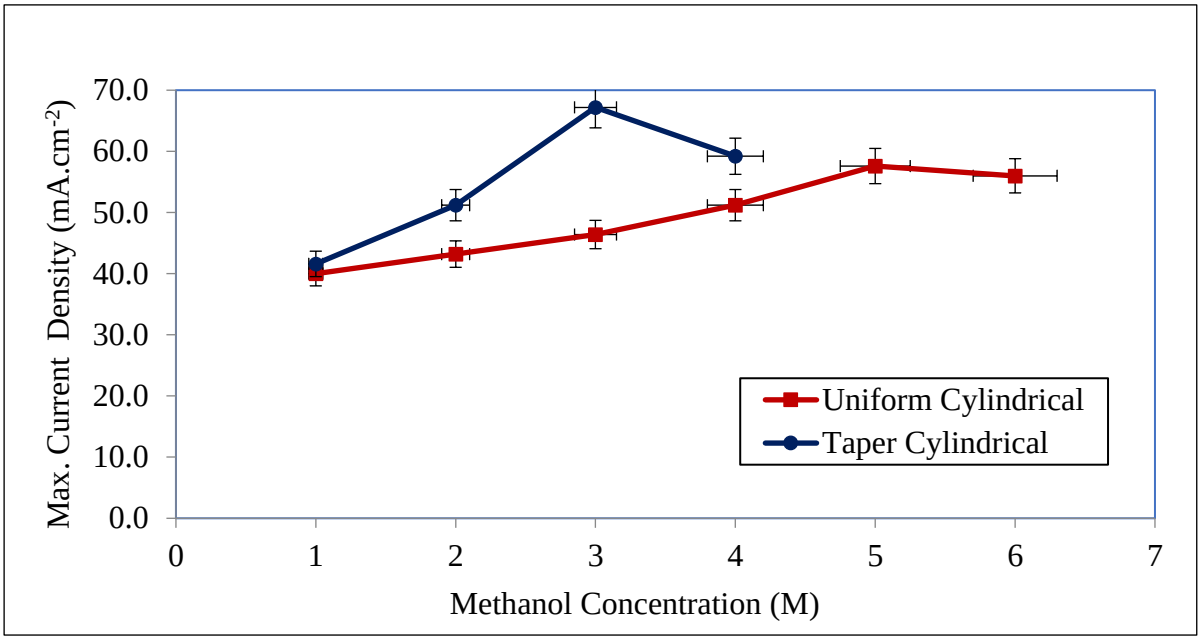

Figure 4.18 Performance of PDMFC using SS-316L with uniform cylindrical and taper cylindrical opening current collectors (at maximum current density) versus methanol concentrations.

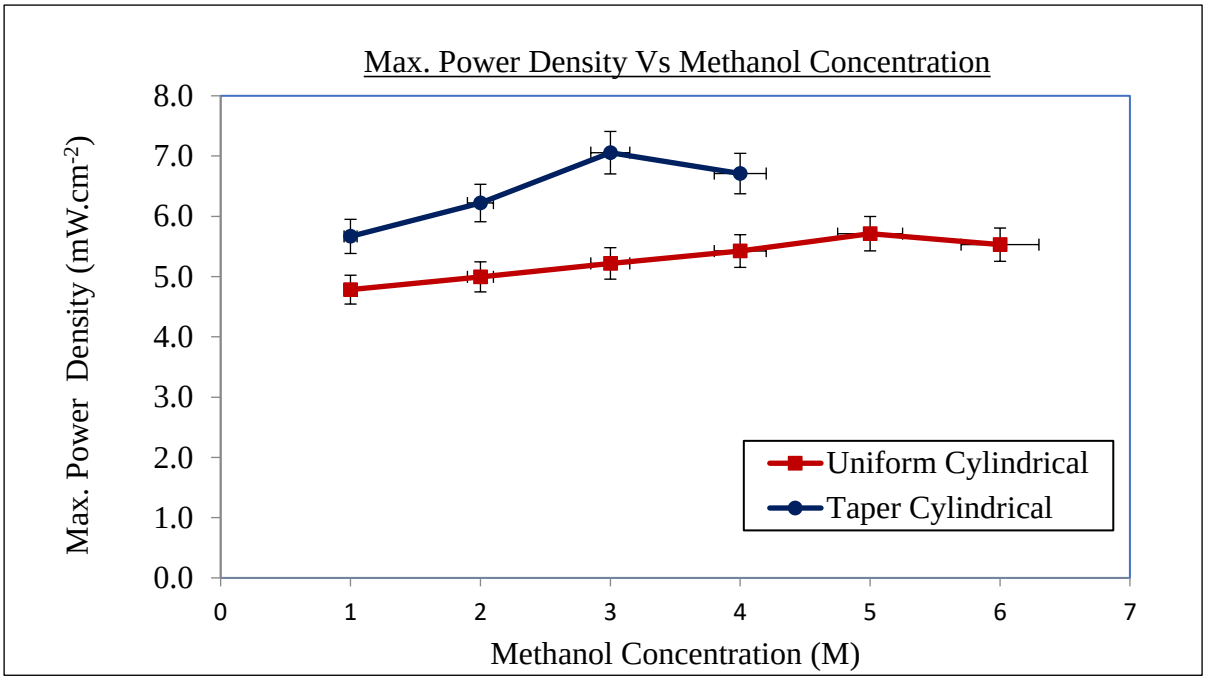

Figure 4.19 Performance of PDMFC using SS-316L with uniform and taper cylindrical opening current collectors (at maximum power density) versus methanol concentration.

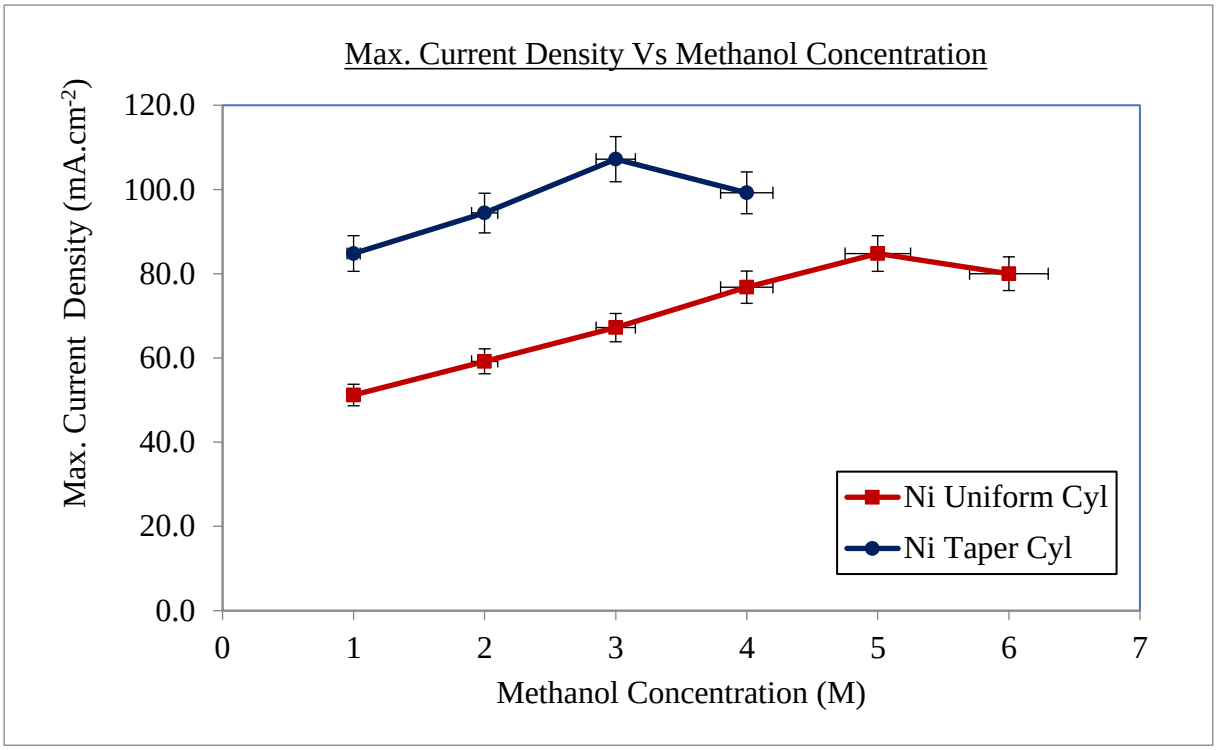

Figure 4.20 Performance of PDMFC using Ni-201 with uniform cylindrical and taper cylindrical opening current collectors (at maximum current density) versus methanol concentration.

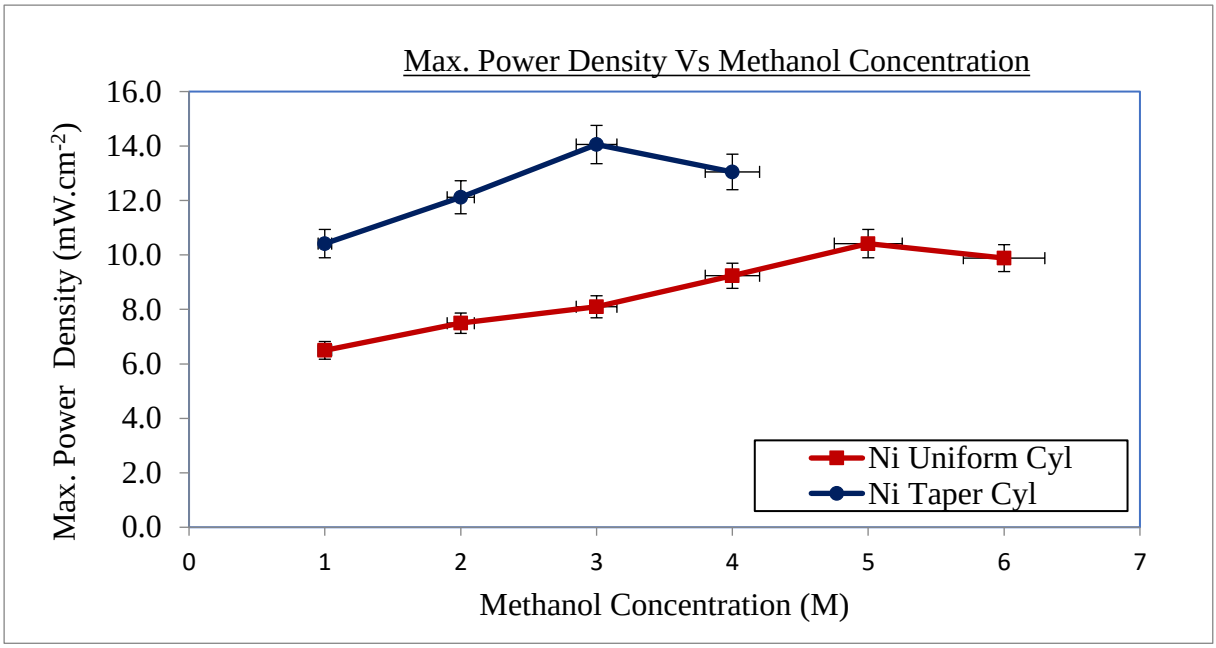

Figure 4.21 Performance of PDMFC using Ni-201 with uniform cylindrical and taper cylindrical opening current collectors (at maximum power density) versus methanol concentrations.

4.2.5 Effect of taper cylindrical current collectors on gravimetrical power density of PDMFC

The taper cylindrical openings of CC are in the shape of truncated cone; hence, there is a reduction in the total volume of the current collectors over uniform cylindrical openings. The difference in the volume of uniform and taper cylindrical opening and their corresponding weight of material removed is calculated (taking the density of SS-316L as 7900 kg/m^3). The Percentage reduction in weight of a Taper Cylindrical opening over uniform cylindrical opening is tabulated in table 4.2. The percentage reduction in weight of Taper Cylindrical openings Current Collector is tabulated in table 4.3.

Table 4.2 Percentage reduction in weight of each Taper Cylindrical opening of Current Collector

Description	**Type of current collectors Opening**	
	Uniform cylindrical	**Taper cylindrical**
Volume of each opening	22.68 mm^3	35.11 mm^3
Weight loss due to each opening in Current Collector	0.179 g	0.246 g
Weight reduction in each opening Taper Cylindrical CC over that of Uniform cylindrical CC	0.067 g	
Percentage reduction in weight of each Taper Cylindrical opening	37.2 %	

Table 4.3 Percentage reduction in weight of Taper Cylindrical opening Current Collector

Description	**Type of current collectors Opening**	
	Uniform cylindrical	**Taper cylindrical**
Volume of Current Collector	11.218 cm^3	10.376 cm^3
Weight of Current Collector	88.623 g	81.968 g
Reduction in Current Collector weight	6.654 g	
Percentage reduction in weight of Taper Cylindrical opening Current Collector	7.50 %	

Each taper cylindrical opening resulted in a reduction of weight by about 37.2% when compared to a uniform cylindrical opening. The total reduction in weight of the taper cylindrical

current collector is 7.50% compared to uniform cylindrical opening current collector. The calculated gravimetric maximum powers using SS-316L CC for taper cylindrical openings is 2.175 W/kg and for uniform cylindrical openings, it is 1.611 W/kg. Similarly, the calculated gravimetric maximum power densities using Ni-201 CC for taper cylindrical openings is 7.60 W/kg and for uniform cylindrical openings, it is 5.20 W/kg. The reduction in weight of taper cylindrical opening current collectors leads to an overall percentage improvement in gravimetric power by 35.0% using SS-316L and 46.1% using Ni-201 against uniform cylindrical opening current collectors. This gravimetric power density improvement using taper cylindrical openings is achieved by keeping the same contact area of current collectors on either side of MEA as is the case with uniform cylindrical openings current collectors.

Similarly, specific power densities at 3M concentration (referring to concentration of methanol corresponding to max. power densities of taper cylindrical openings CC) are calculated and tabulated in table 4.4. Using SS-316L CCs the increased PDMFC specific power density with taper cylindrical openings over uniform cylindrical openings CCs is 26.1%, whereas using Ni-201 CCs, it is 27.8%.

Table 4.4 Improvement in PDMFC specific power density with taper cylindrical openings CC

Current Collectors	**Methanol Concentration**	**Max Power density, $mW.cm^{-2}$**	**Specific Power density, $mW.cm^{-2}.kg^{-1}$**	**Percentage increase in Specific Power density**
SS-316L with Uniform Cylindrical openings	3M	5.219	7.47	26.1
SS-316L with Taper Cylindrical openings	3M	7.056	9.42	
Ni-201 with Uniform Cylindrical openings	3M	9.235	14.28	27.8
Ni-201 with Taper Cylindrical openings	3M	14.054	18.25	

The specific energy generation of PDMFC is calculated based on the maximum power produced against the methanol concentration (fuel) used for a period of 3 hours, during which 50ml of fuel, that is filled in anode fuel reservoir is consumed completely. The calculated specific energy generation for each type of CC is tabulated in table 4.5.

Table 4.5 Specific energy generation of PDMFC for different current collectors

PDMFC Current Collectors	Methanol Concentr-ation	Methanol (density 0.782 g/cc) quantity used for preparing 50 ml of solution, ml	Max Power density, $mW.cm^{-2}$	Max Power obtained in, mW	Specific energy generation, kWh/L
SS-316L with Uniform Cylindrical openings	5M	10	5.712	142.80	0.043
SS-316L with Taper Cylindrical openings	3M	6	7.056	176.40	0.088
Ni-201 with Uniform Cylindrical openings	5M	10	10.416	260.40	0.078
Ni-201 with Taper Cylindrical openings	3M	6	14.054	351.35	0.176

4.2.6 Summary

Experimental investigation of the effect of taper cylindrical openings over uniform cylindrical openings in current collectors made of SS-316L and Ni-201 at various concentrations of methanol solution is carried out. It is observed that the CO_2 generated in the cell is getting expelled easily from taper cylindrical openings than from uniform cylindrical openings. As the taper angle increases, CO_2 gets expelled easily from the openings due to buoyancy and therefore, there is less restriction for methanol flow towards MEA, which leads to better performance of the cell. Cell performance polarisation and power density curves are drawn for comparison of CC performance and to determine maximum power density. The maximum performance of the cell with taper and uniform cylindrical openings in CC is tabulated in table 4.6.

Table 4.6 Best performances of cells with taper and uniform cylindrical openings

Current Collectors	Methanol Concentration	Max Current density, $mA.cm^{-2}$	Max Power density, $mW.cm^{-2}$	Percentage increase in Power density
SS-316L with Uniform Cylindrical openings	5M	56.0	5.712	23.5
SS-316L with Taper Cylindrical openings	3M	67.2	7.056	
Ni-201 with Uniform Cylindrical openings	5M	84.8	10.416	34.92
Ni-201 with Taper Cylindrical openings	3M	107.2	14.054	

Higher performance of PDMFC is achieved using Nickel-201 CC with taper cylindrical openings (34.92% in PD), resulting in ease of CO_2 scavenging due to increased buoyancy, which is a crucial finding.

Specific energy generated by PDMFC per unit fuel consumed for different current collectors is calculated. An improvement is observed when Ni-201 is used as material for CCs over SS-316L and also observed an improvement when CCs with taper cylindrical openings is used over CCs with uniform cylindrical openings for the same material.

Further, with the modification in the geometry of CC openings from uniform cylindrical to taper cylindrical, there is a significant reduction in the cell weight resulting in the following improvements.

- Specific power density (power density per unit weight of the cell) using Ni-201 CC of the fuel cell at 3M methanol concentration got increased by 27.8%, i.e., from 14.28 $mW.cm^{-2}.kg^{-1}$ to 18.25 $mW.cm^{-2}.kg^{-1}$.
- As the weight of the cell got reduced by 3.3 %, its handling and portability becomes easy.

4.3 Performance of PDMFC current collectors with different combinations of anode and cathode materials among SS-316L, Nickel-201and Brass

The experimental investigation is carried out with the combination of different anode and cathode current collectors that are fabricated with SS-316L, Ni-201, and Brass with an opening ratio of 45.3%. The anode-cathode CC combination details are tabulated in table 4.7.

Table 4.7 Experimental Anode/Cathode Combination

Combination	Anode	Cathode
I	Nickel-201 (Ni)	Stainless Steel Gr 316L (SS)
II	Nickel-201 (Ni)	Brass
III	Stainless Steel, Gr 316L(SS)	Nickel-201(Ni)
IV	Stainless Steel, Gr 316L(SS)	Brass

As brass is identified as less durable in dilute methanol environment due to formation of surface metal oxides. Hence the use of brass as current collector material at anode is not considered. The cell performance is examined with the above combinations using uniform cylindrical and taper cylindrical openings current collectors, keeping the same contact area on either side of MEA.While performing the experiment, first set of Voltage and Current readings are taken by varying current characteristic using Ni/SS (Combination-I) materials as current collectors at 5M methanol concentration. The experiment is further repeated with Combination-II, Ni/Brass; Combination-III, SS/Ni; and Combination-IV, SS/Brass current collectors.

4.3.1 Polarisation and Power Density Characteristics

The experimental results of the cell with uniform and taper cylindrical openings CC are plotted as performance characteristic curves and shown in figures 4.22 and 4.23 respectively.

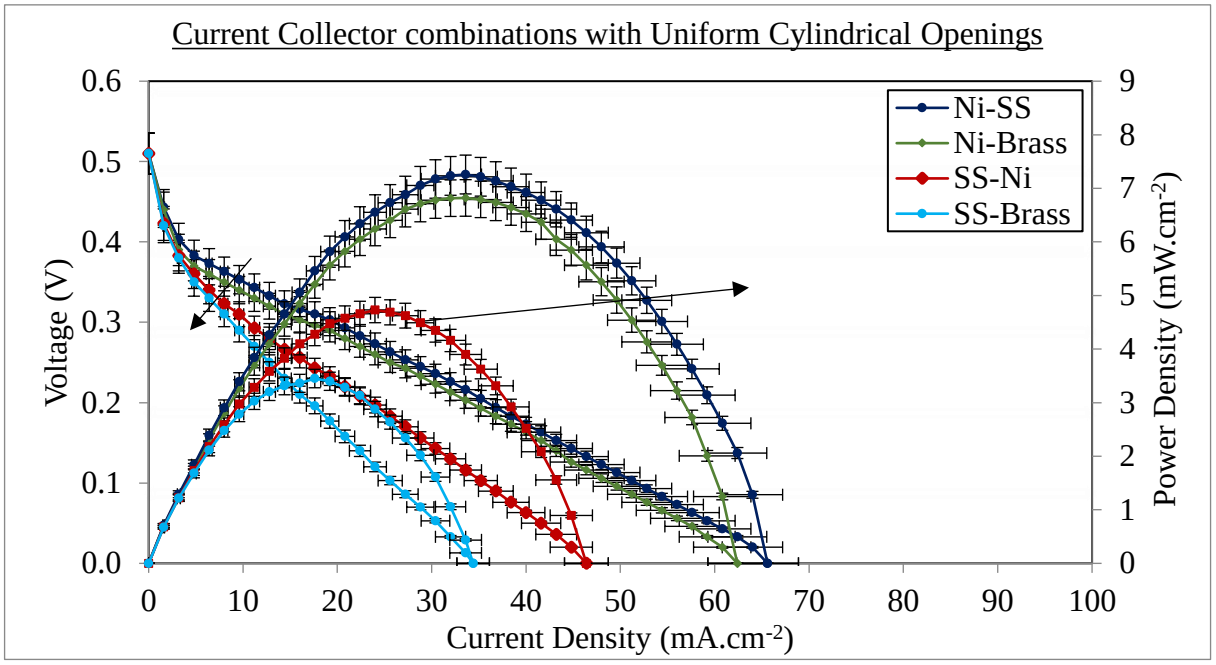

Figure 4.22 Performance characteristic curves of PDMFC using CC with uniform cylindrical openings

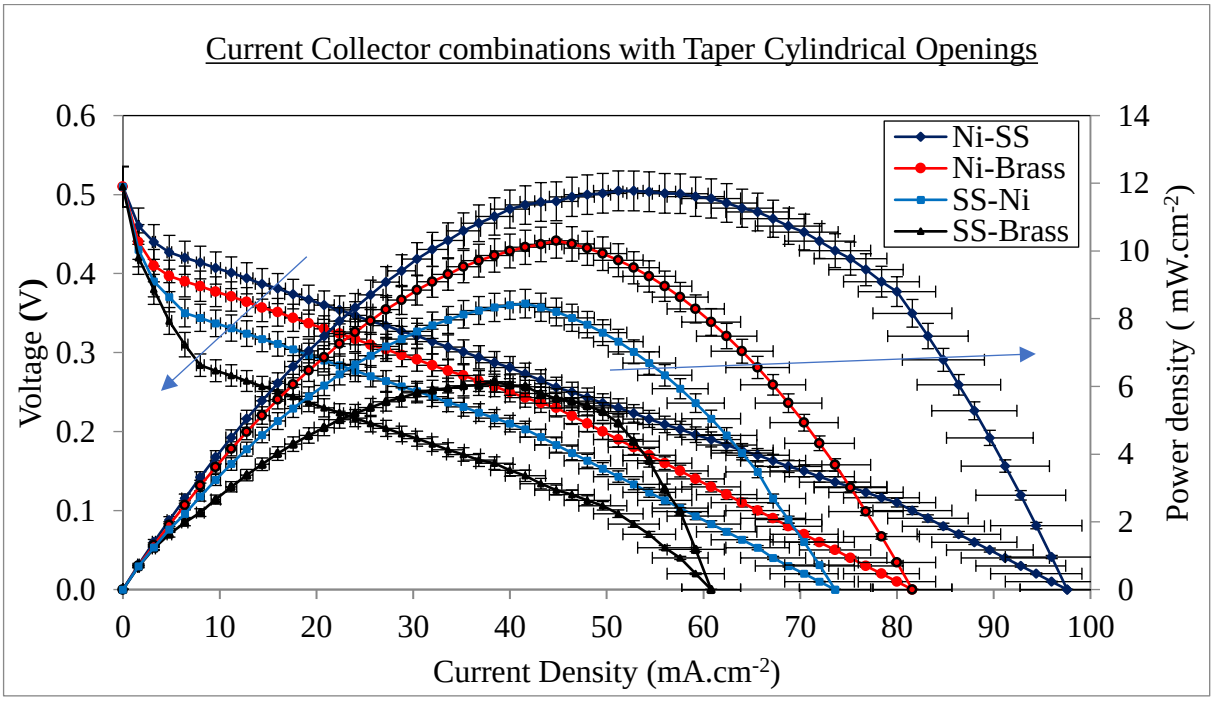

Figure 4.23 Performance characteristic curves PDMFC using CC with taper cylindrical openings

In the Combination-I, with uniform cylindrical openings in the CC, the highest power density recorded is 7.258 $mW.cm^{-2}$ corresponding to a current density of 33.6 $mA.cm^{-2}$ (figure 4.22). During the experiment, the maximum current density recorded is 65.6 $mA.cm^{-2}$. Similarly,

with same setup using taper cylindrical openings in CCs, the highest power density recorded is 11.776 $mW.cm^{-2}$ at a current density of 51.2 $mA.cm^{-2}$ (figure 4.23). During the experiment, the maximum current density recorded is 97.6 $mA.cm^{-2}$.

In the Combination-II, with uniform cylindrical openings in the CC, the highest power density recorded is 6.821 $mW.cm^{-2}$ at a current density of 33.6 $mA.cm^{-2}$ and the maximum current density recorded is 62.4 $mA.cm^{-2}$ (figure 4.22). Similarly, with same setup using taper cylindrical openings in CCs, the highest power density recorded is 10.304 $mW.cm^{-2}$ at a current density of 44.8 $mA.cm^{-2}$ and the maximum current density recorded is 81.6 $mA.cm^{-2}$ (figure 4.23).

In the Combination-III, with uniform cylindrical openings in the CC, the highest power density recorded is 4.728 $mW.cm^{-2}$at a current density of 24.0 $mA.cm^{-2}$ and the maximum current density recorded is 46.4 $mA.cm^{-2}$ (figure 4.22). Similarly, with same setup using taper cylindrical openings in CCs, the highest power density recorded is 8.445 $mW.cm^{-2}$ at a current density of 41.6 $mA.cm^{-2}$ and the maximum current density recorded is 73.6 $mA.cm^{-2}$ (figure 4.23).

In the Combination-IV, with uniform cylindrical openings in the CC, the highest power density recorded is 3.450 $mW.cm^{-2}$ at a current density of 17.6 $mA.cm^{-2}$ and the maximum current density recorded is 34.4 $mA.cm^{-2}$ (figure 4.22). Similarly, with same setup using taper cylindrical openings in CCs, the highest power density recorded is 6.144 $mW.cm^{-2}$ at a current density of 38.4 $mA.cm^{-2}$ and the maximum current density recorded is 60.8 $mA.cm^{-2}$ (figure 4.23).

The maximum power density and maximum current density comparisons of uniform and taper cylindrical openings with different anode-cathode combinations are plotted and shown in figures 4.24 and 4.25 respectively. From these charts, Ni-SS as anode-cathode combination produced the best power and current densities. The combination of SS-Brass showed the lowest performance. Ni-Brass and SS-Ni combinations are performing lower than Ni-SS and higher than SS-Brass. Therefore Ni-SS CCs as anode-cathode combination is identified as the best for the PDMFC performance.

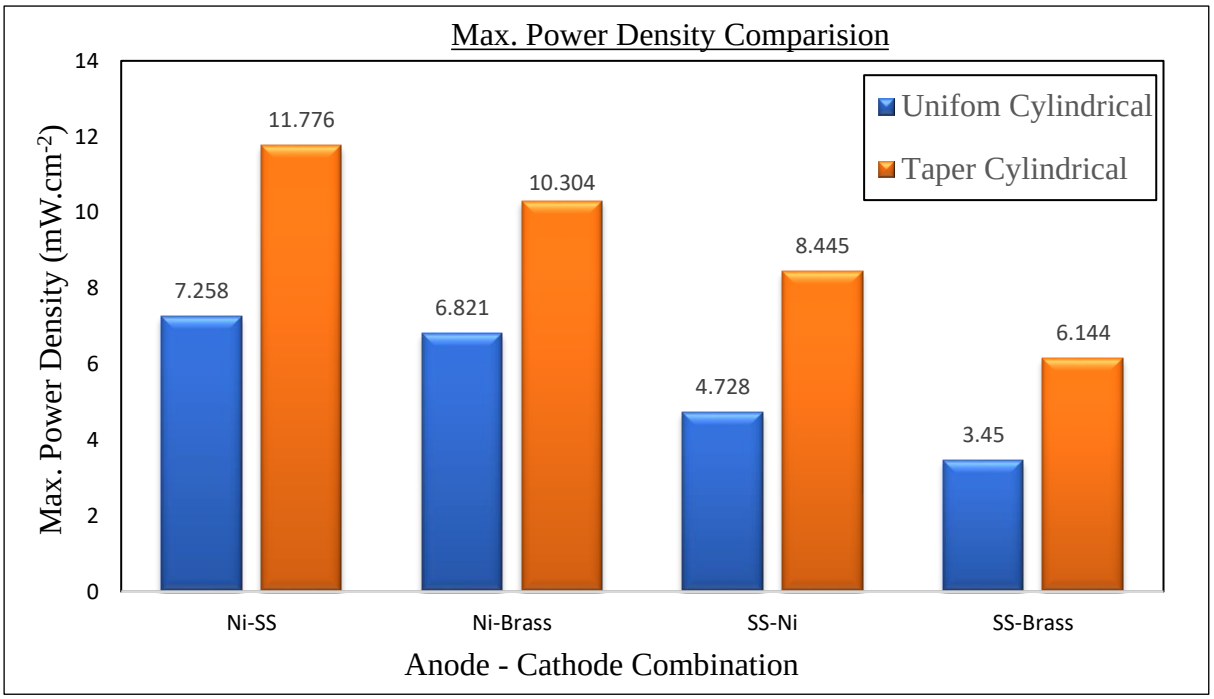

Figure 4.24 Comparison of Maximum power densities of PDMFC using current collectors with uniform and taper cylindrical openings.

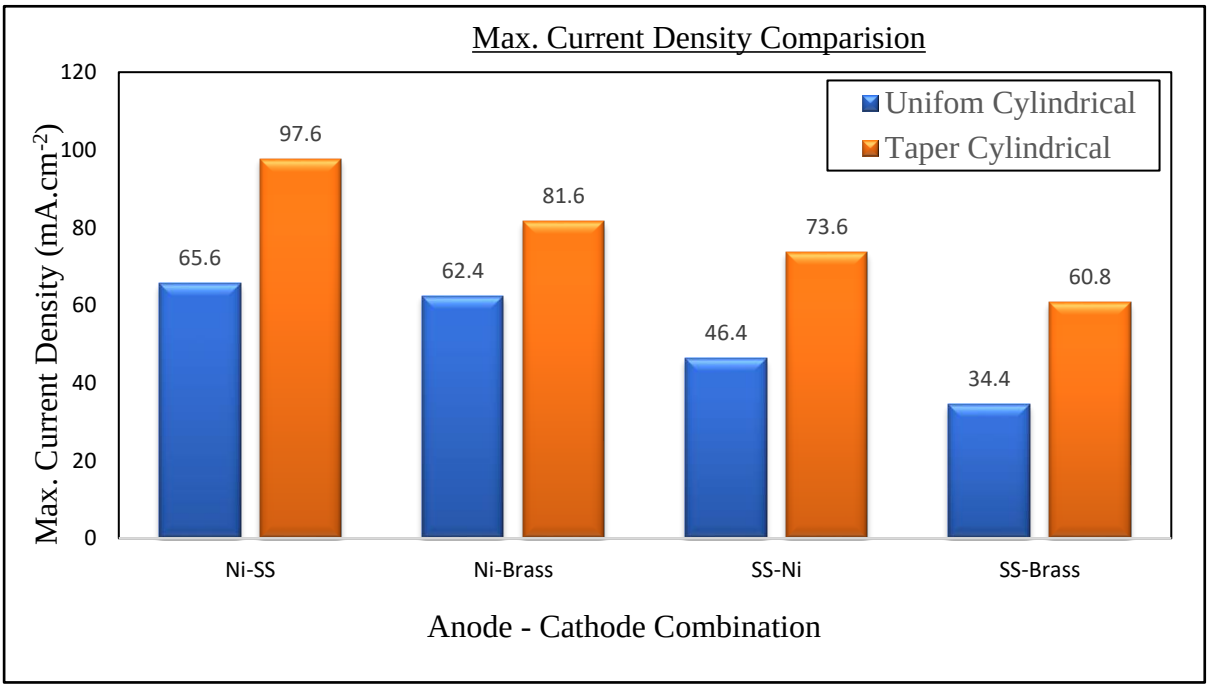

Figure 4.25 Comparison of Maximum current densities of PDMFC using current collectors with uniform and taper cylindrical openings.

The maximum power density produced by taper cylindrical openings on the CC combinations and cost per unit power density is also calculated and placed in table 4.8.

Table 4.8 Cost per unit power density produced.

Combination of Anode – Cathode	**Power Density, mW.cm^{-2}**	**Cost, $/kg**	**Weight of CCs (anode+cathode), x10^{-3} kg**	**Cost/Unit Power Density, $/(mW.cm^{-2})**
Ni-Ni[(i)]	14.054	15.8	195.74	0.22
Ni-SS	11.776	10.6	187.02	0.16
Ni-Brass	10.304	9.66	192.19	0.18
SS - Ni	8.445	10.6	187.02	0.23
SS-Brass	6.144	6.21	183.48	0.18

Note: (i) Data taken from Research Objective -1.

Among the anode-cathode combinations, Ni/Ni combination is found to be superior and has produced maximum power density of 14.054 mW.cm^{-2} and also has better corrosion properties. However, the Ni/SS combination produces 11.776 mW.cm^{-2} power density and the cost per unit power density is the least.

4.3.2 Summary

PDMFC performance is experimentally investigated using different combinations of anode and cathode current collector materials such as Ni-201, SS-316L and brass.

- With taper cylindrical openings in CC, the anode-cathode combination of Ni-201 &SS-316L showed better current density (97.6 mA.cm^{-2}) and power density (11.776 mW.cm^{-2}) than the other combinations.
- SS-316L & Brass combination showed the least performance with respect to current density (60.8 mA.cm^{-2}) and power density (6.144 mW.cm^{-2}).
- Among the anode-cathode combinations, the Ni/SS setup is producing better power density and the least cost per unit power density.
- However, Ni/Ni combination is found to be superior and has produced highest power density and also has better corrosion properties.

4.4 Effect of various shapes and sizes of MEA active regions on the performance of PDMFC.

The performance of Passive Direct Methanol Fuel Cell with different sizes and shapes of active regions such as circle, square, rectangle, and rhombus having Equal Areas and Equal Perimeters is analysed. Circular controlling shape of MEA dynamic zone with an effective area of 1963.5 mm^2 and a perimeter of 177.2 mm is used. Keeping this area and perimeter quantities as reference, dimensions of the other shapes such as square, rectangle, and rhombus are fixed. The same sets of gaskets are used on either side of MEA for achieving desired dynamic MEA region. Ni-201 current collectors are used in the cell at the methanol solution of 5M.

4.4.1 Influence of Effective MEA Shapes on Cell Performance

4.4.1.1 Equal areas of reaction zone

The cell characteristics with various shapes of equal areas in gasket openings are shown in figure 4.26. It is observed that the cell using square shape has produced a maximum power density of 6.344 $mW.cm^{-2}$ among the other shapes chosen that includes rhombus, rectangle, and circle. Whereas the circular shape produces the least power density of 5.541 $mW.cm^{-2}$.

The better performance of the cell with square shape is due to uniform circulation of reactants in the active area and also lower contact resistance between MEA & current collectors.

A bar chart of the power density produced by these dynamic shapes in equal areas is shown in figure 4.27.

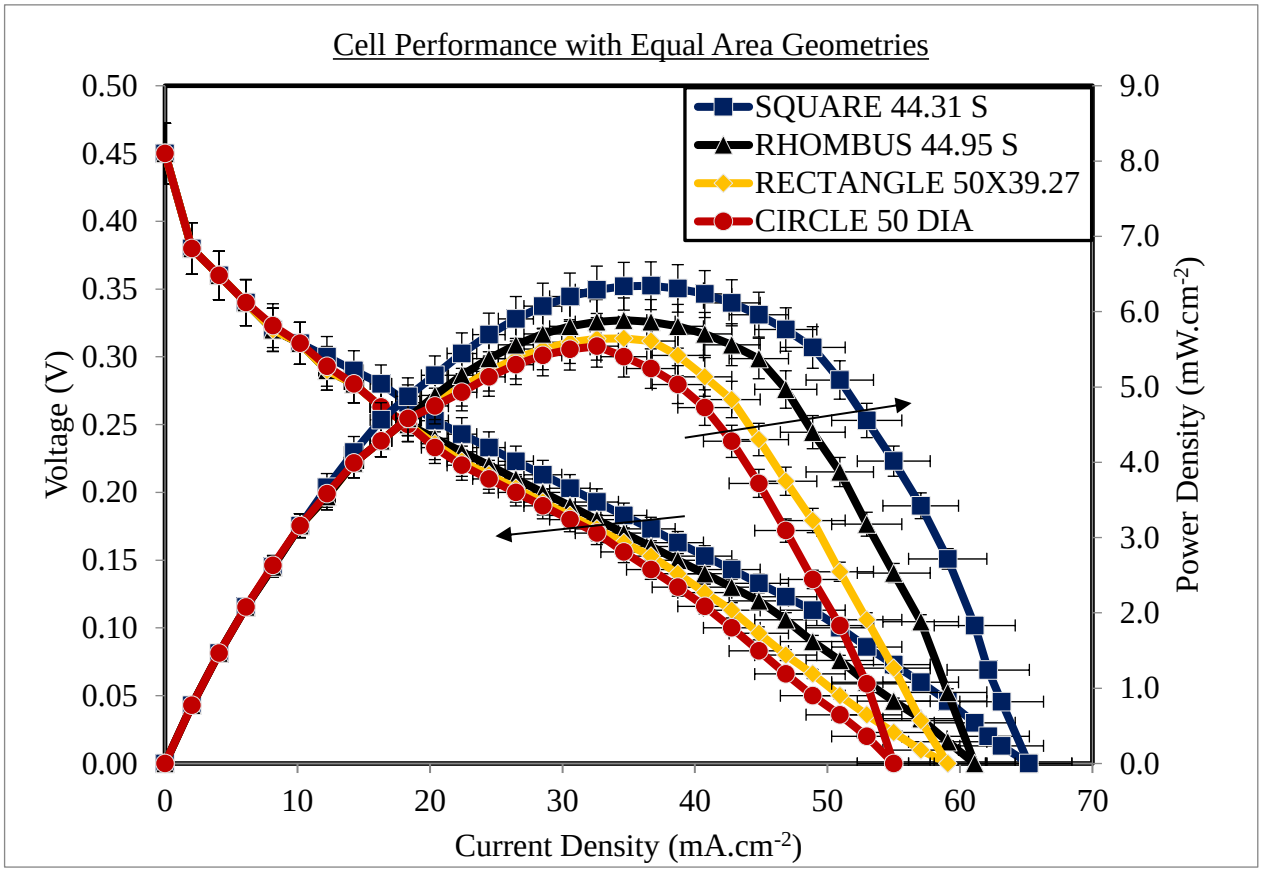

Figure 4.26 Cell characteristics with various shapes of equal areas in gasket openings

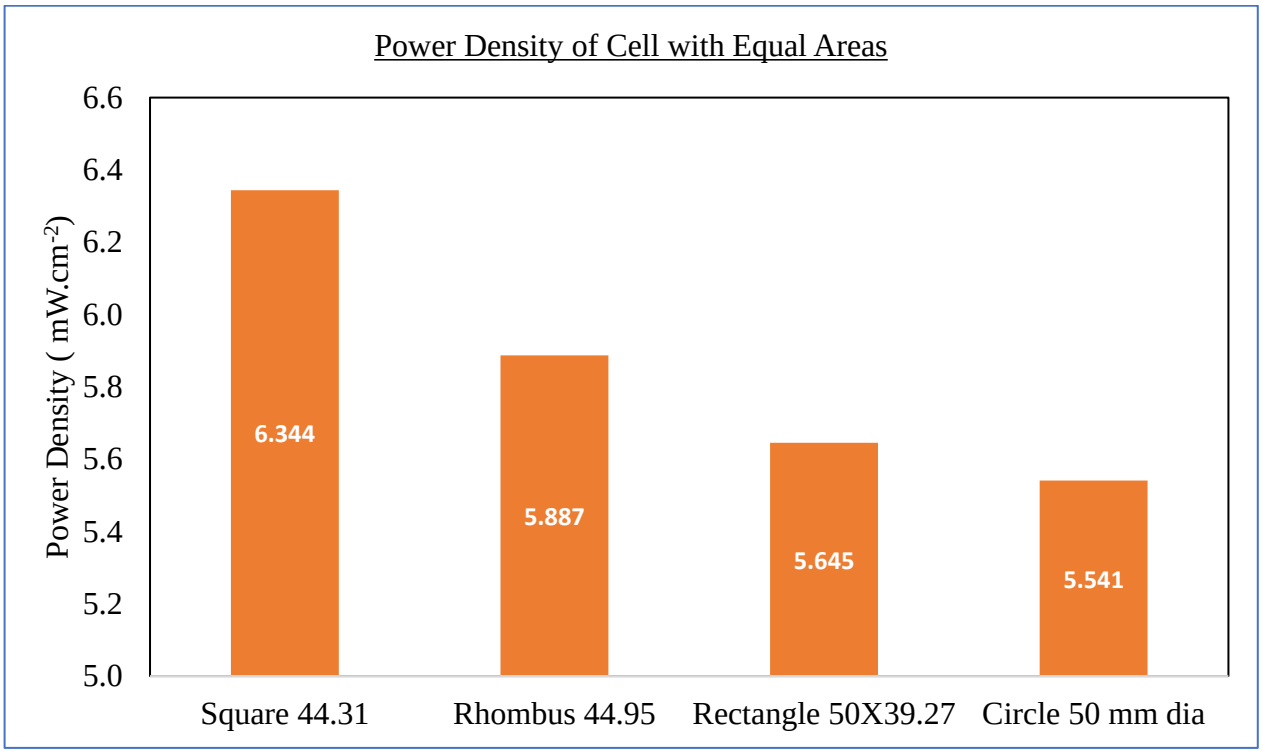

Figure 4.27 Power density with various shapes of equal areas in gasket openings

4.4.1.2 Equal perimeters of reaction zone

The cell characteristics with various shapes of equal perimeters in gasket openings are shown in figure 4.28. It is observed that the cell with a rhombus shape has produced a maximum power density of 7.714 $mW.cm^{-2}$ among the other shapes of square, rectangle, and circle. The circular shape produces the least power density of 5.541 $mW.cm^{-2}$.

The surface-specific concentration (MEA active area per unit methanol solution concentration) of methanol on ion-conducting membrane is greater in larger active areas. Therefore, the diffusion of methanol increases towards cathode which leads to higher crossover of methanol. As a result, current density on the larger active areas is lower when compared to the smaller active areas.

A bar chart of the power density produced with various shapes of equal perimeters in gasket openings is shown in figure 4.29. The better performance of the cell with rhombus shape dynamic zone is attributed to its least effective area among equal perimeters of selected shapes.

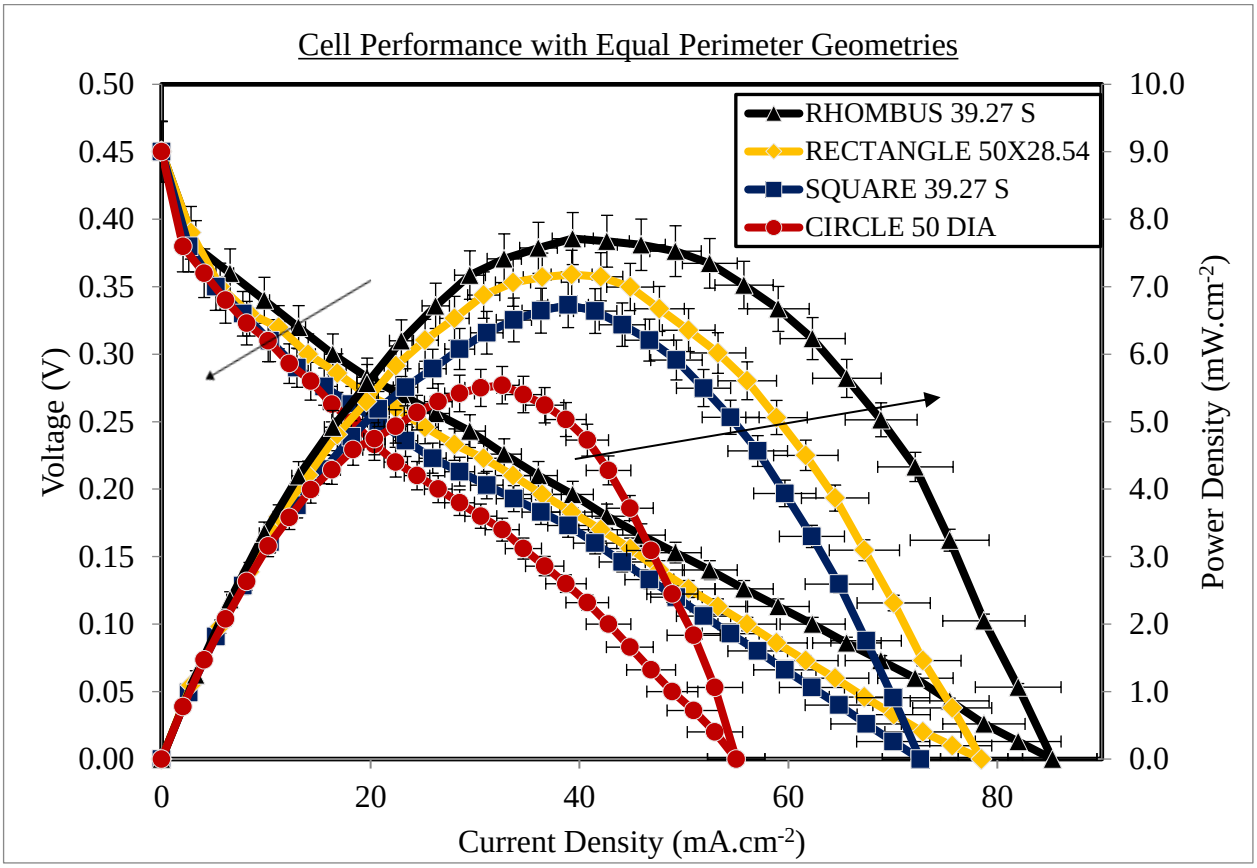

Figure 4.28 Cell characteristics with various shapes of equal perimeters in gasket openings

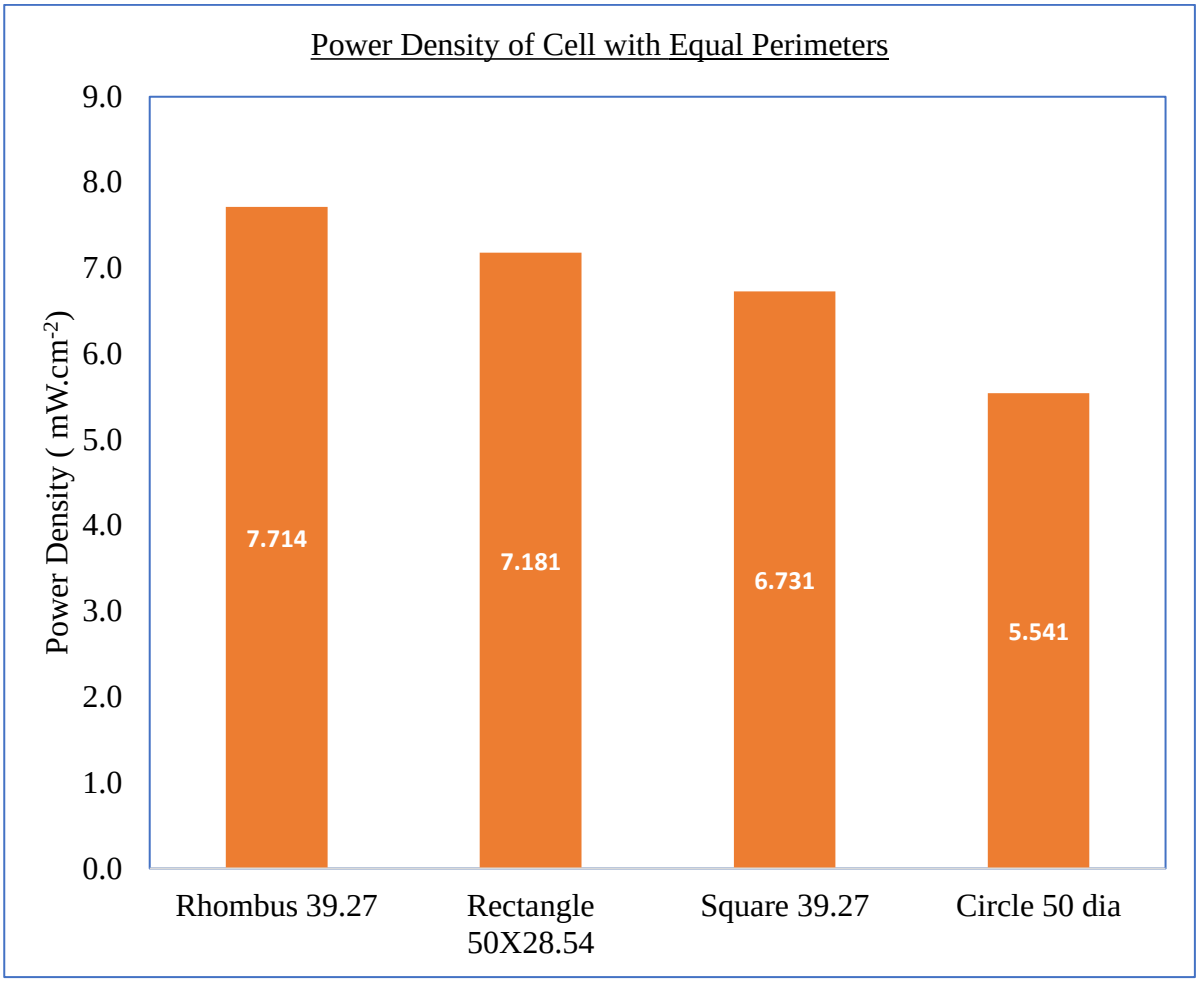

Figure 4.29 Power density with various shapes of equal perimeters in gasket openings

4.4.2 Influence of Effective Opening Shapes on Current Density

4.4.2.1 Equal areas of reaction zone

From the experimental results, it is observed that the cell using a square shape dynamic zone has produced a maximum current density of 65.2 mA.cm^{-2} among the other shapes chosen that include rhombus, rectangle, and circle. The circular shape has produced the least current density of 55.0 mA.cm^{-2}. The cell characteristics with various shapes in equal area geometry openings in gasket are shown in figure 4.30. The better performance of the cell with square shape active area is attributed to equal circulation of reactants on the effective active area.

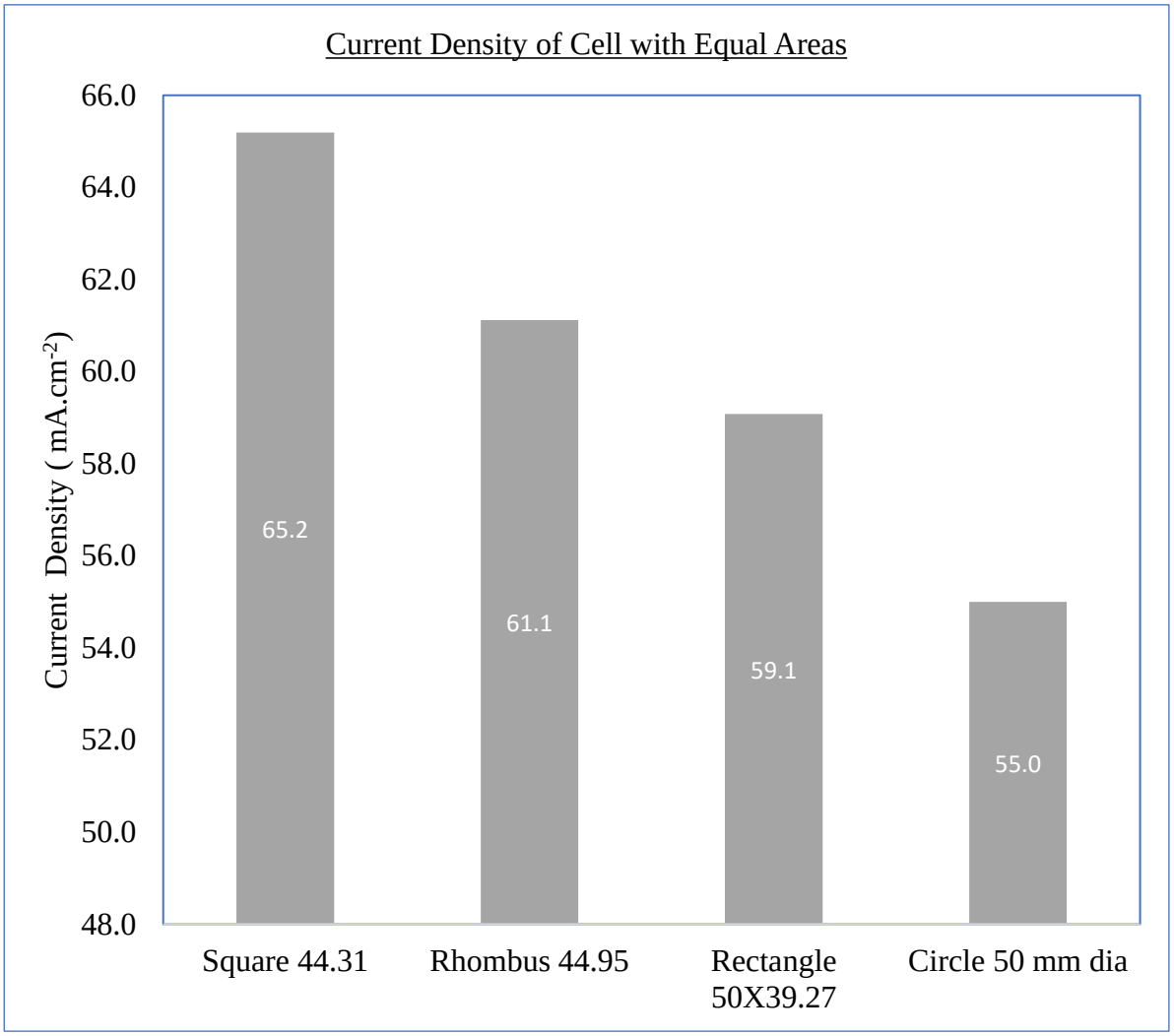

Figure 4.30 Current density with various shapes of equal areas in gasket openings

4.4.2.2 Equal perimeters of reaction zone

From the experimental results, it is observed that the cell with rhombus shape has produced a maximum current density of 85.3 $mA.cm^{-2}$ among the other shapes chosen that include square, rectangle, and circle. The circular shape produces the least current density of 55.0 $mA.cm^{-2}$. The cell characteristics with various shapes of equal perimeters in gasket openings are shown in figure 4.31. The better performance of the cell with rhombus shape is due to least effective area among the selected shapes of equal perimeters.

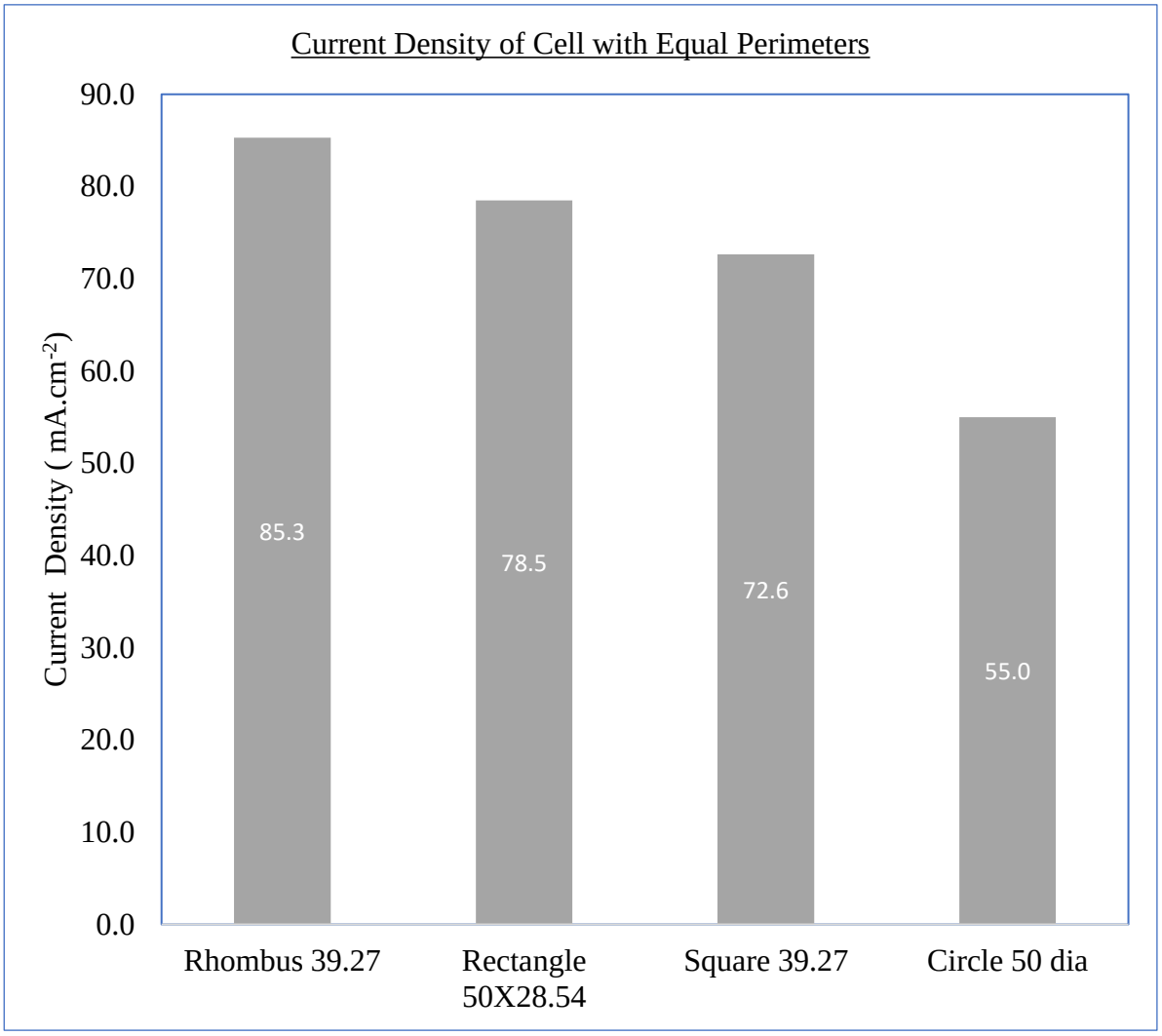

Figure 4.31 Current densities with various shapes of equal perimeters in gasket openings

4.4.3 Comparison of different shapes of Gasket Openings in active region of MEA.

4.4.3.1 Perimeters of different shapes with equal area geometry

From various shapes of dynamic zones with equal areas, it is observed that the rhombus has the largest perimeter and circle has the lowest opening perimeter. The descending order of the opening perimeters is: Rhombus > Rectangle > Square > Circle. The gasket opening perimeters with various shapes of equal areas in gasket openings are shown in figure 4.32.

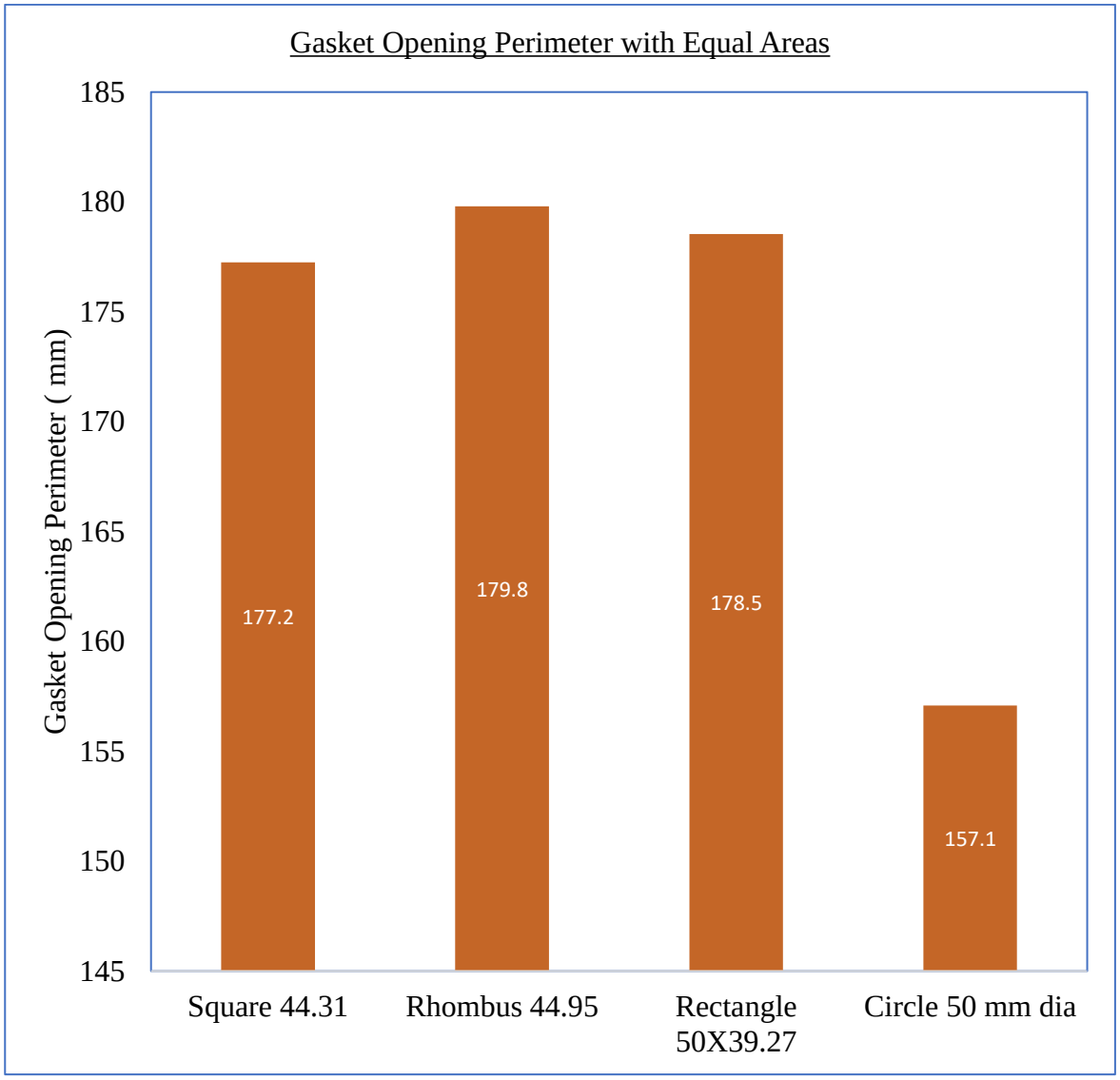

Figure 4.32 Gasket opening perimeter with various shapes of equal areas in gasket openings

4.4.3.2 Areas of different shapes with equal perimeter geometry

From various shapes with equal perimeters, it is observed that the rhombus has the lowest opening area and circle has the largest area. The ascending order of the opening areas is: Rhombus < Rectangle < Square < Circle. Hence power density is influenced by the area of the opening in equal perimeter shapes. The gasket opening perimeters with various shapes of equal areas in gasket openings are shown in figure 4.33.

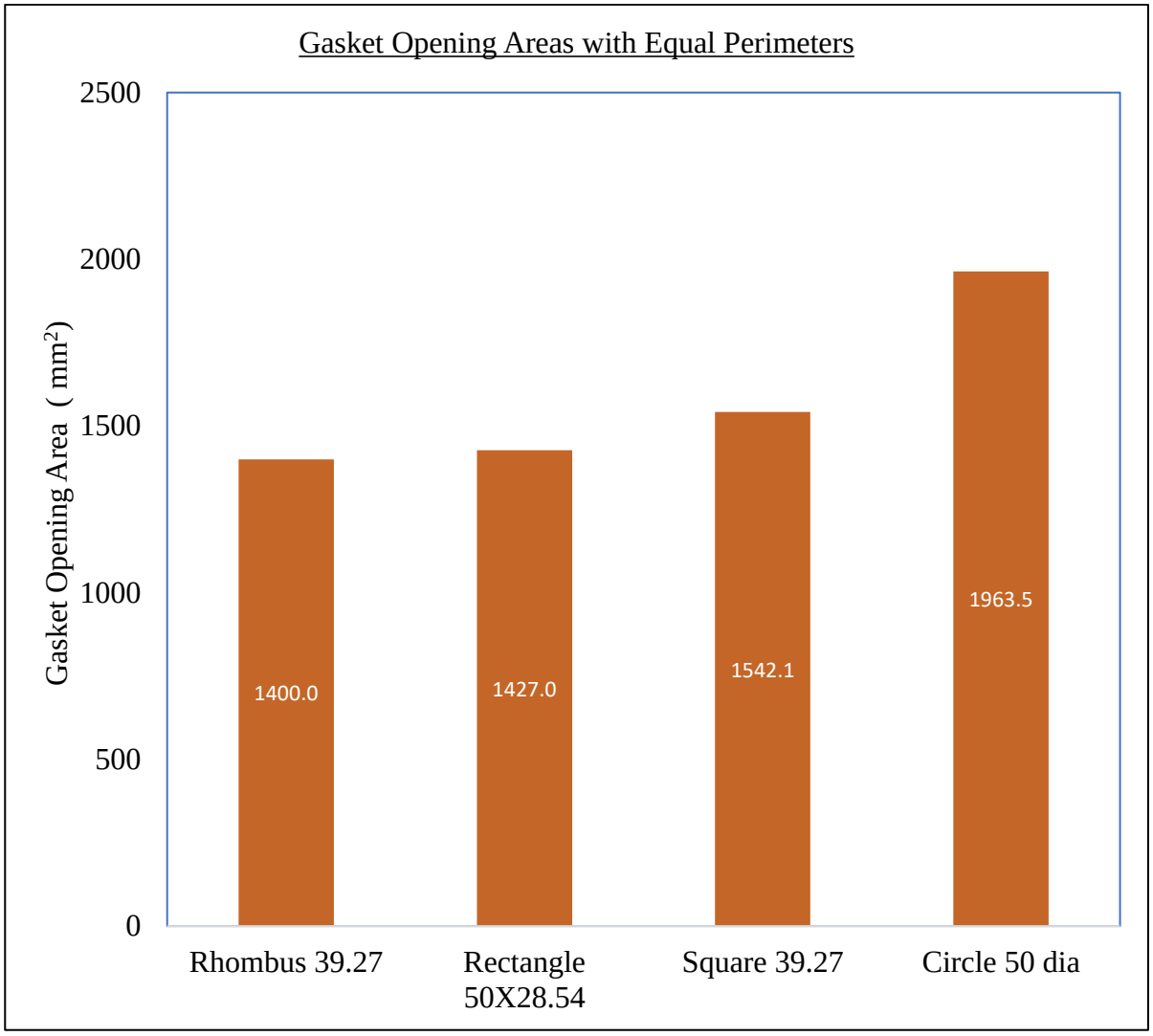

Figure 4.33 Gasket opening area with various shapes of equal perimeters in gasket openings

4.4.4 Influence of Area to Perimeter Ratio (A/P) of Effective Gasket Opening Shapes

4.4.4.1 A/P ratio of shapes with equal areas

It is examined that the ratio of gasket opening area to the perimeter influence the performance of the cell. The gasket opening perimeters with various shapes of equal areas in gasket openings are shown in figure 4.34. The circle has the highest A/P ratio and the rhombus has the least. From the performance graphs, it is revealed that the circular shape gave the least performance due to the influence of the highest gasket opening area to perimeter ratio.

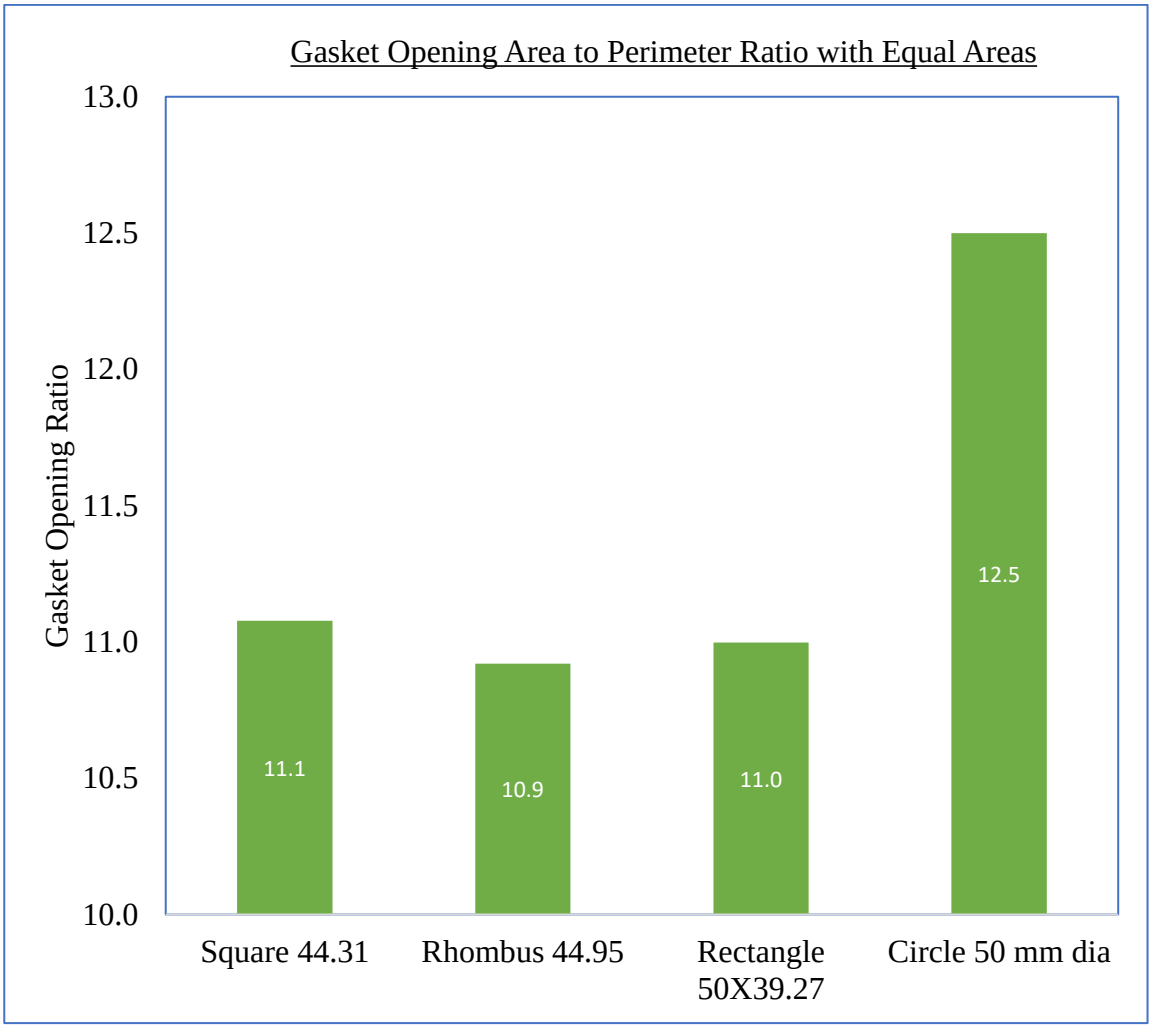

Figure 4.34 Gasket opening area to perimeter ratio with various shapes of equal areas in gasket openings

4.4.4.2 A/P ratio of shapes with equal perimeters

It is predicted that the ratio of gasket opening area to the perimeter influence the performance of the cell. From figure 4.35, it is revealed that the gasket opening areas with various shapes such as rhombus, rectangle, square, and circle have better performance with decreasing gasket opening A/P ratio. The circular shape has the highest opening area to the perimeter ratio and the rhombus has the least. From the performance graphs, it is revealed that the circular shape gave the least performance due to the influence of the highest gasket opening area to perimeter ratio and the rhombus shape has the highest performance due to the lowest gasket opening area to perimeter ratio.

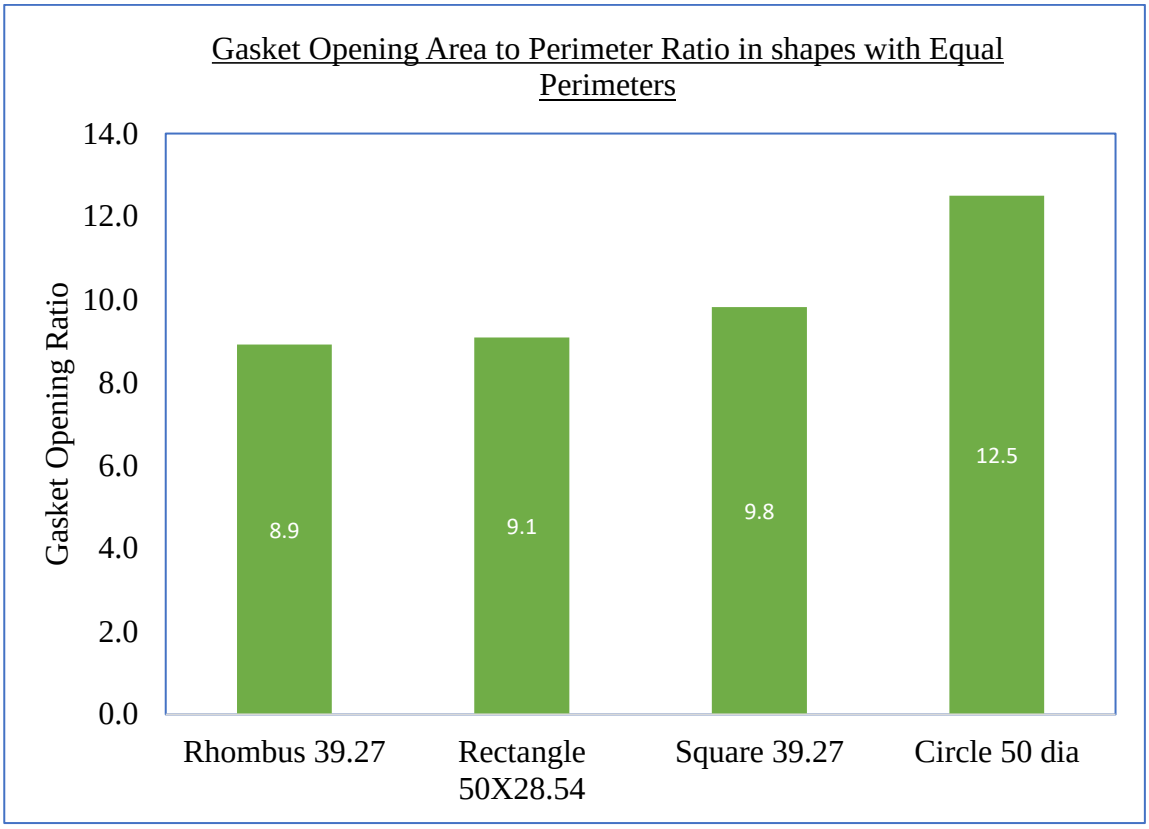

Figure 4.35 Gasket opening area to perimeter ratio with various shapes of equal perimeter geometries.

4.4.5 Comparison of Power and Power Densities of MEA active region with different Shapes and sizes

4.4.5.1 Power generated Vs Various shapes and their sizes.

With two different sizes of selected shapes, a comparison study of size factor (in terms of area of the dynamic zone) on power produced by the cell is carried out. The comparison of power produced against the gasket opening area of various shapes and sizes is shown in figure 4.36. It is observed that the higher the effective MEA area, higher is the power produced by the cell for a given shape.

4.4.5.2 Power Density produced Vs various sizes and shapes.

With two different sizes of selected shapes, a comparison study of *size* factor (in terms of area of the dynamic zone) on power density produced by the cell is carried out. The comparison of power density produced against the gasket opening area with different shapes and sizes is shown in figure 4.37. It is observed that the higher the effective MEA area, lower is the power density produced by the cell for a given shape.

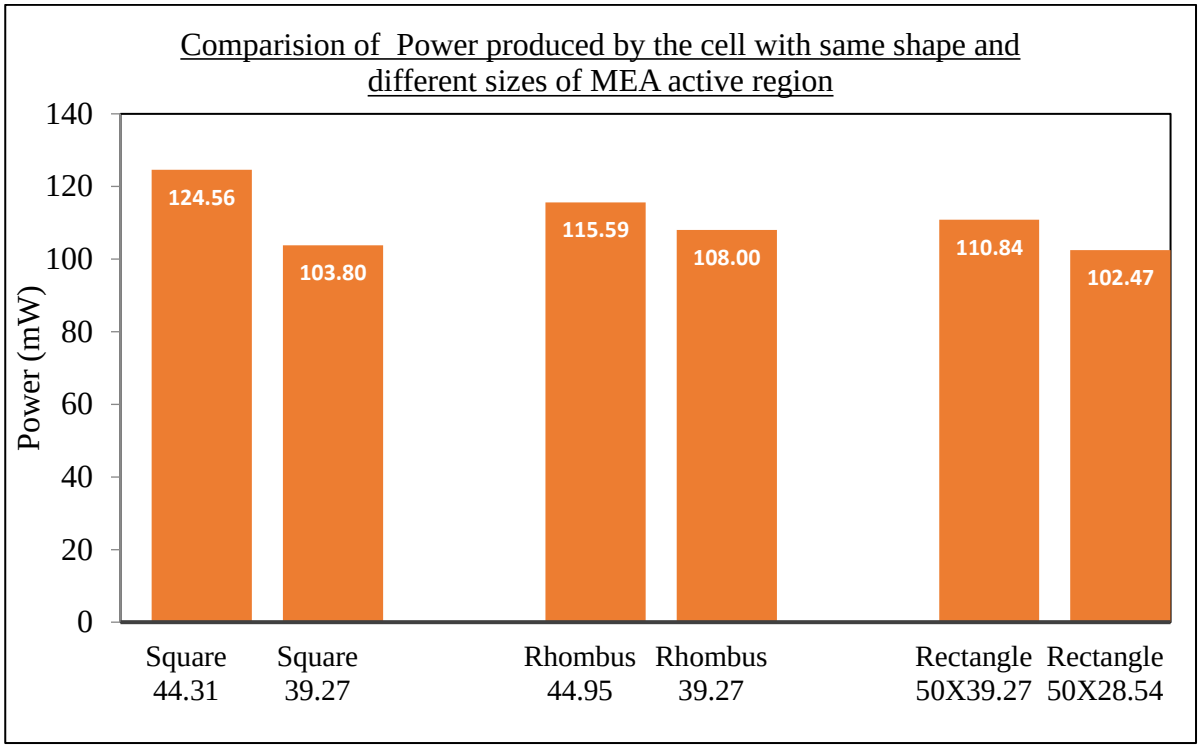

Figure4.36 Power generated by the cell with different shapes and sizes of MEA active area opening.

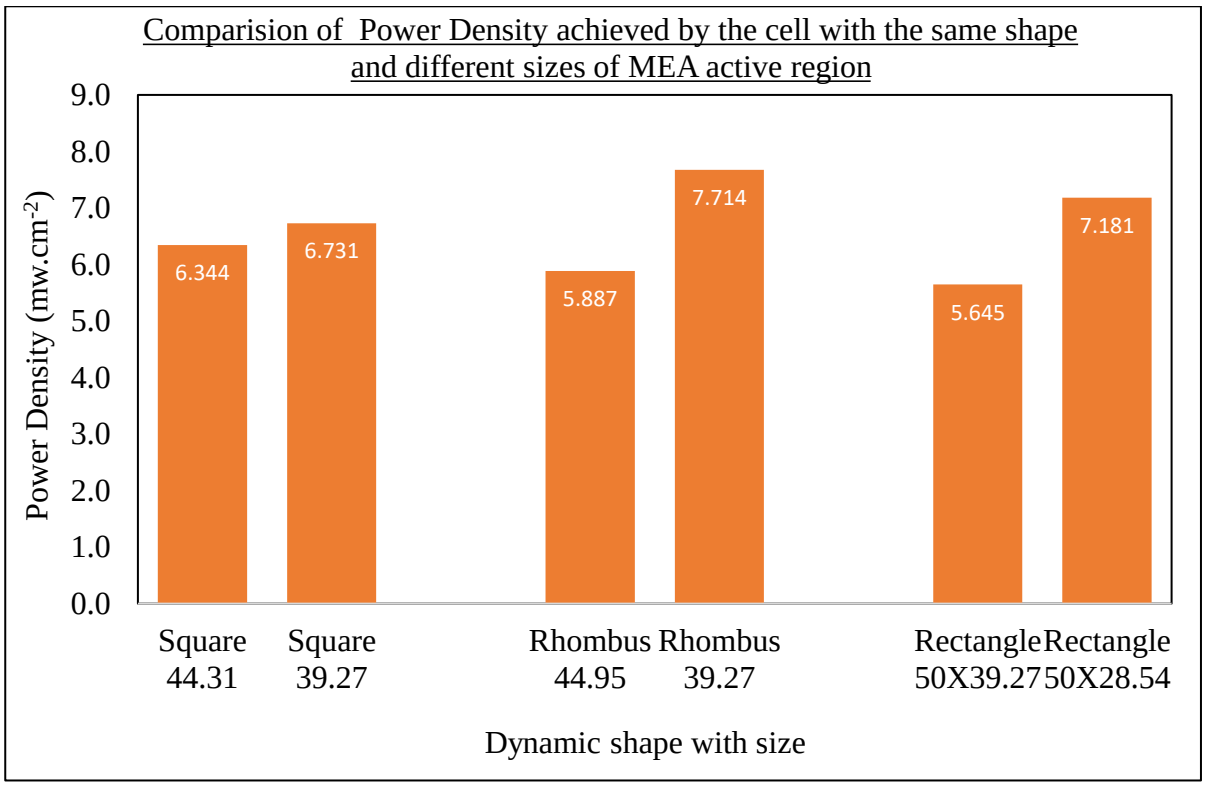

Figure 4.37 Power Density achieved by the cell with various shapes and sizes in MEA active area opening.

4.4.6 Summary

The performance of PDMFC with different shapes of MEA effective openings in equal area and equal perimeter geometries such as square, rectangular, rhombus, and circular is analysed by altering gasket openings of dynamic regions. The Ni-201 current collectors are used in this experimentation.

In equal area geometries, cell with Square shaped dynamic zone has developed the highest power density of 6.344 $mW.cm^{-2}$ and the maximum current density of 65.2 $mA.cm^{-2}$.

In equal perimeter geometries, cell with Rhombus shaped opening with an area of 400 mm^2 has developed the highest power density of 7.714 $mW.cm^{-2}$ and the maximum current density of 85.3 $mA.cm^{-2}$.

It is also learned from the experiment that cell performance depends on the combined effect of (i) Gasket opening shape, opening area, and its perimeter; (ii) Current collector exposed area, its opening ratio, and its opening perimeter.

4.5 Service-oriented degradation of PDMFC components using various Non-Destructive Testing methods

Experimental investigation on PDMFC components is carried out using "shore A hardness gauge" for non-metallic and soft materials, colour contrast penetrant system to identify surface discontinuities, ultrasonic thickness gauge for thickness measurements, and digital balance for weight measurements are used. The instruments, gauges and consumables such as *Shore A* hardness tester, colour contrast liquid penetrant system consumables, ultrasonic thickness gauge, digital balance for weight measurement used in the investigation are shown in figure 4.38.

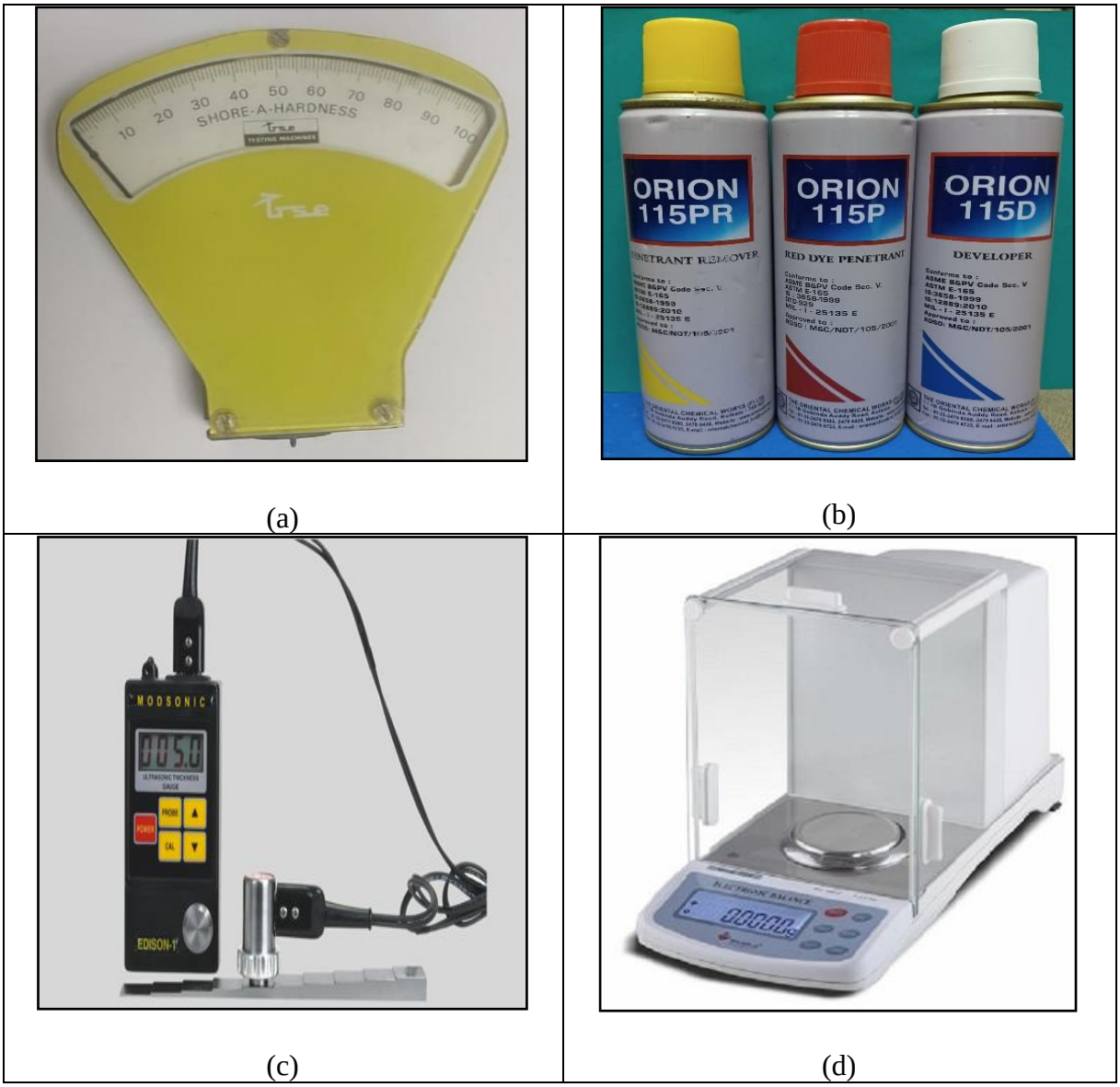

(a) (b)

(c) (d)

(a) Shore A Hardness Tester

(b) Penetrant Kit: Penetrant Remover, Penetrant, and Developer

(c) Ultrasonic Thickness gauge

(d) Digital balance

Figure 4.38 Test Instruments and consumables for NDT

4.5.1 Examination of Anode End Cover

The anode end acrylic cover is shown in figure 4.39(a). This cover is visually examined under daylight to identify visible surface discontinuities if any. The component is evaluated and it is found to be free from visible discontinuities.

Surface Examination is performed using visible Penetrant Testing by solvent removable method. During the evaluation of component, no reportable discontinuities are identified. The component, after the application of developer is shown in figure 4.39(b).

Hardness testing is carried out on the anode end acrylic cover before and after performing the experiment. The measured hardness of the component before and after the experiment is 100 shore A, indicating that there is no change in the material hardness in methanol environment. Hardness testing performed on end cover is shown in figure 4.39(c).

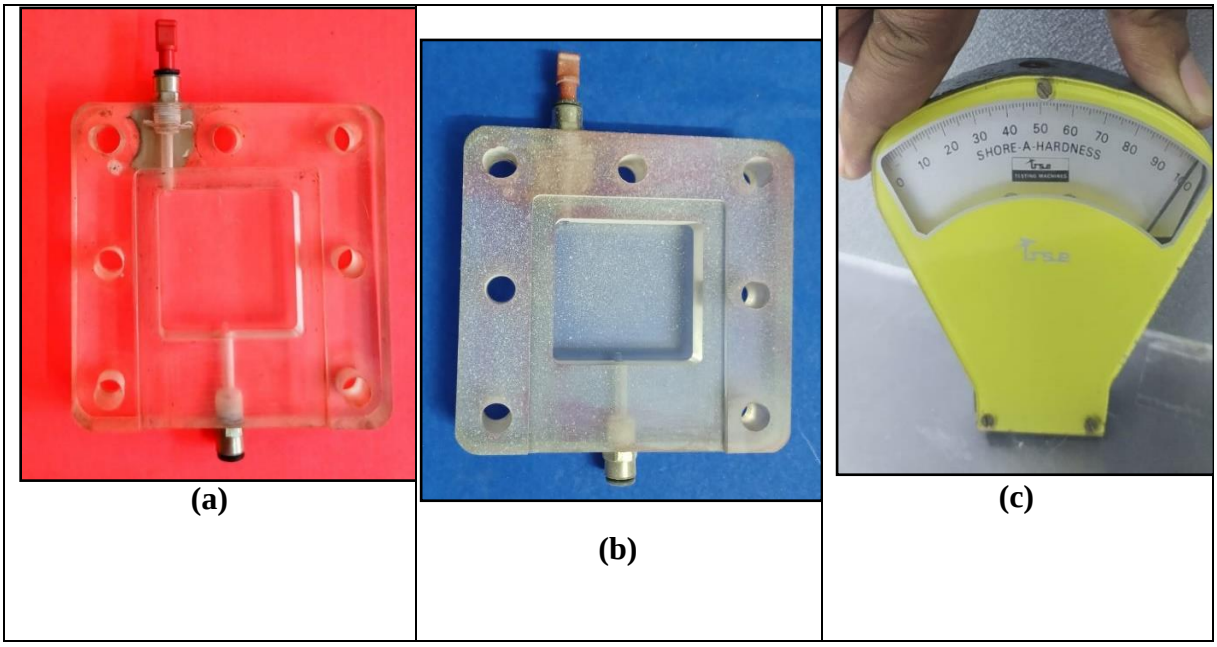

(a) VT-Image (b) PT-Image (c) Hardness Testing

Figure 4.39 Anode End Cover Testing

Evaluation of test results: From the above results, it is interpreted that the anode end acrylic cover is free from deteriorations and intact with the cell operating environment.

4.5.2 Gasket between anode end cover and anode current collector

Viton gasket is used to prevent the leak between the anode end cover and the anode current collector. Image of new Viton gasket is shown in figure 4.40(a) and the gasket which served in PDMFC for two years is shown in figure 4.40(b). Gasket is subjected to Visual Examination for identifying visible discontinuities if present. During the evaluation, gasket tore at one corner is observed and attributed to physical damage during assembling or dismantling

it from the cell. Scratch marks and surface irregularities are also observed resulting from its contact with surface of metallic current collectors. Hardness testing is carried out on new and used gaskets & the measured values are 74 shore A and 76 shore A respectively. Hardness measurements are shown in figures 4.40(c) and 4.40(d). The variation in the hardness is very small, indicating no significant change in hardness of Viton material in methanol environment.

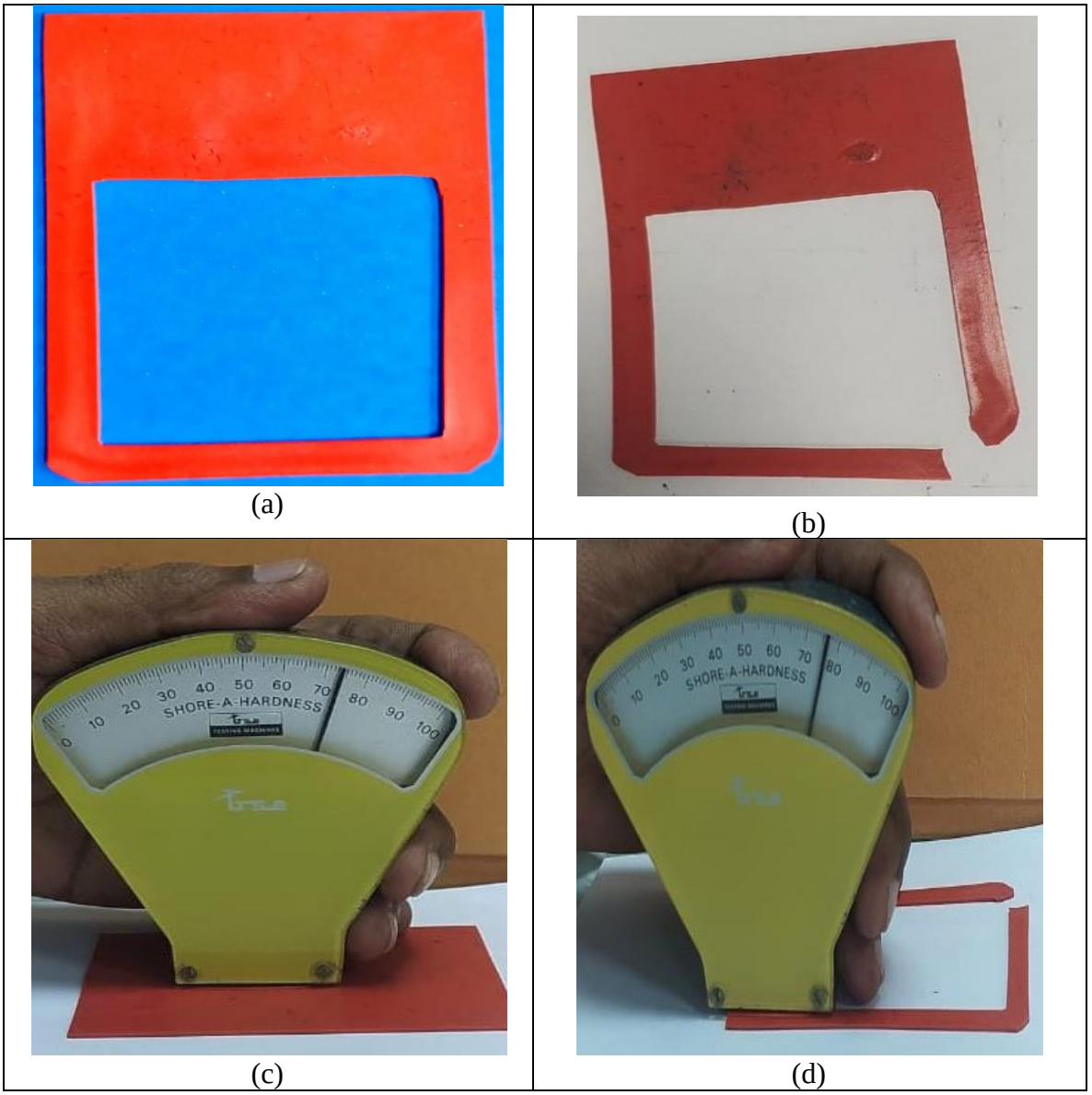

(a) New Viton gasket (b) In-Service Viton gasket (c) Hardness Testing on virgin Viton gasket (d) Hardness Testing on in-service Viton gasket

Figure 4.40 Viton Gasket Testing

Thickness of new and used gaskets is measured. New gasket thickness is 2.00 mm, whereas the used gasket has a thickness of 1.96 mm. Hence there is a compression of 2% (0.04 mm) due to bolting loads over two years of service.

Evaluation of test results: From the above interpretations, it is inferred that compression on gasket is marginal, further, there is no deterioration of the Viton gasket with cell operating environment for a reported period of two years.

4.5.3 Anode Current Collector

From the visual examination, it is observed that the brass reacts with methanol quickly and forms surface oxides. So, the usage of brass materials specific to the anodic end may not be a good choice. Images of the SS-316L and Ni CC are shown in figure 4.41(a). Brass CC before the start of the experiment and after exposure to the methanol environment is shown in Figures 4.41(c) and 4.41(d).

Surface Examination is performed using Penetrant Testing by solvent removable colour contrast method. However, no reportable discontinuities are identified during the evaluation of the component. The component after the application of the developer during the evaluation process is shown in figure 4.41(b).

As it is observed that the current collector at anode deteriorate quickly than that at cathode, anodic current collectors are chosen for the study of corrosion and loss of material.

Short term experimental corrosion rate of the CC materials is calculated and tabulated by taking the weights before and after the experiment and the time of exposure to methanol solution during the test. Thickness of the current collectors before and after conducting the experiment is measured using Ultrasonic thickness gauge. For comparison, the experimental corrosion rates of Ni-201, Brass and SS-316L CC are calculated and tabulated in table 4.9.

4.5.3.1 The durability of Anode Current Collectors: Calculations

Density of the material	= γ g/cm^3
Thickness of CC	= μ mm
Weight Before the experiment	= θ1 g
Weight after the experiment	= θ2 g
Weight Loss	= (θ1- θ2) g
Duration of experiment (in hours)	= τ h
Constant, $\prod$	=3.14
Effective surface area, $\breve{A}$	= (50*50-100*$\prod$/4*3.8*3.8) *2+100*$\prod$*3.8*μ mm^2
Experimental Corrosion Rate, ξ	= [(θ1- θ2)/τ] *[1/ (1000 * γ * $\breve{A}$)] *[24*365] mm/year

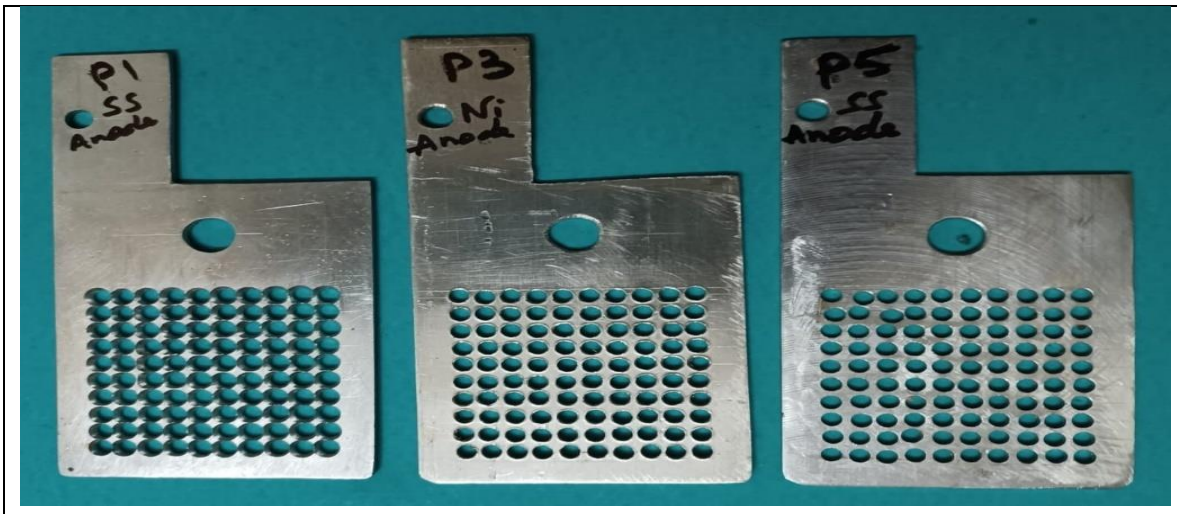

(a)

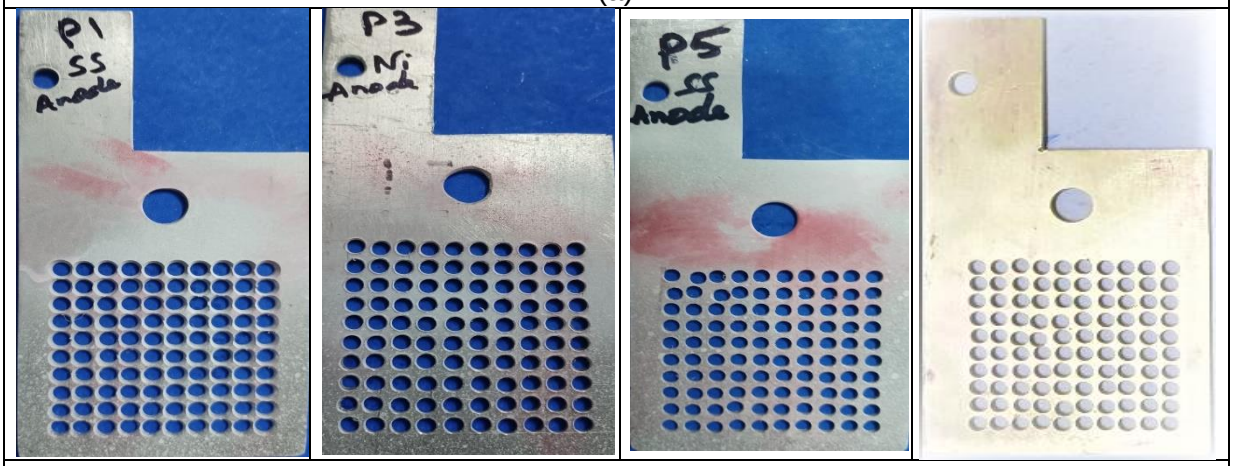

(b)

(c)

(d)

(a) VT on SS-316L and Ni-201 current collectors, (b) Penetrant Test on SS-316L, Ni-201, and Brass current collectors, (c) VT on Brass current collector, (d) Corrosion on Brass at anode side after exposure to 4M methanol

Figure 4.41 Anode Current Collectors

Table 4.9 Anode Current Collectors Short Term Corrosion Measurement Data

Data / Materials	SS-316L	Nickel-201	Brass
Density of the material, γ g/cm^3	7.90	8.89	8.50
Thickness of CC, μ mm	2.01	1.98	1.99
Weight before the experiment, θ1 g	89.1572	97.8724	94.3231
Weight after the experiment, θ2 g	89.1546	97.8720	94.2901
Weight loss, (θ1- θ2) g	0.0026	0.0004	0.0330
Duration of exposure, Ƭ h	12	12	12
Effective Surface area of the current collector, Ă mm^2	5131.25	5095.45	5107.39
Experimental Corrosion rate, ξ mm/year	0.047	0.006	0.555
Comparison of experimental corrosion rates w.r.t SS-316L material	100% (Assumed reference)	12.7% of SS316L corrosion rate	1180% of SS316L corrosion rate

Evaluation of test results: From the above interpretations, it is observed that there is a deterioration in anode current collectors. Among SS-316L, Ni-201, and brass current collectors, the corrosion rate of brass is 11.8 times higher than that of the SS-316L current collector, whereas Ni-201 has a corrosion rate of approximately 1/8 of that of SS-316L.

4.5.4 Gaskets between anode CC & MEA, between MEA & cathode CC, and between cathode CC & cathode end cover

A Teflon-coated woven cloth gasket is used to prevent the leak between the anode current collector & MEA, MEA & cathode current collector, and cathode current collector & cathode end cover. The new gasket and the gasket which served for two years are shown in figure 4.42(a). During the visual examination of the component, no visible defects are identified. However, pressing and scratch marks are observed as a result of compression against the rough surface of metallic current collectors.

Hardness testing is carried out on the new and used gaskets and the values measured are 89 *shore A* and 96 *shore A* respectively. These measurements are shown in Figure 4.42(b). This variation in the hardness is small, indicating no significant change in Teflon in methanol environment.

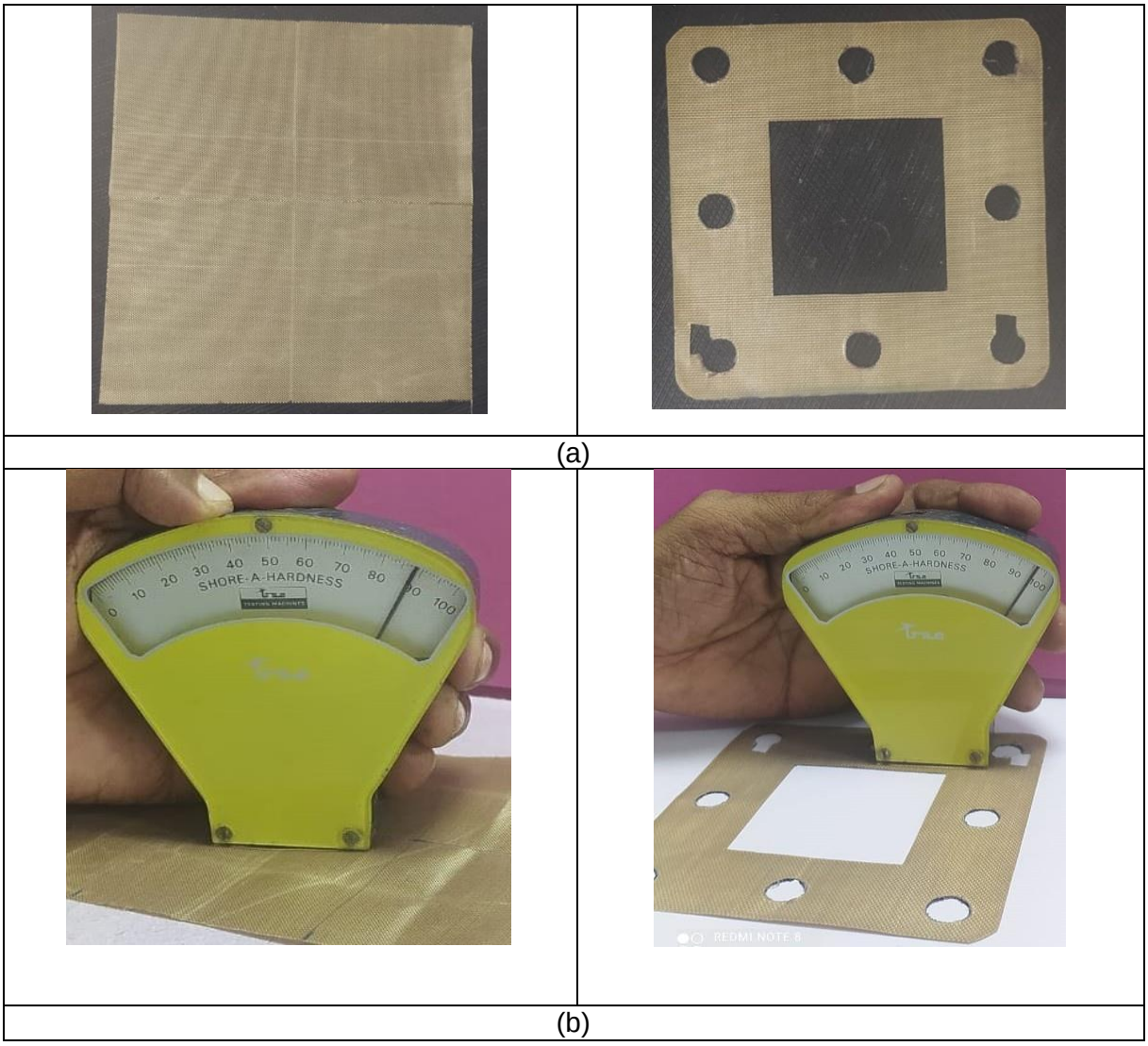

(a) VT on new and used gaskets, (b) Hardness testing on new and used gaskets.

Figure 4.42 Teflon-coated woven cloth Gaskets testing.

Thickness measurement is carried out on the new and used gasket. The new gasket is 0.20 mm thick whereas the used one is 0.18 mm thick. Hence there is a compression of 10% (0.02 mm) due to bolting loads over two years of service.

Evaluation of test results: From the above results, there is no significant deterioration of the Teflon-coated woven cloth gasket and is intact with the cell operating environment for a reported duration of two years.

4.5.5 Membrane Electrode Assembly

Membrane electrode assembly consists of an anode loaded with Platinum-Ruthenium catalyst, a cathode loaded with Platinum catalyst, and a proton-conducting membrane in

between anode and cathode. MEA, facing anode side is shown in figures 4.43(a). From the literature, [105] it is observed that the initial power density of PDMFC is lost about by 30% after a test period of 75 hours. This is due to an increase in resistance because of de-bonding of electrodes with MEA, swelling of membrane and electrodes. SEM images are shown as figures 4.43(b) and 4.43(c) for new and used MEA (for 75 hours), respectively. TEM images of electro-catalysts are shown in figures 4.44(a) and 4.44(b) for new and 75 hours of serviced MEA, respectively. Accumulation of electro-catalysts and metallic particles on membrane indicates the aggressiveness of methanol environment on MEA and fuel cell internals.

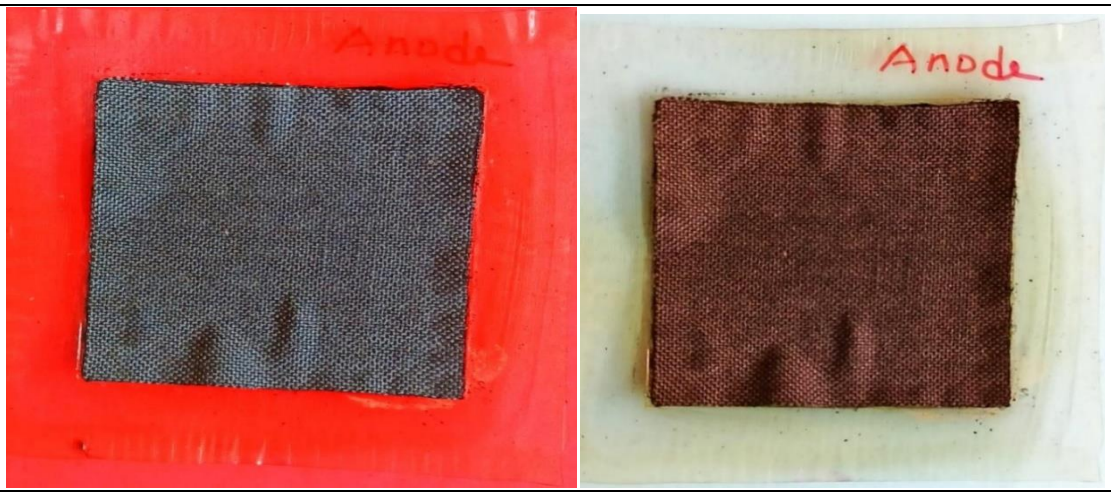

(a)

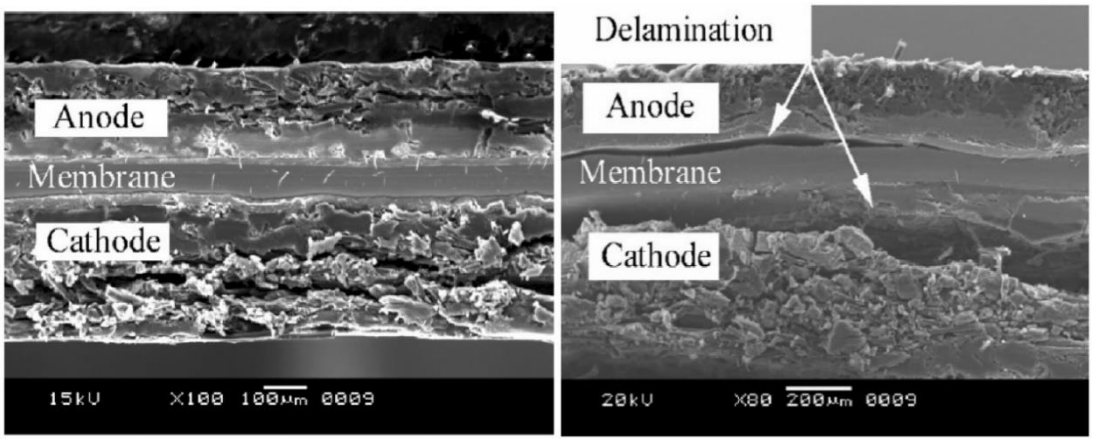

(b) (c)

(a) MEA facing anode side, (b) As received (new) MEA, cross-sectional view under SEM, (c) After 75 hours of MEA in PDMFC, cross-sectional view under SEM [105]

Figure 4.43 MEA Images

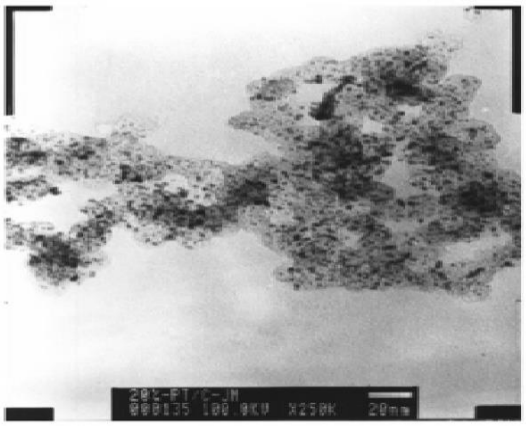

(d)

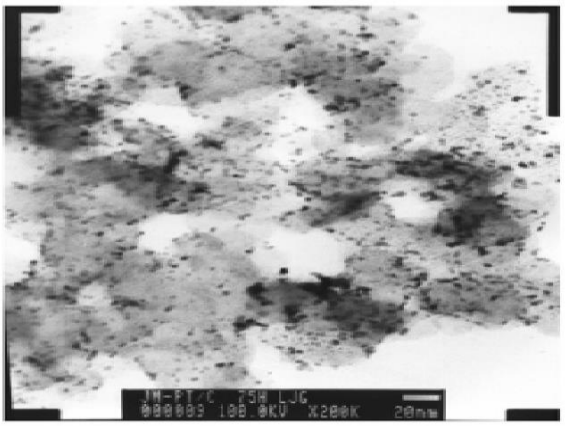

(e)

(a) As received (new) MEA, electro-catalysts view under TEM, (b) After 75 hours of MEA in the cell, electro-catalysts view under TEM [105]

Figure 4.44 MEA TEM Images

Evaluation of test results: From the above microstructures interpretation, the performance degradation of MEA attributes to de-lamination of the MEA with electrodes and agglomeration of electro-catalyst and metals during cell operation.

4.5.6 Cathode Current Collector

In the operation of the cell, the cathode end current collectors are getting corroded at a rate slower than that at the anode side. The corrosion at cathode end CC is attributed to methanol cross-over and the formation of water vapour. From the visual examination, it is observed that the brass reacts with methanol and forms surface oxides. However, Ni-201 and SS-316L are found to be free from visual imperfections. So, the usage of brass materials specific to the cathode end may be considered as long as the surface is free from methanol cross-over that too at lower methanol concentrations. Therefore, brass is not a good choice for higher methanol concentrations and prolonged operation of cell. Images of the SS-316L, Ni-201, and Brass current collectors before conducting the experiment are shown in figure 4.45(a). Brass current collectors before and after exposure to the methanol environment are shown in figures4.45(c) and 4.45(d) respectively.

Surface Examination is performed using Penetrant Testing by colour contrast solvent removable method. No reportable discontinuities are identified during the evaluation of the components. The SS-316L, Ni-201, and brass current collectors after the application of the developer during the evaluation process are shown in figure 4.45(b).

(a)

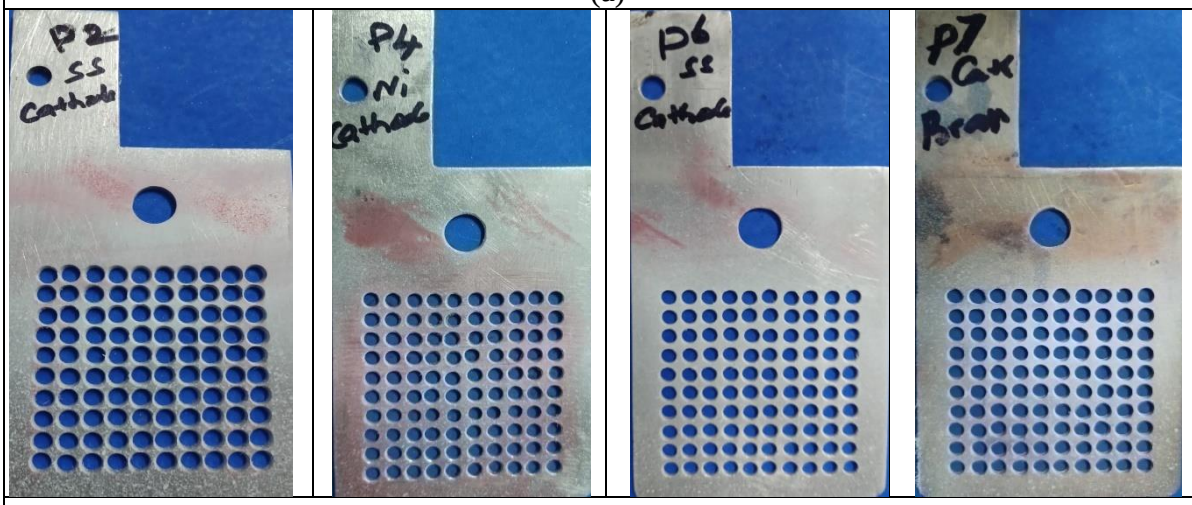

(b)

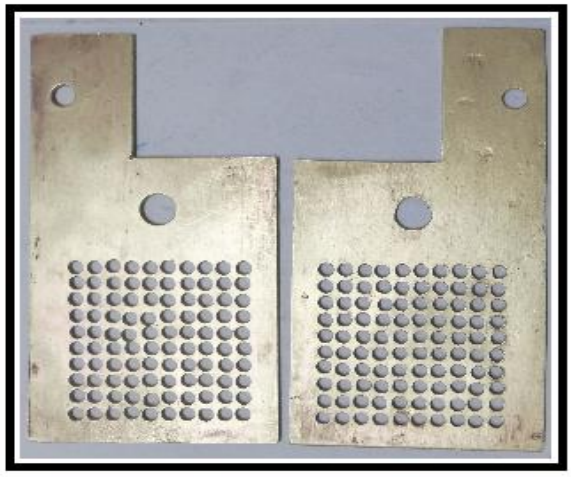

(c)

(d)

(a) VT on SS-316, Ni-201, and Brass current collectors.

(b) Penetrant Test on SS-316, Ni-201, and Brass current collectors.

(c) Brass CC before the experiment.

(d) Corrosion on Brass at cathode side exposed to 4M methanol.

Figure 4.45 Cathode Current Collectors Testing

Evaluation of test results: From the above interpretations, it is observed that there is no deterioration of cathode current collectors made of SS-316L and Ni-201. In Brass current collectors, corrosion is observed due to the reaction with crossover methanol and formation of surface oxides.

4.5.7 Cathode end cover

The cathode end acrylic cover shown in figure 4.46(a) is subjected to visual examination to identify visible discontinuities on the component. However, during the evaluation of the component, linear crack is visible as discontinuity at the top left corner to the drilled hole.

Surface Examination is performed using Penetrant Testing by colour contrast solvent removable method. However, two reportable discontinuities are identified during the evaluation of the component. The component after the application of the developer and during the evaluation process is shown in Figures 4.46(b) and 4.46(c). The evaluated crack length that originated from the inside corner is 32 mm and other crack above the hole is having a length of 8 mm.

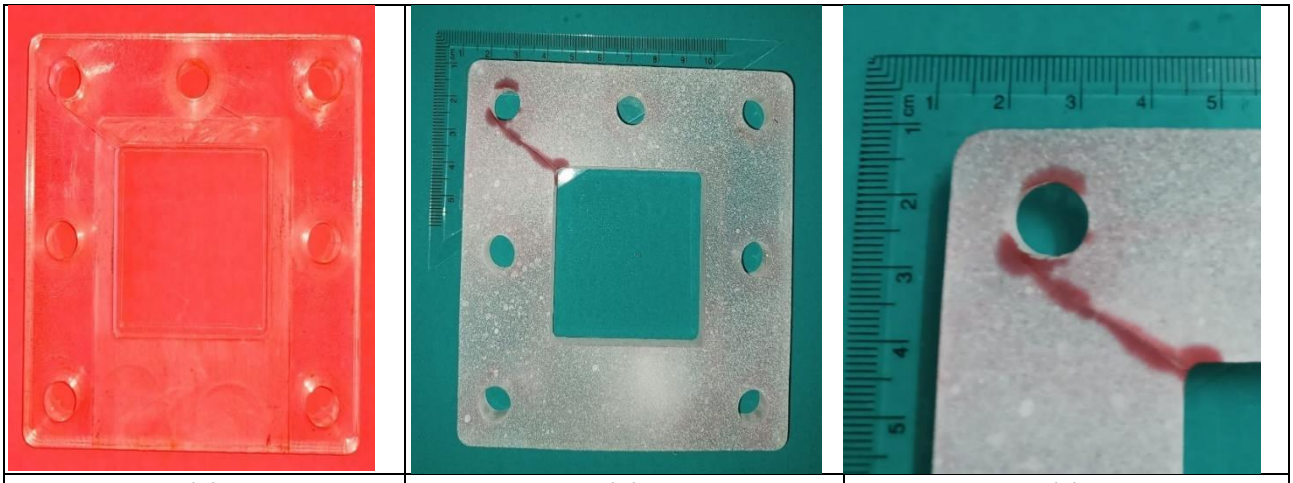

(a) (b) (c)

(a) VT Cathode end acrylic cover.

(b) Penetrant Test on cathode end acrylic cover

(c) Close shot of PT defect indication.

Figure 4.46 Cathode End Cover

Evaluation of test results: The cathode end acrylic cover has two linear defects from the above interpretations of penetrant testing. These defects may cause leakages. These defects originated due to excessive bolt loadings or uneven tightening of fasteners.

4.5.8 Fasteners (bolts, nuts, washers)

Within the PDMFC, it is observed that the fasteners such as bolts, washers, and nuts are getting corroded. From the visual examination, it is observed that the mild steel components react quickly and form surface oxides. Images of the new bolts, nuts, and washers before the start of the experiment are shown in figures 4.47(a) and 4.47(b), and the same after a service period of 2 years are shown in Figures 4.47(c), 4.47(d), 4.47(e) and 4.47(f). The corrosion rate of each fastener is calculated by taking the weights before and after the experiment. An average of seven sets of fasteners are calculated and tabulated in table 4.10.

Calculation details:

Weight Before the experiment = $\theta 1$ g

Weight after the experiment = $\theta 2$ g

Weight Loss = $(\theta 1 - \theta 2)$ g

Duration of experiment = τ years

Experimental Corrosion Rate, ξ = $[(\theta 1 - \theta 2)/ \tau]$ g/year

Table 4.10 Fasteners Short Term Corrosion Measurement Data

Parameter / Component	**MS Bolt**	**MS Nut**	**Spring Washer**	**Plain Washer**
Weight Before Experiment, $\theta 1$g	16.736	4.391	1.125	1.080
Weight after two years, $\theta 2$ g	16.625	4.243	1.013	0.958
Weight loss, $(\theta 1 - \theta 2)$ g	0.111	0.148	0.112	0.122
Duration of exposure, τ years	2	2	2	2
Established Corrosion rate, ξ g/year	0.0555	0.074	0.056	0.061

(a) As received MS Bolts with an insulating cover, (b) As received washers and nuts
(c) Corroded bolts after a service period of 2 years, (d) Corroded nuts after a service period of 2 years, (e) Corroded spring washers after a service period of 2 years, (f) Corroded plain washers after a service period of 2 years

Figure 4.47 Fasteners

Evaluation of test results: From the above examination, it is observed that there is a deterioration of fasteners. The root cause of the deterioration is due to the corrosive environment of the cell.

4.5.9 Wrapping on fasteners.

In the PDMFC, it is observed that the wrapped tubes and sleeves over bolts are getting bulged. From the visual examination, it is observed that the tubes are getting peeled off due to frequent assembling and dismantling of the cell. However, the sleeves are getting bulged under compressive loads of bolts and nuts. Images of the new and used insulating tubes over bolts are shown in figures 4.48(a) and 4.48(b) respectively. The sleeves used for bolts at anode and cathode sides of cell, after a service period of 2 years are shown in figures 4.48(c) and 4.48(d) respectively.

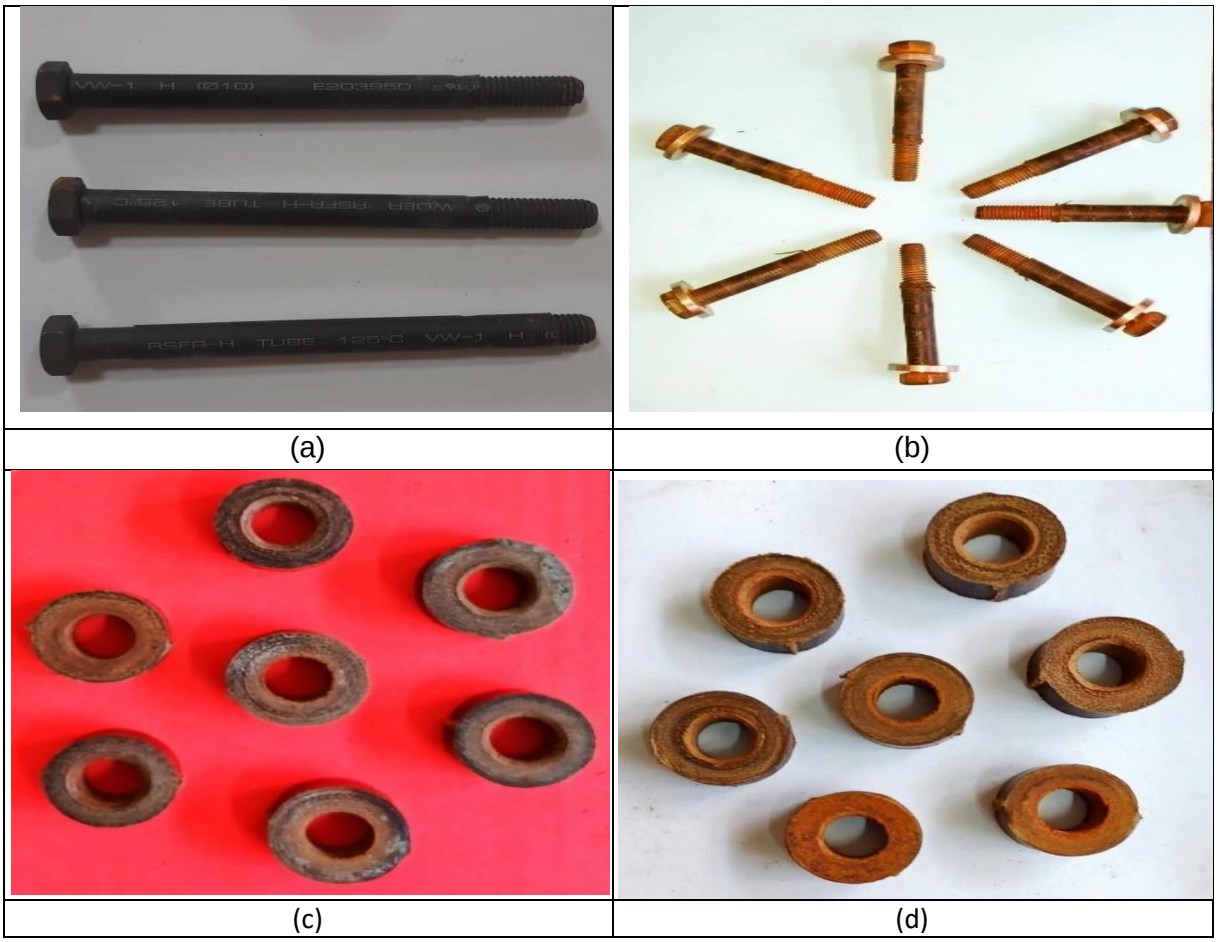

(a) Electrical insulating tube over MS Bolts as received, (b) Electrical insulating tube over MS Bolts after 2 years of service, (c) Anode side bulged insulating sleeves after a service period of 2 years, (d) Cathode side bulged insulating sleeves after a service period of 2 years

Figure 4.48 Wrapping on fasteners.

Evaluation of test results: From the above interpretations, it is observed that there is damage to tubes and sleeves. The root cause of the deterioration is the compressive loading on sleeves and the rubbing of tubes during assembling and dismantling. Physically damaged insulating sleeves and tubes are better to replace to avoid short-circuiting of anode & cathode and for personal protection.

4.5.10 Summary

Fuel cell components and their durability are affected by methanol solution, its concentration, evaporative conditions of water, carbon dioxide evolution, heat generation, and its sealing components. NDT is performed on PDMFC components to evaluate their performance and to ascertain their serviceability, durability, expected life & healthiness. NDT such as Visual Testing, Liquid Penetrant Testing, Ultrasonic Testing for Thickness measurement, hardness measurement, and metallographic examination are used to identify direct or indirect means to find the size and to locate surface and subsurface discontinuities. The materials and components have been examined using Non-Destructive Testing and interpreted for acceptance/rejection or repair and to assure components' safety and reliability. The concluded results of the identified service induced degradations using Non-Destructive Testing Methods on PDMFC Components are tabulated in table 4.11.

Table 4.11 Results of the identified Service-Oriented Degradations using Non-Destructive Testing Methods

Name of the component	Envisaged Degradation Mechanism	Results
Anode End Cover	Brittle Cracks under aging and bolt loading	The anode end acrylic cover has no deterioration and is intact with the cell operating environment.
Gasket between anode end cover & anode	Compression Set, and Lack of softness	There is no deterioration of Viton gasket and is intact with the cell operating environment for a reported duration of two years.
Anode Current Collector	Uniform Corrosion, Corrosion Erosion in openings, and Surface cracks	It is observed that anode current collectors got deteriorated. Among SS-316L, Ni-201, and brass current collectors, the corrosion rate of brass is 11.8 times higher than SS-316L current collector, whereas Ni-201 has a corrosion rate of approximately 1/8 of that of SS-316L.

Gasket between anode and MEA, MEA and cathode, cathode end cover and cathode	Compression Set, and Lack of softness	There is no significant deterioration of the Teflon-coated woven cloth gasket and is intact with the cell operating environment for a reported duration of two years.
MEA	Reduction of Exchange Performance with time	The performance degradation of MEA attributes to delamination of membrane with electrodes and agglomeration of electro-catalyst and metals.
Cathode Current Collector	Uniform Corrosion	It is observed that there is no deterioration of cathode current collectors made of SS-316L and Ni-201. In Brass current collectors, corrosion is observed due to the reaction with crossover methanol and formation of surface oxides.
Cathode end cover	Brittle Cracks	The cathode end acrylic cover has two linear defects as evident in penetrant testing. These defects got originated due to excessive bolt loadings and/or uneven tightening of fasteners.
Fasteners (Bolts, nuts, washers)	Uniform Corrosion	It is observed that there is a deterioration of fasteners. The root cause of the deterioration is corrosive environment of the cell.
Wrapping on fasteners	Cracks under compression, Methanol Tolerance, and Swelling	It is observed that there is damage to tubes and sleeves. The root cause of the deterioration is the compressive loading on sleeves and the rubbing of tubes during assembling and dismantling. Physically damaged insulating sleeves and tubes need to be replaced for equipment and personal protection.

4.6 Comparison and Trend analysis with published research work

The results of the cell performance with Ni-Ni CC combination using taper cylindrical openings are compared with the published results of Boni et al, [11].

In this comparison, both the power density and voltage curves at 3 molar concentrations of methanol are plotted to compare the trends.

Figure 4.49 depicts both the power density curves have similar trends against current density. In the comparison, both the power density curves have initial increasing trend, reached a peak PD, and further falling. Present research experiment on PDMFC has generated higher power density and current density compared to the published research work.

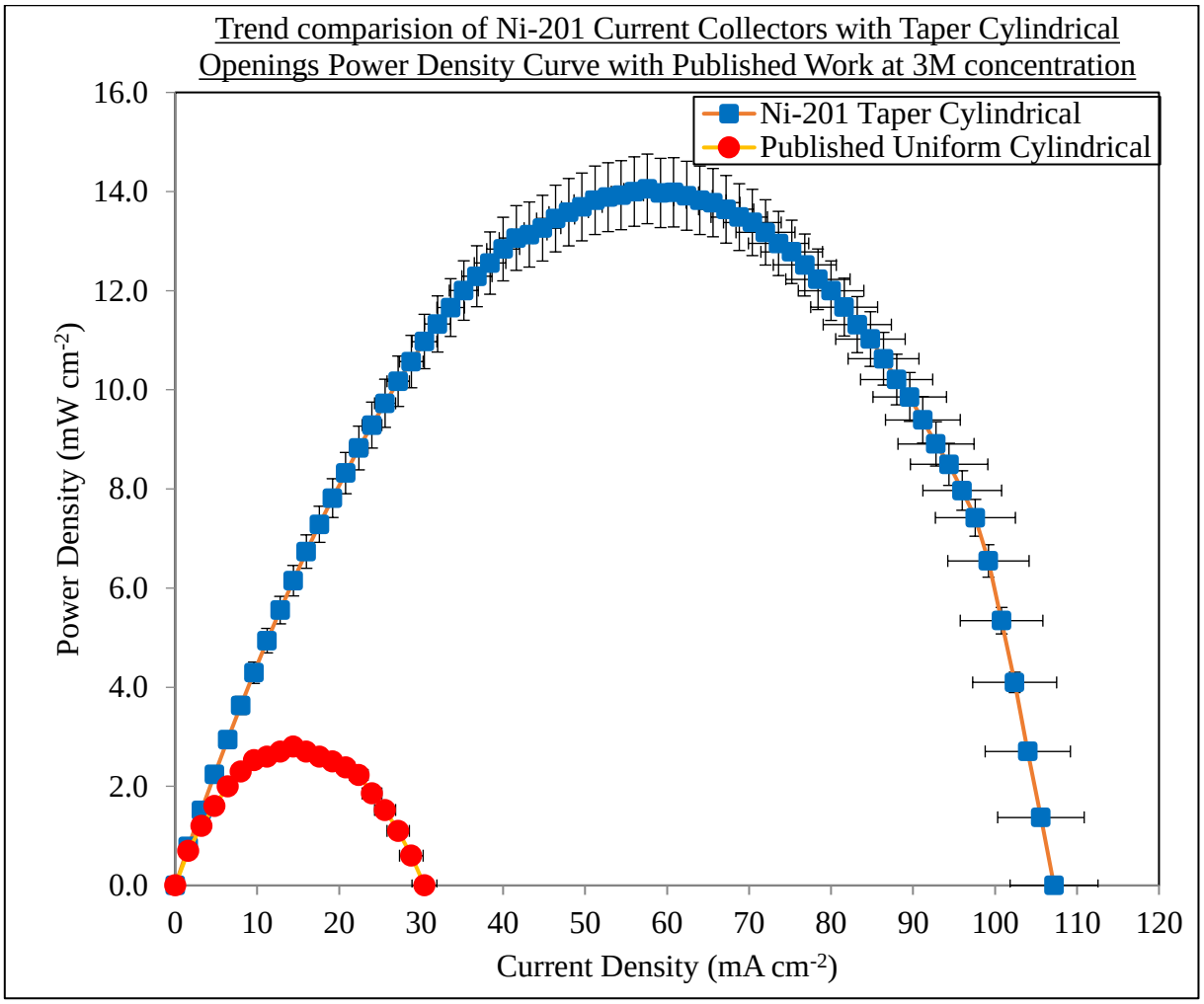

Figure 4.49 Power Density trends

Similarly, Figure 4.50 depicts both the polarisation curves have similar trends against current density. In both the curves, at low current densities, large voltage drop is noticed, which can be attributed to activation losses. Middle portion is flat due to constant voltage reduction attributed to ohmic losses and at the end both the curves falling quickly due to concentration losses. Present research experiment on PDMFC has generated higher current density and the voltage curve is flat compared to the published research work, Boni et al. [11], indicating stable characteristics.

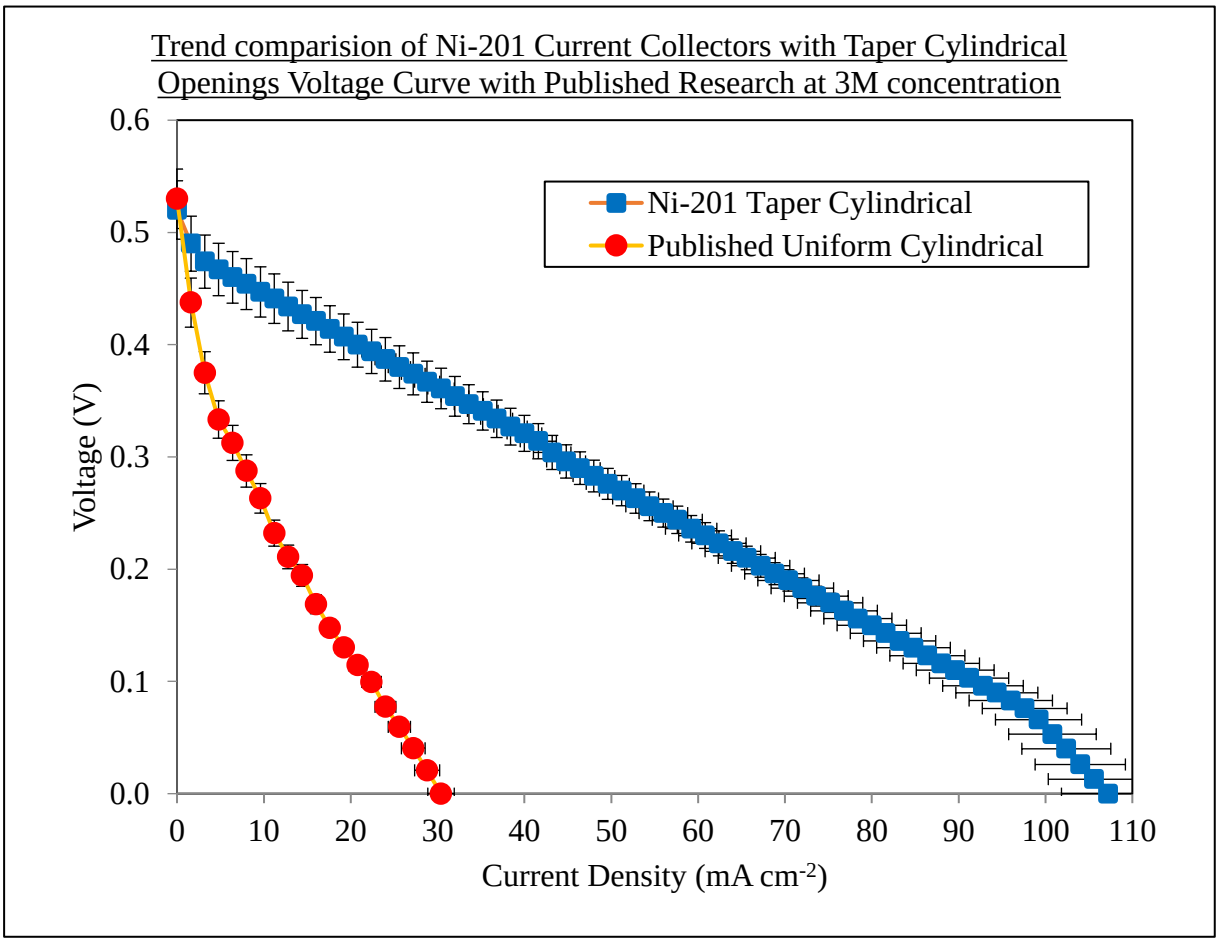

Figure 4.50 Polarization Curve trends

Chapter 5
Conclusions

5.1 Conclusions

Experimental investigations of Passive Direct Methanol Fuel Cell performance with Nickel-201 and Brass current collectors at various methanol concentrations are carried out and compared with the Stainless Steel-316L current collectors. The taper cylindrical openings in the current collectors assist more buoyancy effect on the evolved CO_2 bubbles due to the accommodation of a larger bubble volume compare to the uniform cylindrical opening. The analysis is extended with different combination of anode and cathode current collector materials in PDMFC. The variation in MEA shape/size is achieved by altering gasket openings in the dynamic regions. Non-Destructive Testing is performed on cell components to evaluate their performance and to ascertain their serviceability, durability, expected life and healthiness. From this experimental analysis, the following major conclusions are drawn.

- The maximum power density of cell obtained using Ni-201 current collectors is 10.416 $mW.cm^{-2}$ at 5M methanol concentration.
- From the series of experiments with Ni-201 current collectors, the peak current density achieved is 84.8 $mA.cm^{-2}$ at 5M methanol concentration.
- Cell with Ni-201 current collectors developed 31.92% higher power density than with SS-316L current collectors, whereas with brass current collectors it is 23.52% lower power density than with SS-316L current collectors.
- Among Ni-201, SS-316L and Brass current collector materials chosen for PDMFC experimental performance, it is revealed that the cell with Ni-201 current collectors having uniform cylindrical openings has produced the highest power density & maximum current density compared to brass and SS-316L current collectors.
- In taper cylindrical openings, the positive slope in the tapered surface allows the methanol fuel to flow more easily to the membrane site leading to better performance of the cell.
- Higher performance of PDMFC is achieved using Nickel-201 CC with taper cylindrical openings (34.92% in PD), resulting in ease of CO_2 scavenging due to increased buoyancy, which is a crucial finding.

- Specific power density using Ni-201 CC of the fuel cell at 3M methanol concentration got increased by 27.8%, i.e., from 14.28 $mW.cm^{-2}.kg^{-1}$ to 18.25 $mW.cm^{-2}.kg^{-1}$.
- As the weight of the cell got reduced by 3.3 %, its handling and portability becomes easy.
- With taper cylindrical openings in current collectors, the anode-cathode combination of Ni-201 & SS-316L showed better current density (97.6 $mA.cm^{-2}$) and power density (11.776 $mW.cm^{-2}$) than the other combinations.
- SS-316L & Brass combination showed the least performance with respect to current density (60.8 $mA.cm^{-2}$) and power density (6.144 $mW.cm^{-2}$).
- Among the anode-cathode combinations using taper cylindrical opening current collectors, Cell with Ni-SS combination has showed better polarization and Power Density characteristics, whereas the cell with SS-Brass combination showed the least performance.
- The Ni/SS anode-cathode combination is found economical; however, Ni/Ni anode-cathode combination is proven to be best in terms of maximum power density and corrosion resistance.
- In equal area geometries of MEA, cell with Square shaped dynamic zone has developed the highest power density of 6.344 $mW.cm^{-2}$ and a maximum current density of 65.2 $mA.cm^{-2}$.
- In equal perimeter geometries of MEA, cell with Rhombus shaped opening has developed the highest power density of 7.714 $mW.cm^{-2}$ and the maximum current density of 85.3 $mA.cm^{-2}$.
- The cell performance depends on the combined influence of (i) dynamic zone opening (MEA) shape, opening area, and its perimeter; (ii) Current collector opening ratio and opening perimeter and (iii) Distribution of bolting load.
- From the NDT interpretations, the anode end acrylic cover and Viton gasket are free from deterioration and are intact with the cell operating environment.
- Among the SS-316L, Ni-201, and brass anode current collectors, the corrosion rate on brass is 11.8 times higher than that of SS-316L current collector, whereas Ni-201 has a corrosion rate of approximately 1/8 of that of SS-316L.
- There is no significant deterioration of the Teflon-coated woven cloth gasket and is intact with the cell operating environment for a reported duration of two years.
- The performance degradation of MEA attributes to the de-lamination of the membrane with electrodes and agglomeration of electro-catalyst and metals.

- There is no noticeable deterioration of SS-316L and Ni-201current collectors at cathode side. However, corrosion is observed on brass current collectors, which is attributed to reaction with crossed over methanol leading to the formation of surface oxides.
- The cathode end acrylic cover has two linear defects, which are identified during penetrant testing. These defects originated due to excessive bolt loadings or uneven tightening of fasteners.
- The fasteners of the cell are getting deteriorated due to corrosive environment of the cell. It is required to replace these fasteners whenever the bolt and nut threads get damaged.
- There is damage in tubes and sleeves covering the bolts. The root cause of deterioration is compressive loading on sleeves and rubbing of tubes during assembling and dismantling. Physically damaged insulating sleeves and tubes need to be replaced for equipment and personal protection.

5.2 Research findings from the present work

- PDMFC performance is evaluated using SS-316L, Ni-201, and Brass current collector materials. At 5M methanol concentration, the PDMFC with Ni-201 CC has produced almost twice the maximum power density than that is produced by the cell using SS-316L CC. Therefore, of the above three materials, the cell with Ni-201 CC has shown superior performance.
- The power density of PDMFC with taper cylindrical openings CC is higher (around 35%) than that with uniform cylindrical openings CC. Therefore, the cell performance with taper cylindrical openings design is found better.
- The performance of the cell with different anode-cathode CC combinations among SS, Ni, and Brass is evaluated. Ni-SS combination is found to be better and economical. However, Ni-Ni is producing the highest power density and is showing best corrosion resistance in methanol environment.
- Among circular, rhombus, rectangular, and square-shaped dynamic geometry regions of MEA chosen for investigation of the performance of the cell, square shaped MEA in equal area geometries and rhombus shaped MEA in equal perimeter geometries gave the best performance.

- From the NDT of cell components, current collectors and MEA are identified as prone to deteriorate. From the experiments for compatibility of current collectors, Ni-201 is found to be better corrosion resistant material (about 12% of SS-316L corrosion rate).

5.3 Research contributions from the present work

- PDMFC performance among SS-316L, Ni-201, and Brass current collector materials, Ni-201 CC is identified as best material.
- The cell performance with taper cylindrical openings design is found better than uniform cylindrical openings.
- The performance of the cell with Ni-SS combination is found to be better and economical. However, Ni-Ni is producing the highest power density and is showing best corrosion resistance in methanol environment.

5.4 Limitations of the present work

The passive DMFC has lower power outputs compared to other fuel cells. This is due to the characteristic chemical kinetics of the methanol fuel cell. The limitations are listed below:

- Slower anode kinetic reaction rate at ambient conditions.
- Lower power output due to smaller active area of membrane.
- Higher power can be generated with multi stacking or with higher size active area of MEA or by doping additional catalyst loading.

5.5 Scope for future work

- To evaluate PDMFC performance with other membranes to reduce methanol permeation.
- To explore and employ new current collector materials compatible with methanol solution.
- In the present research, the planar shape fuel cell is considered, future work may be attempted with different geometrical shapes of the cell.

References

[1] O'hayre, R.P., Suk-Won Cha, Colella, W.G. and Prinz, F.B. (2016). *Fuel cell fundamentals*. Hoboken, New Jersey: John Wiley & Sons Inc.

[2] Narayanan, S., Valdez, T.I., Rohatgi, N., Chun, W., Hoover, W.G. and Halpert, G. (1999). Recent advances in direct methanol fuel cells. *Annual Battery Conference on Applications and Advances*. doi:https://doi.org/10.1109/bcaa.1999.795969.

[3] Barbir,F. (2013). Introduction. *PEM Fuel Cells*, pp.1–16. doi:https://doi.org/10.1016/b978-0-12-387710-9.00001-1.

[4] Braz BA, Oliveira VB, Pinto AMFR, Hernandez, R. and Dunning, C. (2017). Recent developments in passive direct methanol fuel cells. In: Direct methanol fuel cells applications, performance and technology, *Direct Methanol Fuel Cells*. pp. 143-203. Nova Science Publishers.

[5] N.V. Raghavaiah, G. Naga Srinivasulu and HariPrasad, I. (2020). Review of Challenges in Direct Methanol Fuel Cell and Contemporary Status. doi:https://doi.org/10.5281/zenodo.3989515.

[6] Braz, B.A., Oliveira, V.B. and Pinto, A.M.F.R. (2020). Optimization of a passive direct methanol fuel cell with different current collector materials. *Energy*, 208, p.118394. doi:https://doi.org/10.1016/j.energy.2020.118394.

[7] Das, P.K., Li, X. and Liu, Z.-S. (2008). A three-dimensional agglomerate model for the cathode catalyst layer of PEM fuel cells. *Journal of Power Sources*, 179(1), pp.186–199. doi:https://doi.org/10.1016/j.jpowsour.2007.12.085.

[8] Lim, C. and Wang, C.Y. (2004). Effects of hydrophobic polymer content in GDL on power performance of a PEM fuel cell. *Electrochimica Acta*, 49(24), pp.4149–4156. doi:https://doi.org/10.1016/j.electacta.2004.04.009.

[9] Narayanan, S.R. (1999). Design and Operation of an Electrochemical Methanol Concentration Sensor for Direct Methanol Fuel Cell Systems. *Electrochemical and Solid-State Letters*, 3(3), p.117. doi:https://doi.org/10.1149/1.1390975.

[10] Braz, B.A., Oliveira, V.B. and Pinto, A.M.F.R. (2020). Experimental Evaluation of the Effect of the Anode Diffusion Layer Properties on the Performance of a Passive Direct Methanol Fuel Cell. *Energies*, 13(19), p.5198. doi:https://doi.org/10.3390/en13195198.

[11] Boni, M., Srinivasa Rao Surapaneni, Naga Srinivasulu Golagani and Sateesh Kumar Manupati (2021). Experimental investigations on the effect of current collector open ratio on the performance of a passive direct methanol fuel cell with liquid electrolyte layer. *Chemical Papers*, 75(1), pp.27–38. doi:https://doi.org/10.1007/s11696-020-01277-0.

[12] Mallick, R.K., Thombre, S.B. and Shrivastava, N.K. (2015). A critical review of the current collector for passive direct methanol fuel cells. *Journal of Power Sources*, 285, pp.510–529. doi:https://doi.org/10.1016/j.jpowsour.2015.03.089.

[13] Boni, M., Rao, S.S. and Srinivasulu, G.N. (2019). Influence of intermediate liquid electrolyte layer on the performance of passive direct methanol fuel cell. *International Journal of Green Energy*, 16(15), pp.1475–1484. doi:https://doi.org/10.1080/15435075.2019.1671419.

[14] Yuan, W., Tang, Y., Yang, X., Liu, B. and Wan, Z. (2012). Structural diversity and orientation dependence of a liquid-fed passive air-breathing direct methanol fuel cell. *International Journal of Hydrogen Energy*, 37(11), pp.9298–9313. doi:https://doi.org/10.1016/j.ijhydene.2012.03.013.

[15] Juan Pablo Esquivel, NeusSabaté, Santander, J., N. Torres-Herrero, Gràcia, I., Ivanov, P., Fonseca, L. and Jaromir Hubalek (2009). Influence of current collectors design on the performance of a silicon-based passive micro direct methanol fuel cell. *Journal of Power Sources*, 194(1), pp.391–396. doi:https://doi.org/10.1016/j.jpowsour.2009.04.065

[16] Gholami, O., Imen, S. J., &Shakeri, M. (2013). Effect of non-uniform parallel channel on performance of passive direct methanol fuel cell. *International Journal of Hydrogen Energy*, *38*(8), 3395–3400. https://doi.org/10.1016/j.ijhydene.2013.01.020

[17] Yuan, W., Tang, Y., Yang, X., Bu, L. and Wan, Z. (2013). Corrosion Behavior of Porous Metal Fiber-Sintered Felt in Both Simulated and Practical Environments of a Direct Methanol Fuel Cell. *CORROSION*, 69(1), pp.25–34. doi:https://doi.org/10.5006/0666.

[18] Wilberforce, T., Ijaodola, O., Ogungbemi, E., Hassan, Z.E., Thompson, J. and Olabi, A.G. (2018). Effect of bipolar plate materials on performance of fuel cells. *Reference Module in Materials Science and Materials Engineering*, [online] pp.1–15. doi:https://doi.org/10.1016/B978-0-12-803581-8.11272-X.

[19] Munjewar, S.S., Thombre, S.B. and Mallick, R.K. (2016). A comprehensive review on recent material development of passive direct methanol fuel cell. *Ionics*, 23(1), pp.1–18. doi:https://doi.org/10.1007/s11581-016-1864-1.

[20] Mallick, R.K., Thombre, S.B. and Shrivastava, N.K. (2015). A critical review of the current collector for passive direct methanol fuel cells. *Journal of Power Sources*, 285, pp.510–529. doi:https://doi.org/10.1016/j.jpowsour.2015.03.089.

[21] Boni, M., Srinivasa Rao, S. and Naga Srinivasulu, G. (2020). Performance evaluation of an air breathing–direct methanol fuel cell with different cathode current collectors with liquid electrolyte layer. *Asia-Pacific Journal of Chemical Engineering*, 15(4). doi:https://doi.org/10.1002/apj.2465.

[22] Escudero-Cid, R., Pérez-Flores, J.C., Fatás, E. and Ocón, P. (2014). Degradation of DMFC using a New Long-Term Stability Cycle. *International Journal of Green Energy*, 12(6), pp.641–653. doi:https://doi.org/10.1080/15435075.2013.867269.

[23] N. V. Raghavaiah, Overview of Pressure Vessel Design using ASME Boiler and Pressure Vessel Code Section VIII Division-1 and Division- 2 (2019) International Journal of Research in Engineering, Science and Management, Volume-2, Issue-6, June-2019, page 525-526, www.ijresm.com | ISSN (Online): 2581-5792.

[24] Yang, W.M., Chou, S.K. and Shu, C. (2007). Effect of current-collector structure on performance of passive micro direct methanol fuel cell. *Journal of Power Sources*, 164(2), pp.549–554. doi:https://doi.org/10.1016/j.jpowsour.2006.11.014.

[25] Dohle, H. (2002). Heat and power management of a direct-methanol-fuel-cell (DMFC) system. *Journal of Power Sources*, 111(2), pp.268–282. doi:https://doi.org/10.1016/s0378-7753(02)00339-7.

[26] Huang, J., Baird, D.G. and McGrath, J.E. (2005). Development of fuel cell bipolar plates from graphite filled wet-lay thermoplastic composite materials. *Journal of Power Sources*, 150, pp.110–119. doi:https://doi.org/10.1016/j.jpowsour.2005.02.074.

[27] Abraham, B.G. and Chetty, R. (2021). Design and fabrication of a quick-fit architecture air breathing direct methanol fuel cell. *International Journal of Hydrogen Energy*, 46(9), pp.6845–6856. doi:https://doi.org/10.1016/j.ijhydene.2020.11.184.

[28] Song, S.Q., Liang, Z.X., Zhou, W.J., Sun, G.Q., Xin, Q., Stergiopoulos, V. and Tsiakaras, P. (2005). Direct methanol fuel cells: The effect of electrode fabrication procedure on MEAs structural properties and cell performance. *Journal of Power Sources*, 145(2), pp.495–501. doi:https://doi.org/10.1016/j.jpowsour.2005.02.069.

[29] Das, S., Dutta, K. and PatitPaban Kundu (2015). Nickel nanocatalysts supported on sulfonated polyaniline: potential toward methanol oxidation and as anode materials for DMFCs. *Journal of materials chemistry. A, Materials for energy and sustainability*, 3(21), pp.11349–11357. doi:https://doi.org/10.1039/c5ta01837d.

[30] Cha, H.-C., Chen, C.-Y. and Shiu, J.-Y. (2009). Investigation on the durability of direct methanol fuel cells. *Journal of Power Sources*, 192(2), pp.451–456. doi:https://doi.org/10.1016/j.jpowsour.2009.03.028.

[31] Kuan, Y.-D., Lee, S.-M. and Sung, M.-F. (2014). Development of a Direct Methanol Fuel Cell with Lightweight Disc Type Current Collectors. *Energies*, 7(5), pp.3136–3147. doi:https://doi.org/10.3390/en7053136.

[32] Sgroi, M., Zedde, F., Barbera, O., Stassi, A., Sebastián, D., Lufrano, F., Baglio, V., Aricò, A., Bonde, J. and Schuster, M. (2016). Cost Analysis of Direct Methanol Fuel Cell Stacks for Mass Production. *Energies*, 9(12), p.1008. doi:https://doi.org/10.3390/en9121008.

[33] Xu, Q., Sun, W., Zhang, J., Zhang, W., Ma, Q., Su, H. and Xing, L. (2021). Constructing a graphene-contained layer in anode to improve the performance of direct methanol fuel cells using high-concentration fuel. *International Journal of Green Energy*, 18(6), pp.566–577. doi:https://doi.org/10.1080/15435075.2020.1865374.

[34] Braz, B.A., Oliveira, V.B. and Pinto, A.M.F.R. (2020). Experimental Evaluation of the Effect of the Anode Diffusion Layer Properties on the Performance of a Passive Direct Methanol Fuel Cell. *Energies*, 13(19), p.5198. doi:https://doi.org/10.3390/en13195198.

[35] Shrivastava, N.K. and Tequila (2017). Direct Methanol Fuel Cells. *Elsevier eBooks*, pp.343–357. doi:https://doi.org/10.1016/b978-0-12-409548-9.10121-6.

[36] Braz, B.A., Oliveira, V.B. and Pinto, A.M.F.R. (2020). Optimization of a passive direct methanol fuel cell with different current collector materials. *Energy*, 208, p.118394. doi:https://doi.org/10.1016/j.energy.2020.118394.

[37] Compatibility of Metals & Alloys in Neat Methanol Service. (n.d.). Available at: https://www.methanol.org/wp-content/uploads/2016/06/Compatibility-of-Metals-Alloys-in-Neat-Methanol-Service.pdf.

[38] Meenakshi, H.N. and More, S.S. (2021). Corrosion Behavior of Brass in Methanol-Gasoline Fuel Blends. *Springer Proceedings in Materials*, pp.393–401. doi:https://doi.org/10.1007/978-981-15-8319-3_40.

[39] Braz, B.A., Oliveira, V.B. and Pinto, A.M.F.R. (2019). Experimental studies of the effect of cathode diffusion layer properties on a passive direct methanol fuel cell power output. *International Journal of Hydrogen Energy*, 44(35), pp.19334–19343. doi:https://doi.org/10.1016/j.ijhydene.2019.03.162.

[40] Braz, B. A., Moreira, C., & Alexandra M.F.R. Pinto. (2019). Effect of the current collector design on the performance of a passive direct methanol fuel cell. *Electrochimica Acta, 300*, 306–315. https://doi.org/10.1016/j.electacta.2019.01.131

[41] Calabriso, A., Cedola, L., Del Zotto, L., Rispoli, F. and Santori, S.G. (2015). Performance investigation of Passive Direct Methanol Fuel Cell in different structural configurations. *Journal of Cleaner Production*, [online] 88, pp.23–28. doi:https://doi.org/10.1016/j.jclepro.2014.06.087.

[42] Yousefi, S., Shakeri, M. and Sedighi, K. (2013). The effect of cell orientations and environmental conditions on the performance of a passive DMFC single cell. *Ionics*, 19(11), pp.1637–1647. doi:https://doi.org/10.1007/s11581-013-0889-y.

[43] Yousefi, S. and Ganji, D.D. (2012). Experimental investigation of a passive direct methanol fuel cell with 100cm2 active areas. *Electrochimica Acta*, 85, pp.693–699. doi:https://doi.org/10.1016/j.electacta.2012.08.045.

[44] Ahmad, H., Kamarudin, S.K., Hasran, U.A. and Daud, W.R.W. (2011). A novel hybrid Nafion-PBI-ZP membrane for direct methanol fuel cells. *International Journal of Hydrogen Energy*, 36(22), pp.14668–14677. doi:https://doi.org/10.1016/j.ijhydene.2011.08.044.

[45] Gholami, O., Imen, S.J. and Shakeri, M. (2013). Effect of non-uniform parallel channel on performance of passive direct methanol fuel cell. *International Journal of Hydrogen Energy*, 38(8), pp.3395–3400. doi:https://doi.org/10.1016/j.ijhydene.2013.01.020.

[46] Argyropoulos, P., Scott, K. and Taama, W.M. (1999). Carbon dioxide evolution patterns in direct methanol fuel cells. *Electrochimica Acta*, 44(20), pp.3575–3584. doi:https://doi.org/10.1016/s0013-4686(99)00102-4.

[47] Hsieh, S.-S., Huang, C.-F. and Feng, C.-L. (2008). A novel design and micro-fabrication for copper (Cu) electroforming bipolar plates. *Micron*, 39(3), pp.263–268. doi:https://doi.org/10.1016/j.micron.2007.03.003.

[48] Sgroi, M., Zedde, F., Barbera, O., Stassi, A., Sebastián, D., Lufrano, F., Baglio, V., Aricò, A., Bonde, J. and Schuster, M. (2016). Cost Analysis of Direct Methanol Fuel Cell Stacks for Mass Production. *Energies*, 9(12), p.1008. doi:https://doi.org/10.3390/en9121008.

[49] Argyropoulos, P., Scott, K. and Taama, W.M. (1999). *Journal of Applied Electrochemistry*, 29(6), pp.663–671. doi:https://doi.org/10.1023/a:1003589319211.

[50] Tang, Y., Yuan, W., Pan, M., Tang, B. and Wan, Z. (2010). Effects of structural aspects on the performance of a passive air-breathing direct methanol fuel cell. *Journal of Power Sources*, 195(17), pp.5628–5636. doi:https://doi.org/10.1016/j.jpowsour.2010.03.069.

[51] Govindarasu, Ramasamy, R. Parthiban and P. K. Bhaba. (2014).Recent evolutions in modeling of direct methanol fuel cell. Elixir Chem. Engg., 72, 25428-25433

[52] Chang, J.-Y., Kuan, Y.-D. and Lee, S.-M. (2014). Experimental Investigation of a Direct Methanol Fuel Cell with Hilbert Fractal Current Collectors. *Journal of Chemistry*, 2014, pp.1–7. doi:https://doi.org/10.1155/2014/371616.

[53] Vasco S. Silva, Adélio M. Mendes, Luis M. Madeira and Suzana P. Nunes, (2005)Membranes for direct methanol fuel cell applications: Analysis based on characterization, experimentation and modeling, *Advances in Fuel Cells*, ISBN: 81-308-0026-8.

[54] Hashemi, R., Yousefi, S. and Faraji, M. (2015). Experimental studying of the effect of active area on the performance of passive direct methanol fuel cell. *Ionics*, 21(10), pp.2851–2862. doi:https://doi.org/10.1007/s11581-015-1479-y.

[55] Govindarasu, R. and Somasundaram, S. (2020). Studies on Influence of Cell Temperature in Direct Methanol Fuel Cell Operation. *Processes*, 8(3), p.353. doi:https://doi.org/10.3390/pr8030353.

[56] Claycomb, J.R., Audrius Brazdeikis, Le, M., Yarbrough, R.A., GrigoriyGogoshin and Miller, J.M. (2003). Nondestructive testing of PEM fuel cells. *IEEE Transactions on Applied Superconductivity*. doi:https://doi.org/10.1109/tasc.2003.813687.

[57] Frikkie C. De Beer, NDT.net Issue: 2018-04 Publication: SAINT-2018 Conference & Exhibition of the South African Institute for NDT, 17-18 Feb 2018, Johannesburg, South Africa (SAINT 2018), Hydrogen Fuel Cells Optimization through NDT using Neutron Radiography, 5 Nuclear Energy Corporation of South Africa (NECSA)8, Pretoria, South Africa V

[58] axenics.com. (2019). *Non-Destructive Weld Testing | Alternative Energy Manufacturing | Axenics*. [online] Available at: https://axenics.com/blog/non-destructive-weld-testing-alternative-energy-manufacturing [Accessed 29 Apr. 2023].

[59] Zhou, W., Wang, J., Pan, Z., Liu, J., Ma, L., Zhou, J. and Su, Y. (2022). Review on optimization design, failure analysis and non-destructive testing of composite hydrogen storage vessel. *International Journal of Hydrogen Energy*, [online] 47(91), pp.38862–38883. doi:https://doi.org/10.1016/j.ijhydene.2022.09.028.

[60] N. V. Raghavaiah.(2019).Overview of Pressure Vessel Design using ASME Boiler and Pressure Vessel Code Section VIII Division-1 and Division- 2 *International Journal of Research in Engineering, Science and Management*, Volume-2, Issue-6, June-2019, page 525-526, www.ijresm.com | ISSN (Online): 2581-5792.

[61] Siti Aminah Osman, Siti KartomKamarudin, Karim, N.A. and SahriahBasri (2021). Application of graphene in low-temperature fuel cell technology: An overview. *International Journal of Energy Research*, 45(13), pp.18318–18336. doi:https://doi.org/10.1002/er.6969.

[62] Deng, H., Ma, Z., Zhang, X., Zhang, Y. and Liu, X. (2015). Corrosion resistance in simulated DMFC environment of plasma electrolytic oxidation coating prepared on aluminum alloy. *Surface and Coatings Technology*, 269, pp.108–113. doi:https://doi.org/10.1016/j.surfcoat.2015.02.027.

[63] Kim, Y., Kim, S. and Choe, B. (2019). The Role of Hydrogen in Hydrogen Embrittlement of Metals: The Case of Stainless Steel. *Metals*, 9(4), p.406.

[64] PavolDlhý, Poduška, J., Arbeiter, F., Gosch, A., OndrejSlávik, LubošNáhlík and Pavel Hutař (2021). Crack Propagation Analysis of Compression Loaded Rolling Elements. *Materials*, 14(10), pp.2656–2656. doi:https://doi.org/10.3390/ma14102656.

[65] Prabhuraj, P. et al. “Evaluating stress corrosion cracking behaviour of high strength AA7075-T651 aluminium alloy.” *Journal of the Mechanical Behavior of Materials* 26 (2017): 105 - 112.

[66] Bayerl, H. (2009). Compression Set of Silicone Elastomers. *International polymer science and technology*. doi:https://doi.org/10.1177/0307174x0903600801.

[67] Autor: Harold Berger, Mordfin, L. and American Society For Testing And Materials. Committee E-7 On Nondestructive Testing (1992). *Nondestructive testing standards--present and future*. Editorial: Philadelphia, Pa: Astm.

[68] Dwivedi, S.K., Vishwakarma, M. and Soni, Prof.Akhilesh. (2018). Advances and Researches on Non Destructive Testing: A Review. *Materials Today: Proceedings*, [online] 5(2), pp.3690–3698. doi:https://doi.org/10.1016/j.matpr.2017.11.620.

[69] Zillmann, R. W. (1977). Nondestructive Testing Standards in the ASME Boiler and Pressure Vessel Code. *ASTM International*.

[70] DalalanaBertoglio, D. and Zorzo, A.F. (2017). Overview and open issues on penetration test. *Journal of the Brazilian Computer Society*, 23(1). doi:https://doi.org/10.1186/s13173-017-0051-1.

[71] Tesfaye, T., Mohammed, M.S. and Ki-Seong, K. (2019). Mapping of ultrasonic thickness measurements using laser grid projection and image processing. *Insight - Non-Destructive Testing and Condition Monitoring*, 61(11), pp.643–649. doi:https://doi.org/10.1784/insi.2019.61.11.643.

[72] Sharma, A. and Sinha, A.K. (2018). Ultrasonic testing for mechanical engineering domain: present and future perspective. *International Journal of Research*, 7(2), pp.243–253. doi:https://doi.org/10.22105/riej.2018.100730.1018.

[73] Qi, H.J., Joyce, K. and Boyce, M.C. (2003). Durometer Hardness and the Stress-Strain Behavior of Elastomeric Materials. *Rubber Chemistry and Technology*, 76(2), pp.419–435. doi:https://doi.org/10.5254/1.3547752.

[74] Zhao, H., Allanson, D. and Ren, X.J. (2015). Use of Shore Hardness Tests for In-Process Properties Estimation/Monitoring of Silicone Rubbers. *Journal of Materials Science and Chemical Engineering*, 03(07), pp.142–147. doi:https://doi.org/10.4236/msce.2015.37019.

[75] www.astm.org. (n.d.). *Standard Practice for Microetching Metals and Alloys*. [online] Available at: https://www.astm.org/e0407-07r15e01.html.

[76] Tcr, P. and Llc, A. (n.d.). *09012 Use of In-Situ Metallography for Plant Health Assessment Studies and Failure Investigations*. [online] Available at: https://www.evolvetcr.com/download/Paper-on-Use-of-In-Situ-Metallography-for-Plant-Health-Assessment-Studies-and-Failure-Investigations.pdf [Accessed 29 Apr. 2023].

[77] www.astm.org. (n.d.). *Standard Practice for Scanning Electron Microscope Beam Size Characterization*. [online] Available at: https://www.astm.org/e0986-04r17.html [Accessed 29 Apr. 2023].

[78] Matsuyama, H. and Koike, K. (1991). A data acquisition and display system for spin-polarized scanning electron microscopy (spin SEM). *Review of Scientific Instruments*, 62(4), pp.970–981. doi:https://doi.org/10.1063/1.1141987.

[79] 14:00-17:00 (n.d.). *ISO 29301:2010*. [online] ISO. Available at: https://www.iso.org/standard/45399.html [Accessed 29 Apr. 2023].

[80] Mast, J., Verleysen, E., Hodoroaba, V.-D. and Kaegi, R. (2020). Characterization of nanomaterials by transmission electron microscopy: Measurement procedures. *Characterization of Nanoparticles*, pp.29–48. doi:https://doi.org/10.1016/b978-0-12-814182-3.00004-3.

[81] Nicole Gleichmann (2020). *SEM vs TEM*. [online] Analysis & Separations from Technology Networks. Available at: https://www.technologynetworks.com/analysis/articles/sem-vs-tem-331262.

[82] Tsen, W.-C. (2020). Composite Proton Exchange Membranes Based on Chitosan and Phosphotungstic Acid Immobilized One-Dimensional Attapulgite for Direct Methanol Fuel Cells. *Nanomaterials*, 10(9), p.1641. doi:https://doi.org/10.3390/nano10091641.

[83] Awang, N., Jaafar, J. and Ismail, A.F. (2018). Thermal Stability and Water Content Study of Void-Free Electrospun SPEEK/Cloisite Membrane for Direct Methanol Fuel Cell Application. *Polymers*, 10(2), p.194. doi:https://doi.org/10.3390/polym10020194.

[84] Pavlin, M., Predan, J., Gubeljak, N. and Ćelić, R. (2019). Determination of the modulus of linearity of acrylic bases and acrylic teeth. *Materials Testing*, 61(10), pp.953–959. doi:https://doi.org/10.3139/120.111415.

[85] K. Deepak (2020). Effect of cathode end plate on passive direct methanol fuel cell performance. *IOP conference series*, 998, pp.012063–012063. doi:https://doi.org/10.1088/1757-899x/998/1/012063.

[86] Yousefi, S. and Zohoor, M. (2014). Conceptual design and statistical overview on the design of a passive DMFC single cell. *International Journal of Hydrogen Energy*, 39(11), pp.5972–5980. doi:https://doi.org/10.1016/j.ijhydene.2014.01.117.

[87] Calabriso, A., Cedola, L., Del Zotto, L., Rispoli, F. and Santori, S.G. (2015). Performance investigation of Passive Direct Methanol Fuel Cell in different structural configurations. *Journal of Cleaner Production*, [online] 88, pp.23–28. doi:https://doi.org/10.1016/j.jclepro.2014.06.087.

[88] Zhao, T., Chen, R., Yang, W. and Xu, C. (2009). Small direct methanol fuel cells with passive supply of reactants. *Journal of Power Sources*, 191(2), pp.185–202. doi:https://doi.org/10.1016/j.jpowsour.2009.02.033.

[89] Padhy, B.R. and Reddy, R.G. (2006). Performance of DMFC with SS 316 bipolar/end plates. *Journal of Power Sources*, 153(1), pp.125–129. doi:https://doi.org/10.1016/j.jpowsour.2005.02.089.

[90] Raja Maallah, Abdelilah Chtaini. (2021). Nickel-Modified Carbon Paste Electrode for the Methanol Fuel Cell. *Significances of Bioengineering & Biosciences*. 5(3). SBB. 000614. 2021. DOI: 10.31031/SBB.2021.05.000614

[91] M. Sunitha, N. Durgadevi, Sathish, A. and Ramachandran, T. (2018). Performance evaluation of nickel as anode catalyst for DMFC in acidic and alkaline medium. *Journal of fuel chemistry & technology*, 46(5), pp.592–599. doi:https://doi.org/10.1016/s1872-5813(18)30026-4.

[92] Raghavaiah, N.V. and Naga Srinivasulu, G. (2022). Experimental investigations on performance of passive direct methanol fuel cell using Nickel-201 and brass current collector materials. *Chemical Papers*, 76(7), pp.4581–4595. doi:https://doi.org/10.1007/s11696-022-02200-5.

[93] Yousefi, S. and Zohoor, M. (2014). Conceptual design and statistical overview on the design of a passive DMFC single cell. *International Journal of Hydrogen Energy*, 39(11), pp.5972–5980. doi:https://doi.org/10.1016/j.ijhydene.2014.01.117.

[94] Krishnamurthy, B. and S. Deepalochani (2009). Effect of PTFE content on the performance of a Direct Methanol fuel cell. *International Journal of Hydrogen Energy*, 34(1), pp.446–452. doi:https://doi.org/10.1016/j.ijhydene.2008.09.093.

[95] Munjewar, S.S., Thombre, S.B. and Mallick, R.K. (2017). Approaches to overcome the barrier issues of passive direct methanol fuel cell – Review. *Renewable and Sustainable Energy Reviews*, 67, pp.1087–1104. doi:https://doi.org/10.1016/j.rser.2016.09.002.

[96] Okada, T., Xie, G., Gorseth, O., Kjelstrup, S., Nakamura, N. and Arimura, T. (1998). Ion and water transport characteristics of Nafion membranes as electrolytes. *Electrochimica Acta*, 43(24), pp.3741–3747. doi:https://doi.org/10.1016/s0013-4686(98)00132-7.

[97] Mustafa Ercelik, Adnan Ozden, Yılser Devrim and C. Ozgur Colpan (2017). Investigation of Nafion based composite membranes on the performance of DMFCs. *International Journal of Hydrogen Energy*, 42(4), pp.2658–2668. doi:https://doi.org/ 10.1016/ j.ijhydene.2016.06.215.

[98] Boni, M., Rao, S.S. and Srinivasulu, G.N. (2019). Influence of intermediate liquid electrolyte layer on the performance of passive direct methanol fuel cell. *International Journal of Green Energy*, 16(15), pp.1475–1484. doi:https://doi.org/10.1080/ 15435075.2019.1671419.

[99] Ahmad, H., Kamarudin, S.K., Hasran, U.A. and Daud, W.R.W. (2011). A novel hybrid Nafion-PBI-ZP membrane for direct methanol fuel cells. *International Journal of Hydrogen Energy*, 36(22), pp.14668–14677. doi:https://doi.org/10.1016/ j.ijhydene. 2011.08.044.

[100] Yousefi, S., Shakeri, M. and Sedighi, K. (2013). The effect of cell orientations and environmental conditions on the performance of a passive DMFC single cell. *Ionics*, 19(11), pp.1637–1647. doi:https://doi.org/10.1007/s11581-013-0889-y.

[101] Kablou, Y., Cruickshank, C.A. and Matida, E. (2015). Experimental Analysis of a Small-Scale Flowing Electrolyte–Direct Methanol Fuel Cell Stack. *Journal of Fuel Cell Science and Technology*, 12(4). doi:https://doi.org/10.1115/1.4031423.

[102]Glüsen, A., Konradi, I., Detlef Stolten, Mergel, J., Grube, T., Detlef Stolten, Müller, M.J. and N. Kimiaie (2010). Manufacturing Technologies for Direct Methanol Fuel Cells (DMFCs). *18th World Hydrogen Energy Conference*.

[103]Munjewar, S.S., Thombre, S.B. and Mallick, R.K. (2016). A comprehensive review on recent material development of passive direct methanol fuel cell. *Ionics*, 23(1), pp.1–18. doi:https://doi.org/10.1007/s11581-016-1864-1.

[104]Horst Czichos (2021). Technology in the 21st Century – The role of materials and materials testing. *MP MATERIALPRUEFUNG - MP MATERIALS TESTING*. doi: https://doi.org/10.1515/mt-2020-0015.

[105]Liu, J., Zhou, Z., Zhao, X., Xin, Q., Sun, G. and Yi, B. (2004). Studies on performance degradation of a direct methanol fuel cell (DMFC) in life test. *Physical Chemistry Chemical Physics*, 6(1), pp.134–134. doi:https://doi.org/10.1039/b313478d.

[106]Ermilova, E., Kazak, F. and Weiß, S. (2019). Stability of structured sheet metals during buckling. *Materials Testing*, 61(10), pp.929–935. doi:https://doi.org/10.3139/ 120. 111403.

[107]Sandmeyer Steel. (n.d.). *Alloy 316/316L Austenitic Stainless Steel Plate*. [online] Available at: https://www.sandmeyersteel.com/316-316L.html.

[108]Properties of Some Metals and Alloys. (n.d.). Available at: https: //nickelinstitute.org/ media/1771/propertiesofsomemetalsandalloys_297_.pdf.

Publications

S. No	Name of the journal	Paper title	Remarks Index
1	Chemical Papers (Springer)	Experimental Investigations on Performance of Passive Direct Methanol Fuel Cell using Nickel-201 and Brass Current Collector Materials	Published (SCI)
2	Fuel Cells (Wiley)	Analysis and Experimental Investigation on Passive Direct Methanol Fuel Cell Current Collectors with Taper Cylindrical Openings	Published (SCI)
3	World Journal of Engineering (Emerald)	Experimental Investigations on Passive Direct Methanol Fuel Cell using Variable Membrane Electrode Assembly Dynamic Regions by Altering Gasket Shapes	Published (SCOPUS)
4	IEOM	Identification of Service-Oriented Degradations using Non-Destructive Testing Methods on Passive Direct Methanol Fuel Cell Components	Published (IEOM)
5	RESGA-2021: Renewable Energy for Sustainable Growth Assessment	Fuel Cells for Alternative and Sustainable Energy Systems (Book Chapter)	Published (Wiley Scrivener)
6	Patent (1), Govt. of India	Experimental Investigation on Performance of Passive Direct Methanol Fuel Cell using Taper Cylindrical Openings on Current Collectors	Published in Intellectual Properties of India
7	Patent (2), Govt. of India	Experimental Investigation on Performance of Passive Direct Methanol Fuel Cell using dynamic active regions of Membrane Electrode Assembly with Nickel Current Collectors	Published in Intellectual Properties of India

Conferences

S. No	National/ International	Name of the conference	Paper title	Place held
1	International	International Conference on Advances in Fluid Flow and Thermal Sciences (*ICAFFTS* 2021)	Experimental Investigation on Passive Direct Methanol Fuel Cell with combination of different anode and cathode current collectors	SVNIT, Surat, India.
2	International	2nd Indian International Conference on Industrial Engineering and Operations Management (*IEOM*-2022)	Identification of Service-Oriented Degradations using Non-Destructive Testing Methods on Passive Direct Methanol Fuel Cell Components	NIT, Warangal, India.

Appendix-I

Uncertainty Analysis

Uncertainty analysis is performed on the experimental results to identify inherent errors associated with the experimental instruments. In the experiment, voltage value is measured by keeping the current reading as constant. Hence, the error is reflected in voltage readings. To calculate the uncertainty in the results, standard deviation method is chosen using voltage measurements at constant current value.

The measured voltage readings average can be expressed as,

$$V_{avg} = \frac{1}{n}\sum_{i=1}^{i=n} V_i$$

Here,

V_i : individual voltage measurement,

i : individual entity of measurements,

V_{avg} : average of the voltage measurement; and

n : number of voltage measurements.

Uncertainty in the measured experimental data is evaluated from standard deviation and is expressed as:

$$U_v = \sqrt{\frac{1}{(n-1)}\sum (V_i - V_{avg})^2}$$

Where, U_v: uncertainty over the measurements V_i

Error in the measurement = $\frac{U_v}{n}$

For this experimental PDMFC setup, at 5M methanol concentration and using 45.30% open ratio current collectors at a current density of 49.6 $mA.cm^{-2}$, following three readings are recorded.

V_1=0.207 V, V_2=0.210 V and V_3=0.213 V

Percentage error in the voltage measurement is 0.17%, which is within the stated error of 0.28%, provided by the manufacturer.